Deep transcriptome annotation suggests that small and large proteins encoded in the same genes often cooperate

Sondos Samandi[1,7] †, Annie V. Roy[1,7] †, Vivian Delcourt[1,7,8], Jean-François Lucier[2], Jules Gagnon[2], Maxime C. Beaudoin[1,7], Benoît Vanderperre[1], Marc-André Breton[1], Julie Motard[1,7], Jean-François Jacques[1,7], Mylène Brunelle[1,7], Isabelle Gagnon-Arsenault[6,7], Isabelle Fournier[8], Aida Ouangraoua[3], Darel J. Hunting[4], Alan A. Cohen[5], Christian R. Landry[6,7], Michelle S. Scott[1], Xavier Roucou[1,7]*

[1]Department of Biochemistry, [2]Department of Biology and Center for Computational Science, [3]Department of Computer Science, [4]Department of Nuclear Medicine & Radiobiology, [5]Department of Family Medicine, Université de Sherbrooke, Québec, Canada; [6]Département de biologie and IBIS, Université Laval, Québec, Canada; [7]PROTEO, Québec Network for Research on Protein Function, Structure, and Engineering, Québec, Canada; [8]Université Lille, INSERM U1192, Laboratoire Protéomique, Réponse Inflammatoire & Spectrométrie de Masse (PRISM) F-59000 Lille, France

†These authors contributed equally to this work

*Correspondance to Xavier Roucou: Département de biochimie (Z8-2001), Faculté de Médecine et des Sciences de la Santé, Université de Sherbrooke, 3201 Jean Mignault, Sherbrooke, Québec J1E 4K8, Canada, Tel. (819) 821-8000x72240; Fax. (819) 820 6831;

E-Mail: xavier.roucou@usherbrooke.ca

Abstract

Recent studies in eukaryotes have demonstrated the translation of alternative open reading frames (altORFs) in addition to annotated protein coding sequences (CDSs). We show that a large number of small proteins could in fact be coded by altORFs. The putative alternative proteins translated from altORFs have orthologs in many species and evolutionary patterns indicate that altORFs are particularly constrained in CDSs that evolve slowly. Thousands of predicted alternative proteins are detected in proteomic datasets by reanalysis using a database containing predicted alternative proteins. Protein domains and co-conservation analyses suggest a potential functional relationship between small and large proteins encoded in the same genes. This is illustrated with specific examples, including altMiD51, a 70 amino acid mitochondrial fission-promoting protein encoded in *MiD51*/*Mief1*/*SMCR7L*, a gene encoding an annotated protein promoting mitochondrial fission. Our results suggest that many coding genes code for more than one protein that are often functionally related.

Introduction

Current protein databases are cornerstones of modern biology but are based on a number of assumptions. In particular, a mature mRNA is predicted to contain a single CDS; yet, ribosomes can select more than one translation initiation site (TIS)[1–3] on any single mRNA. Also, minimum size limits are imposed on the length of CDSs, resulting in many RNAs being mistakenly classified as non-coding (ncRNAs)[4–11]. As a result of these assumptions, the size and complexity of most eukaryotic proteomes have probably been greatly underestimated[12–15]. In particular, few small proteins (defined as of 100 amino acids or less) are annotated in current databases. The absence of annotation of small proteins is a major bottleneck in the study of their function and their roles in health and disease. This is further supported by classical and recent examples of small proteins of functional importance, for instance many critical regulatory molecules such as the F0 subunit of the F0F1-ATPsynthase[16], the sarcoplasmic reticulum calcium ATPase regulator phospholamban[17], and the key regulator of iron homeostasis hepcidin[18]. This limitation also impedes our understanding of the process of origin of new genes, which are thought to contribute to evolutionary innovations. Because these genes generally code for small proteins [19–22], they are difficult to unambiguously detect by proteomics and in fact are impossible to detect if they are not included in proteomics databases.

Functional annotation of ORFs encoding small proteins is particularly challenging since an unknown fraction of small ORFs may occur by chance in the transcriptome, generating a significant level of noise [13]. However, given that many small proteins have

important functions and are ultimately one of the most important sources of functional novelty, it is time to address the challenge of their functional annotations[13].

We systematically reanalyzed several eukaryotic transcriptomes to annotate previously unannotated ORFs which we term alternative ORFs (altORFs), and we annotated the corresponding hidden proteome. Here, altORFs are defined as potential protein-coding ORFs in ncRNAs, in UTRs or in different reading frames from annotated CDSs in mRNAs (Figure 1a). For clarity, predicted proteins translated from altORFs are termed alternative proteins and proteins translated from annotated CDSs are termed reference proteins.

Our goal was to provide functional annotations of alternative proteins by (1) analyzing relative patterns of evolutionary conservation between alternative and reference proteins and their corresponding coding sequences; (2) estimating the prevalence of alternative proteins both by bioinformatics analysis and by detection in large experimental datasets; (3) detecting functional signatures in alternative proteins; and (4) predicting and testing functional cooperation between alternative and reference proteins.

Results

Prediction of altORFs and alternative proteins. We predicted a total of 539,134 altORFs compared to 68,264 annotated CDSs in the human transcriptome (Figure 1b, Table 1). Because identical ORFs can be present in different RNA isoforms transcribed from the same genomic locus, the number of unique altORFs and CDSs becomes 183,191

87 and 54,498, respectively. AltORFs were also predicted in other organisms for comparison
88 (Table 1). By convention, only reference proteins are annotated in current protein
89 databases. As expected, altORFs are on average small, with a size ranging from 30 to
90 1480 codons. Accordingly, the median size of predicted human alternative proteins is 45
91 amino acids compared to 460 for reference proteins (Figure 1c), and 92.96 % of
92 alternative proteins have less than 100 amino acids. Thus, the bulk of the translation
93 products of altORFs would be small proteins. The majority of altORFs either overlap
94 annotated CDSs in a different reading frame (35.98%) or are located in 3'UTRs (40.09%)
95 (Figure 1d). 9.83% of altORFs are located in repeat sequences (Figure 1-figure
96 supplement 1a), compared to 2.45% of CDSs. To assess whether observed altORFs could
97 be attributable solely to random occurrence, due for instance to the base composition of
98 the transcriptome, we estimated the expected number of altORFs generated in 100
99 shuffled human transcriptomes. Overall, we observed 62,307 more altORFs than would
100 be expected from random occurrence alone (Figure 1e; $p < 0.0001$). This analysis suggests
101 that a large number are expected by chance alone but that at the same time, a large
102 absolute number could potentially be maintained and be functional. The density of
103 altORFs observed in the CDSs, 3'UTRs and ncRNAs (Figure 1f) was markedly higher
104 than in the shuffled transcriptomes, suggesting that these are maintained at frequencies
105 higher than expected by chance, again potentially due to their coding function. In
106 contrast, the density of altORFs observed in 5'UTRs was much lower than in the shuffled
107 transcriptomes, supporting recent claims that negative selection eliminates AUGs (and
108 thus the potential for the evolution of altORFs) in these regions[23,24].
109

110 Although the majority of human annotated CDSs do not have a TIS with a Kozak motif
111 (Figure 1g)[25], there is a correlation between a Kozak motif and translation efficiency[26].
112 We find that 27,539 (15% of 183,191) human altORFs encoding predicted alternative
113 proteins have a Kozak motif (A/GNNAUGG), as compared to 19,745 (36% of 54,498)
114 for annotated CDSs encoding reference proteins (Figure 1g). The number of altORFs
115 with Kozak motifs is significantly higher in the human transcriptome compared to
116 shuffled transcriptomes (Figure 1-figure supplement 2), again supporting their potential
117 role as protein coding.
118
119 **Conservation analyses.** Next, we compared evolutionary conservation patterns of
120 altORFs and CDSs. A large number of human alternative proteins have homologs in other
121 species. In mammals, the number of homologous alternative proteins is higher than the
122 number of homologous reference proteins (Figure 2a), and 9 are even conserved from
123 human to yeast (Figure 2b), supporting a potential functional role. As phylogenetic
124 distance from human increases, the number and percentage of genes encoding
125 homologous alternative proteins decreases more rapidly than the percentage of genes
126 encoding reference proteins (Figures 2a and c). This observation indicates either that
127 altORFs evolve more rapidly than CDSs or that distant homologies are less likely to be
128 detected given the smaller sizes of alternative proteins. Another possibility is that they
129 evolve following the patterns of evolution of genes that evolve *de novo*, with a rapid birth
130 and death rate, which accelerates their turnover over time[20].
131 Since the same gene may contain a conserved CDS and one or several conserved
132 altORFs, we analyzed the co-conservation of orthologous altORF-CDS pairs. Our results

show a very large fraction of co-conserved alternative-reference protein pairs in several species (Figure 3). Detailed results for all species are presented in Table 2.

If altORFs play a functional role, they would be expected to be under purifying selection. The first and second positions of a codon experience stronger purifying selection than the third because of redundancy in the genetic code[27]. In the case of CDS regions overlapping altORFs with a shifted reading frame, the third codon positions of the CDSs are either the first or the second in the altORFs, and should thus also undergo purifying selection. We analyzed conservation of third codon positions of CDSs for 100 vertebrate species for 1,088 altORFs completely nested within and co-conserved across vertebrates (human to zebrafish) with their 889 CDSs from 867 genes (Figure 4). We observed that in regions of the CDS overlapping altORFs, third codon positions were evolving at significantly more extreme speeds (slow or quick) than third codon positions of random control sequences from the entire CDS (Figure 4), reaching up to 67-fold for conservation at $p<0.0001$ and 124-fold for accelerated evolution at $p<0.0001$. We repeated this analysis with the 53,862 altORFs completely nested within the 20,814 CDSs from 14,677 genes, independently of their co-co-conservation. We observed a similar trend, with a 22-fold for conservation at $p<0.0001$, and a 24-fold for accelerated evolution at $p<0.0001$ (Figure 4-figure supplement 1).This is illustrated with three altORFs located within the CDS of *NTNG1*, *RET* and *VTI1A* genes (Figure 5). These three genes encode a protein promoting neurite outgrowth, the proto-oncogene tyrosine-protein kinase receptor Ret and a protein mediating vesicle transport to the cell surface, respectively. Two of these alternative proteins have been detected by ribosome profiling (*RET*, IP_182668.1) or mass spectrometry (*VTI1A*, IP_188229.1) (see below, Supplementary files 1 and 2).

157

158 **Evidence of expression of alternative proteins.** We provide two lines of evidence
159 indicating that thousands of altORFs are translated into proteins. First, we re-analyzed
160 detected TISs in publicly available ribosome profiling data[28,29], and found 26,531 TISs
161 mapping to annotated CDSs and 12,616 mapping to altORFs in these studies (Figure 6a;
162 Supplementary file 1). Only a small fraction of TISs detected by ribosomal profiling
163 mapped to altORFs[3'] even if those are more abundant than altORF[5'] relative to shuffled
164 transcriptomes, likely reflecting a recently-resolved technical issue which prevented TIS
165 detection in 3'UTRs [30]. New methods to analyze ribosome profiling data are being
166 developed and will likely uncover more translated altORFs [9]. In agreement with the
167 presence of functional altORFs[3'], cap-independent translational sequences were recently
168 discovered in human 3'UTRs[31]. Second, we re-analyzed proteomic data using our
169 composite database containing alternative proteins in addition to annotated reference
170 proteins (Figure 6b; Supplementary file 2). We selected four studies representing
171 different experimental paradigms and proteomic applications: large-scale [32] and targeted
172 [33] protein/protein interactions, post-translational modifications [34], and a combination of
173 bottom-up, shotgun and interactome proteomics [35] . In the first dataset, we detected 3,957
174 predicted alternative proteins in the interactome of reference proteins[32], providing a
175 framework to uncover the function of these proteins. In a second proteomic dataset
176 containing about 10,000 reference human proteins[35], a total of 549 predicted alternative
177 proteins were detected. Using a phosphoproteomic large data set[34], we detected 384
178 alternative proteins. The biological function of these proteins is supported by the
179 observation that some alternative proteins are specifically phosphorylated in cells

180 stimulated by the epidermal growth factor, and others are specifically phosphorylated
181 during mitosis (Figure 7; Supplementary file 3). We provide examples of spectra
182 validation (Figure 7-figure supplement 1). A fourth proteomic dataset contained 77
183 alternative proteins in the epidermal growth factor receptor interactome[33] (Figure 6b). A
184 total of 4,872 different alternative proteins were detected in these proteomic data. The
185 majority of these proteins are coded by altORF^{CDS}, but there are also significant
186 contributions of altORF$^{3'}$, altORF^{nc} and altORF$^{5'}$ (Figure 6c). Overall, by mining the
187 proteomic and ribosomal profiling data, we detected the translation of a total of 17,371
188 unique alternative proteins. 467 of these alternative proteins were detected by both MS
189 and ribosome profiling (Figure 8), providing a high-confidence collection of small
190 alternative proteins for further studies.
191
192 **Functional annotations of alternative proteins.** An important goal of this study is to
193 associate potential functions to alternative proteins, which we can do through
194 annotations. Because the sequence similarities and the presence of particular signatures
195 (families, domains, motifs, sites) are a good indicator of a protein's function, we analyzed
196 the sequence of the predicted alternative proteins in several organisms with InterProScan,
197 an analysis and classification tool for characterizing unknown protein sequences by
198 predicting the presence of combined protein signatures from most main domain
199 databases[36] (Figure 9; Figure 9-figure supplement 1). We found 41,511 (23%) human
200 alternative proteins with at least one InterPro signature (Figure 9b). Of these, 37,739 (or
201 20.6%) are classified as small proteins. Interestingly, the reference proteome has a
202 smaller proportion (840 or 1.68%) of small proteins with at least one InterPro signature,

203 supporting a biological activity for alternative proteins.

204 Similar to reference proteins, signatures linked to membrane proteins are abundant in the
205 alternative proteome and represent more than 15,000 proteins (Figures 9c-e; Figure 9-
206 figure supplement 1). With respect to the targeting of proteins to the secretory pathway or
207 to cellular membranes, the main difference between the alternative and the reference
208 proteomes lies in the very low number of proteins with both signal peptides and
209 transmembrane domains. Most of the alternative proteins with a signal peptide do not
210 have a transmembrane segment and are predicted to be secreted (Figures 9c, d),
211 supporting the presence of large numbers of alternative proteins in plasma[37]. The majority
212 of predicted alternative proteins with transmembrane domains have a single membrane
213 spanning domain but some display up to 27 transmembrane regions, which is still within
214 the range of reference proteins that show a maximum of 33 (Figure 9e).

215 We extended the functional annotation using the Gene Ontology. A total of 585
216 alternative proteins were assigned 419 different InterPro entries, and 343 of them were
217 tentatively assigned 192 gene ontology terms (Figure 10). 15.5% (91/585) of alternative
218 proteins with an InterPro entry were detected by MS or/and ribosome profiling, compared
219 to 13.7% (22,055/161,110) for alternative proteins without an InterPro entry (*p*-value =
220 1.13e-05, Fisher's exact test and chi-square test). Thus, predicted alternative proteins with
221 InterPro entries are more likely to be detected, supporting their functional role. The most
222 abundant class of predicted alternative proteins with at least one InterPro entry are C2H2
223 zinc finger proteins with 110 alternative proteins containing 187 C2H2-type/integrase
224 DNA-binding domains, 91 C2H2 domains and 23 C2H2-like domains (Figure 11a).
225 Eighteen of these (17.8%) were detected in public proteomic and ribosome profiling

226 datasets, a percentage that is similar to reference zinc finger proteins (20.1%) (Figure 6,
227 Table 3). Alternative proteins have between 1 and 23 zinc finger domains (Figure 11b).
228 Zinc fingers mediate protein-DNA, protein-RNA and protein-protein interactions[38]. The
229 linker sequence separating adjacent finger motifs matches or resembles the consensus
230 TGEK sequence in nearly half the annotated zinc finger proteins[39]. This linker confers
231 high affinity DNA binding and switches from a flexible to a rigid conformation to
232 stabilize DNA binding. The consensus TGEK linker is present 46 times in 31 alternative
233 zinc finger proteins (Supplementary file 4). These analyses show that a number of
234 alternative proteins can be classified into families and will help deciphering their
235 functions.
236
237 **Evidence of functional relationships between reference and alternative proteins**
238 **coded by the same genes.** Since one gene may code for both a reference and one or
239 several alternative proteins, we asked whether paired (encoded in the same gene)
240 alternative and reference proteins have functional relationships. The functional
241 associations discussed here are potential functional interactions that do not necessarily
242 imply physical interactions; however, there are a few known examples of functional
243 linkage between different proteins encoded in the same gene (Table 4). If there is a
244 functional relationship, one would expect orthologous alternative- reference protein pairs
245 to be co-conserved more often than expected by chance[40]. Our results show a large
246 fraction of co-conserved alternative-reference protein pairs in several species (Figure 3).
247 Detailed results for all species are presented in Table 2.
248 Another mechanism that could show functional relationships between alternative and

249 reference proteins encoded in the same gene would be that they share protein domains.
250 We compared the functional annotations of the 585 alternative proteins with an InterPro
251 entry with the reference proteins expressed from the same genes. Strikingly, 89 of 110
252 altORFs coding for zinc finger proteins (Figure 11) are present in transcripts in which the
253 CDS also codes for a zinc finger protein. Overall, 138 alternative/reference protein pairs
254 share at least one InterPro entry and many pairs share more than one entry (Figure 12a).
255 The number of shared entries was much higher than expected by chance (Figure 12b,
256 $p<0.0001$). The correspondence between InterPro domains of alternative proteins and
257 their corresponding reference proteins coded by the same genes also indicates that even
258 when entries are not identical, the InterPro terms are functionally related (Figure 12c;
259 Figure 12-figure supplement 1), overall supporting a potential functional linkage between
260 reference and predicted alternative proteins. Domain sharing remains significant
261 ($p<0.001$) even when the most frequent domains, zinc fingers, are not considered (Figure
262 12-figure supplement 2).
263
264 Recently, the interactome of 118 human zinc finger proteins was determined by affinity
265 purification followed by mass spectrometry [41]. This study provides a unique opportunity
266 to test if, in addition to possessing zinc finger domains, thus being functionally connected
267 some pairs of reference and alternative proteins coded by the same gene also interact. We
268 re-analyzed the MS data using our alternative protein sequence database to detect
269 alternative proteins in this interactome (Supplementary file 5). Five alternative proteins
270 (IP_168460.1, IP_168527.1, IP_270697.1, IP_273983.1, IP_279784.1) were identified
271 within the interactome of their reference zinc finger proteins. This number was higher

272 than expected by chance ($p<10^{-6}$) based on 1 million binomial simulations of randomized
273 interactomes. This result strongly supports the hypothesis of functional relationships
274 between alternative and reference proteins coded by the same genes, and indicates that
275 there are examples of physical interactions.
276
277 Finally, we integrated the co-conservation and expression analyses to produce a high-
278 confidence list of alternative proteins predicted to have a functional relationship with
279 their reference proteins and found 2,715 alternative proteins in mammals (*H. sapiens* to
280 *B. taurus*), and 44 in vertebrates (H. *sapiens* to *D. rerio*) (Supplementary file 6). In order
281 to further test for functional relationship between alternative/reference protein pairs in
282 this list, we focused on alternative proteins detected with at least two peptide spectrum
283 matches or with high TIS reads. From this subset, we selected altMiD51 (IP_294711.1)
284 among the top 2% of alternative proteins detected with the highest number of unique
285 peptides in proteomics studies, and altDDIT3 (IP_211724.1) among the top 2% of
286 altORFs with the most cumulative reads in translation initiation ribosome profiling
287 studies.
288 AltMiD51 is a 70 amino acid alternative protein conserved in vertebrates[42] and co-
289 conserved with its reference protein MiD51 from humans to zebrafish (Supplementary
290 file 6). Its coding sequence is present in exon 2 of the *MiD51/MIEF1/SMCR7L* gene. This
291 exon forms part of the 5'UTR for the canonical mRNA and is annotated as non-coding in
292 current gene databases (Figure 13a). Yet, altMiD51 is robustly detected by MS in several
293 cell lines (Supplementary file 2: HEK293, HeLa Kyoto, HeLa S3, THP1 cells and gut
294 tissue), and we validated some spectra using synthetic peptides (Figure 13-figure

295 supplement 1), and it is also detected by ribosome profiling (Supplementary file 1)[37,42,43].
296 We confirmed co-expression of altMiD51 and MiD51 from the same transcript (Figure
297 13b). Importantly, the tripeptide LYR motif predicted with InterProScan and located in
298 the N-terminal domain of altMiD51 (Figure 13a) is a signature of mitochondrial proteins
299 localized in the mitochondrial matrix[44]. Since *MiD51/MIEF1/SMCR7L* encodes the
300 mitochondrial protein MiD51, which promotes mitochondrial fission by recruiting
301 cytosolic Drp1, a member of the dynamin family of large GTPases, to mitochondria[45], we
302 tested for a possible functional connection between these two proteins expressed from the
303 same mRNA. We first confirmed that MiD51 induces mitochondrial fission (Figure 13-
304 figure supplement 2). Remarkably, we found that altMiD51 also localizes at the
305 mitochondria (Figure 13c; Figure 13-figure supplement 3) and that its overexpression
306 results in mitochondrial fission (Figure 13d). This activity is unlikely to be through
307 perturbation of oxidative phosphorylation since the overexpression of altMiD51 did not
308 change oxygen consumption nor ATP and reactive oxygen species production (Figure 13-
309 figure supplement 4). The decrease in spare respiratory capacity in altMiD51-expressing
310 cells (Figure 13-figure supplement 4a) likely resulted from mitochondrial fission[46]. The
311 LYR domain is essential for altMiD51-induced mitochondrial fission since a mutant of
312 the LYR domain, altMiD51(LYR→AAA) was unable to convert the mitochondrial
313 morphology from tubular to fragmented (Figure 13d). Drp1(K38A), a dominant negative
314 mutant of Drp1 [47], largely prevented the ability of altMiD51 to induce mitochondrial
315 fragmentation (Figure 13d; Figure 13-figure supplement 5a). In a control experiment, co-
316 expression of wild-type Drp1 and altMiD51 proteins resulted in mitochondrial
317 fragmentation (Figure 13-figure supplement 5b). Expression of the different constructs

318 used in these experiments was verified by western blot (Figure 13-figure supplement 6).
319 Drp1 knockdown interfered with altMiD51-induced mitochondrial fragmentation (Figure
320 14), confirming the proposition that Drp1 mediates altMiD51-induced mitochondrial
321 fragmentation. It remains possible that altMiD51 promotes mitochondrial fission
322 independently of Drp1 and is able to reverse the hyperfusion induced by Drp1
323 inactivation. However, Drp1 is the key player mediating mitochondrial fission and most
324 likely mediates altMiD51-induced mitochondrial fragmentation, as indicated by our
325 results.
326 AltDDIT3 is a 31 amino acid alternative protein conserved in vertebrates and co-
327 conserved with its reference protein DDIT3 from human to bovine (Supplementary file
328 6). Its coding sequence overlaps the end of exon 1 and the beginning of exon 2 of the
329 *DDIT3/CHOP/GADD153* gene. These exons form part of the 5'UTR for the canonical
330 mRNA (Figure 15a). To determine the cellular localization of altDDIT3 and its possible
331 relationship with DDIT3, confocal microscopy analyses were performed on HeLa cells
332 co-transfected with altDDIT3^{GFP} and DDIT3^{mCherry}. Expression of these constructs was
333 verified by western blot (Figure 15-figure supplement 1). Interestingly, both proteins
334 were mainly localized in the nucleus and partially localized in the cytoplasm (Figure
335 15b). This distribution for DDIT3 confirms previous studies [48,49]. Both proteins seemed to
336 co-localize in these two compartments (Pearson correlation coefficient 0.92, Figure 15c).
337 We further confirmed the statistical significance of this colocalization by applying
338 Costes' automatic threshold and Costes' randomization colocalization analysis and
339 Manders Correlation Coefficient (Figure 15d; Figure 15-figure supplement 2) [50]. Finally,
340 in lysates from cells co-expressing altDDIT3^{GFP} and DDIT3^{mCherry}, DDIT3^{mCherry} was

341 immunoprecipitated with GFP-trap agarose, confirming an interaction between the small
342 altDDTI3 and the large DDIT3 proteins encoded in the same gene (Figure 15e).
343
344
345 **Discussion**
346 We have provided the first functional annotation of altORFs with a minimum size of 30
347 codons in different genomes. The comprehensive annotation of *H sapiens* altORFs is
348 freely available to download at https://www.roucoulab.com/p/downloads (Homo sapiens
349 functional annotation of alternative proteins based on RefSeq GRCh38 (hg38)
350 predictions). In light of the increasing evidence from approaches such as ribosome
351 profiling and MS-based proteomics that the one mRNA-one canonical CDS assumption
352 is strongly challenged, our findings provide the first clear functional insight into a new
353 layer of regulation in genome function. While many observed altORFs may be
354 evolutionary accidents with no functional role, several independent lines of evidence
355 support translation and a functional role for thousands of alternative proteins: (1)
356 overrepresentation of altORFs relative to shuffled sequences; (2) overrepresentation of
357 altORF Kozak sequences; (3) active altORF translation detected via ribosomal profiling;
358 (4) detection of thousands of alternative proteins in multiple existing proteomic datasets;
359 (5) correlated altORF-CDS conservation, but with overrepresentation of highly conserved
360 and fast-evolving altORFs; (6) overrepresentation of identical InterPro signatures
361 between alternative and reference proteins encoded in the same mRNAs; (7) several
362 thousand co-conserved paired alternative-reference proteins encoded in the same gene;
363 and (8) presence of clear, striking examples in altMiD51, altDDIT3 and 5 alternative

364 proteins interacting with their reference zinc finger proteins. While 5 of these 8 lines of
365 evidence support an unspecified functional altORF role, 4 of them (5, 6, 7 and 8)
366 independently support a specific functional/evolutionary interpretation of their role: that
367 alternative proteins and reference proteins have paired functions. Note that this
368 hypothesis does not require binding, just functional cooperation such as activity on a
369 shared pathway.
370
371 The presence of different coding sequences in the same gene provides a coordinated
372 transcriptional regulation. Consequently, the transcription of different coding sequences
373 can be turned on or off together, similar to prokaryotic operons. Thus, the observation
374 that alternative-reference protein pairs encoded in the same genes have functional
375 relationships is not completely unexpected. This observation is also in agreement with
376 increasing evidence that small proteins regulate the function of larger proteins[51]. We
377 speculate that clustering of a CDS and one or more altORFs in the same genes, and thus
378 in the same transcription unit allows cells to adapt more quickly with optimized energy
379 expenditure to environmental changes.
380
381 Upstream ORFs here labeled altORFs$^{5'}$ are important translational regulators of canonical
382 CDSs in vertebrates[52]. Interestingly, the altORF$^{5'}$ encoding altDDIT3 was characterized
383 as an inhibitory upstream ORF [53,54], but evidence of endogenous expression of the
384 corresponding small protein was not sought. The detection of altMiD51 and altDDIT3
385 suggests that a fraction of altORFs$^{5'}$ may have dual functions as translation regulators and
386 functional proteins.

387

388 Our results raise the question of the evolutionary origins of these altORFs. A first
389 possible mechanism involves the polymorphism of initiation and stop codons during
390 evolution [55,56]. For instance, the generation of an early stop codon in the 5'end of a CDS
391 could be followed by the evolution of another translation initiation site downstream,
392 creating a new independent ORF in the 3'UTR of the canonical gene. This mechanism of
393 altORF origin, reminiscent of gene fission, would at the same time produce a new altORF
394 that shares protein domains with the annotated CDS, as we observed for a substantial
395 fraction (24%) of the 585 alternative proteins with an InterPro entry. A second
396 mechanism would be de novo origin of ORFs, which would follow the well-established
397 models of gene evolution *de novo*[20,57,58] in which new ORFs are transcribed and
398 translated and have new functions or await the evolution of new functions by mutations.
399 The numerous altORFs with no detectable protein domains may have originated this way
400 from previously non-coding regions or in regions that completely overlap with CDS in
401 other reading frames.

402

403 Detection is an important challenge in the study of small proteins. A TIS detected by
404 ribosome profiling does not necessarily imply that the protein is expressed as a stable
405 molecule, and proteomic analyses more readily detect large proteins that generate several
406 peptides after enzymatic digestion. In addition, evolutionarily novel genes tend to be
407 poorly expressed, again reducing the probability of detection [20]. Here, we used a
408 combination of five search engines, thus increasing the confidence and sensitivity of hits
409 compared to single-search-engine processing[59,60]. This strategy led to the detection of

410 several thousand alternative proteins. However, ribosome profiling and MS have
411 technical caveats and the comprehensive contribution of small proteins to the proteome
412 will require more efforts, including the development of new tools such as specific
413 antibodies.
414
415 Only a relatively small percentage of alternative proteins (22.6%) are functionally
416 annotated with Interpro signatures, compared to reference proteins (96.9%). An obvious
417 explanation is the small size of alternative proteins with a median size of 45 amino acids,
418 which may not be able to accommodate large domains. It has been proposed that small
419 proteins may be precursors of new proteins but require an elongation of their coding
420 sequence before they display a useful cellular activity [19,51]. According to this hypothesis,
421 it is possible that protein domains appear only after elongation of the coding sequence.
422 Alternatively, InterPro domains were identified by investigating the reference proteome,
423 and alternative proteins may have new domains and motifs that remain to be
424 characterized. Finally, an unknown fraction of predicted altORFs may not be translated or
425 may code for non-functional peptides.
426
427 In conclusion, our deep annotation of the transcriptome reveals that a large number of
428 small eukaryotic proteins, which may even represent the majority, are still officially
429 unannotated. Our results also suggest that many small and large proteins coded by the
430 same mRNA may cooperate by regulating each other's function or by functioning in the
431 same pathway, confirming the few examples in the literature of unrelated proteins
432 encoded in the same genes and functionally cooperating[61–65]. To determine whether or not

433 this functional cooperation is a general feature of small/large protein pairs encoded in the
434 same gene will require much more experimental evidence, but our results strongly
435 support this hypothesis.
436

437 Materials and methods

438 **Generation of alternative open reading frames (altORFs) and alternative protein**
439 **databases.** Throughout this manuscript, annotated protein coding sequences and proteins
440 in current databases are labelled annotated coding sequences or CDSs and reference
441 proteins, respectively. For simplicity reasons, predicted alternative protein coding
442 sequences are labelled alternative open reading frames or altORFs.
443 To generate MySQL databases containing the sequences of all predicted alternative
444 proteins translated from reference annotation of different organisms, a computational
445 pipeline of Perl scripts was developed as previously described with some modifications[37].
446 Genome annotations for *H. sapiens* (release hg38, Assembly: GCF_000001405.26), *P.*
447 *troglodytes* (Pan_troglodytes-2.1.4, Assembly: GCF_000001515.6), *M. musculus*
448 (GRCm38.p2, Assembly: GCF_000001635.22), *D. melanogaster* (release 6, Assembly:
449 GCA_000705575.1), *C. elegans* (WBcel235, Assembly: GCF_000002985.6) and *S.*
450 *cerevisiae* (Sc_YJM993_v1, Assembly: GCA_000662435.1) were downloaded from the
451 NCBI website (http://www.ncbi.nlm.nih.gov/genome). For *B. taurus* (release UMD
452 3.1.86), *X. tropicalis* (release JGI_4.2) and *D. rerio* (GRCz10.84), genome annotations
453 were downloaded from Ensembl (http://www.ensembl.org/info/data/ftp/). Each annotated
454 transcript was translated *in silico* with Transeq[66]. All ORFs starting with an AUG and
455 ending with a stop codon different from the CDS, with a minimum length of 30 codons

456 (including the stop codon) and identified in a distinct reading frame compared to the
457 annotated CDS when overlapping the CDS, were defined as altORFs.
458 An additional quality control step was performed to remove initially predicted altORFs
459 with a high level of identity with reference proteins. Such altORFs typically start in a
460 different coding frame than the reference protein but through alternative splicing, end
461 with the same amino acid sequence as their associated reference protein. Using BLAST,
462 altORFs overlapping CDSs chromosomal coordinates and showing more than 80%
463 identity and overlap with an annotated CDS were rejected.
464 AltORF localization was assigned according to the position of the predicted translation
465 initiation site (TIS): altORFs$^{5'}$, altORFs^{CDS} and altORFs$^{3'}$ are altORFs with TISs located
466 in 5'UTRs, CDSs and 3'UTRs, respectively. Non-coding RNAs (ncRNAs) have no
467 annotated CDS and all ORFs located within ncRNAs are labelled altORFs^{nc}.
468 The presence of the simplified Kozak sequence (A/GNNATGG) known to be favorable
469 for efficient translation initiation was also assessed for each predicted altORF[67].
470
471 **Identification of TISs.** The global aggregates of initiating ribosome profiles data were
472 obtained from the initiating ribosome tracks in the GWIPS-viz genome browser[28] with
473 ribosome profiling data collected from five large scale studies[2,9,68–70]. Sites were mapped
474 to hg38 using a chain file from the UCSC genome browser
475 (http://hgdownload.soe.ucsc.edu/goldenPath/hg19/liftOver/hg19ToHg38.over.chain.gz)
476 and CrossMap v0.1.6 (RRID:SCR_001173). Similar to the methods used in these studies,
477 an altORF is considered as having an active TIS if it is associated with at least 10 reads at
478 one of the 7 nucleotide positions of the sequence NNNAUGN (AUG is the predicted

479 altORF TIS). An additional recent study was also included in our analysis[29]. In this study,
480 a threshold of 5 reads was used. Raw sequencing data for ribosome protected fragments
481 in harringtonine treated cells was aligned to the human genome (GRCh38) using bowtie2
482 (2.2.8)[71]. Similar to the method used in this work, altORFs with at least 5 reads
483 overlapping one position in the kozak region were considered as having an
484 experimentally validated TIS.
485
486 **Generation of shuffled transcriptomes.** Each annotated transcript was shuffled using
487 the Fisher-Yates shuffle algorithm. In CDS regions, all codons were shuffled except the
488 initiation and stop codons. For mRNAs, we shuffled the 5'UTRs, CDSs and 3'UTRs
489 independently to control for base composition. Non-coding regions were shuffled at the
490 nucleotide level. The resulting shuffled transcriptome has the following features
491 compared to hg38: same number of transcripts, same transcripts lengths, same nucleotide
492 composition, and same amino-acid composition for the proteins translated from the
493 CDSs. Shuffling was repeated 100 times and the results are presented with average values
494 and standard deviations. The total number of altORFs is 539,134 for hg38, and an
495 average of 489,073 for shuffled hg38. AltORFs and kozak motifs in the 100 shuffled
496 transcriptomes were detected as described above for hg38.
497
498 **Identification of paralogs/orthologs in alternative proteomes.** Both alternative and
499 reference proteomes were investigated. Pairwise ortholog and paralog relationships
500 between the human proteomes and the proteomes from other species, were calculated
501 using an InParanoid-like approach[72], as described below (RRID:SCR_006801). The

502 following BLAST (RRID:SCR_001010) procedure was used. Comparisons using our
503 datasets of altORFs/CDS protein sequences in multiple FASTA formats from
504 *Saccharomyces cerevisiae, Caenorhabditis elegans, Drosophila melanogaster, Danio*
505 *rerio, Xenopus tropicalis Bos taurus, Mus musculus, Pan troglodytes, Homo sapiens* were
506 performed between each pair of species (*Homo sapiens* against the other species),
507 involving four whole proteome runs per species pair: pairwise comparisons (organism A
508 vs organism B, organism B vs organism A), plus two self-self runs (organism A vs
509 organism A, organism B vs organism B). BLAST homology inference was accepted when
510 the length of the aligned region between the query and the match sequence equalled or
511 exceeded 50% of the length of the sequence, and when the bitscore reached a minimum
512 of 40[73]. Orthologs were detected by finding the mutually best scoring pairwise hits
513 (reciprocal best hits) between datasets A-B and B-A. The self-self runs were used to
514 identify paralogy relationships as described[72].
515
516 **Co-conservation analyses.** For each orthologous alternative protein pair A-B between
517 two species, we evaluated the presence and the orthology of their corresponding
518 reference proteins A'-B' in the same species. In addition, the corresponding altORFs and
519 CDSs had to be present in the same gene.
520 In order to develop a null model to assess co-conservation of alternative proteins and
521 their reference pairs, we needed to establish a probability that any given orthologous
522 alternative protein would by chance occur encoded on the same transcript as its paired,
523 orthologous reference protein. Although altORFs might in theory shift among CDSs (and
524 indeed, a few examples have been observed), transposition events are expected to be

525 relatively rare; we thus used the probability that the orthologous alternative protein is
526 paired with any orthologous CDS for our null model. Because this probability is by
527 definition higher than the probability that the altORF occurs on the paired CDS, it is a
528 conservative estimate of co-conservation. We took two approaches to estimating this
529 percentage, and then used whichever was higher for each species pair, yielding an even
530 more conservative estimate. First, we assessed the percentage of orthologous reference
531 proteins under the null supposition that each orthologous alternative protein had an equal
532 probability of being paired with any reference protein, orthologous or not. Second, we
533 assessed the percentage of non-orthologous alternative proteins that were paired with
534 orthologous reference proteins. This would account for factors such as longer CDSs
535 having a higher probability of being orthologous and having a larger number of paired
536 altORFs. For example, between *Homo sapiens* and *Mus musculus*, we found that 22,304
537 of 54,498 reference proteins (40.9%) were orthologs. Of the 157,261 non-orthologous
538 alternative proteins, 106,987 (68%) were paired with an orthologous reference protein.
539 Because 68% is greater than 40.9%, we used 68% as the probability for use in our null
540 model. Subsequently, our model strongly indicates co-conservation (Fig. 3 and Table 2;
541 $p<10^{-6}$ based on 1 million binomial simulations; highest observed random percentage
542 =69%, much lower than the observed 96% co-conservation).
543
544 **Analysis of third codon position (wobble) conservation.** Basewise conservation scores
545 for the alignment of 100 vertebrate genomes including *H. sapiens* were obtained from
546 UCSC genome browser
547 (http://hgdownload.soe.ucsc.edu/goldenPath/hg38/phyloP100way/)

548 (RRID:SCR_012479). Conservation PhyloP scores relative to each nucleotide position
549 within codons were extracted using a custom Perl script and the Bio-BigFile module
550 version 1.07 (see code file). The PhyloP conservation score for the wobble nucleotide of
551 each codon within the CDS was extracted. For the 53,862 altORFs completely nested
552 inside 20,814 CDSs, the average PhyloP score for wobble nucleotides within the altORF
553 region was compared to the average score for the complete CDS. To generate controls,
554 random regions in CDSs with a similar length distribution as altORFs were selected and
555 PhyloP scores for wobble nucleotides were extracted. We compared the differences
556 between altORF and CDS PhyloP scores (altORF PhyloP – CDS PhyloP) to those
557 generated based on random regions. We identified expected quantiles of the differences
558 ("DQ" column in the table), and compared these to the observed differences. Because
559 there was greater conservation of wobble nucleotide PhyloP scores within altORFs
560 regions located farther from the center of their respective genes ($r = 0.08$, $p < 0.0001$),
561 observed differences were adjusted using an 8-knot cubic basis spline of percent distance
562 from center. These observed differences were also adjusted for site-specific signals as
563 detected in the controls.
564

565 **Human alternative protein classification and in silico functional annotation.**

566 *Repeat and transposable element annotation*

567 RepeatMasker, a popular software to scan DNA sequences for identifying and classifying
568 repetitive elements (RRID:SCR_012954), was used to investigate the extent of altORFs
569 derived from transposable elements[74]. Version 3-3-0 was run with default settings.

570 *Alternative protein analysis using InterProScan* (RRID:SCR_005829)

571 InterProScan combines 15 different databases, most of which use Hidden Markov models
572 for signature identification[75]. Interpro merges the redundant predictions into a single
573 entry and provides a common annotation. A recent local version of InterProScan 5.14-
574 53.0 was run using default parameters to scan for known protein domains in alternative
575 proteins. Gene ontology (GO) and pathway annotations were also reported if available
576 with -goterm and -pa options. Only protein signatures with an E-value $\leq 10^{-3}$ were
577 considered.
578 We classified the reported InterPro hits as belonging to one or several of three clusters;
579 (1) alternative proteins with InterPro entries; (2) alternative proteins with signal peptides
580 (SP) and/or transmembrane domains (TM) predicted by at least two of the three SignalP,
581 PHOBIUS, TMHMM tools and (3) alternative proteins with other signatures.
582 The GO terms assigned to alternative proteins with InterPro entries were grouped and
583 categorised into 13 classes within the three ontologies (cellular component, biological
584 process, molecular function) using the CateGOrizer tool[76] (RRID:SCR_005737).
585 Each unique alternative protein with InterPro entries and its corresponding reference
586 protein (encoded in the same transcript) were retrieved from our InterProscan output.
587 Alternative and reference proteins without any InterPro entries were ignored. The overlap
588 in InterPro entries between alternative and reference proteins was estimated as follows.
589 We went through the list of alternative/reference protein pairs and counted the overlap in
590 the number of entries between the alternative and reference proteins as
591 100*intersection/union. All reference proteins and the corresponding alternative proteins
592 were combined together in each comparison so that all domains of all isoforms for a
593 given reference protein were considered in each comparison. The random distribution of

594 the number of alternative/reference protein pairs that share at least one InterPro entry was
595 computed by shuffling the alternative/reference protein pairs and calculating how many
596 share at least one InterPro entry. This procedure was repeated 1,000 times. Finally, we
597 compared the number and identity of shared InterPro entries in a two dimensional matrix
598 to illustrate which Interpro entries are shared. In many instances, including for zinc-finger
599 coding genes, InterPro entries in alternative/reference protein pairs tend to be related
600 when they are not identical.
601
602 **Mass Spectrometry identification.** Wrapper Perl scripts were developed for the use of
603 SearchGUI v2.0.11[77] (RRID:SCR_012054) and PeptideShaker v1.1.0[59]
604 (RRID:SCR_002520) on the *Université de Sherbrooke's* 39,168 core high-performance
605 *Mammouth Parallèle 2* computing cluster
606 (http://www.calculquebec.ca/en/resources/compute-servers/mammouth-parallele-ii).
607 SearchGUI was configured to run the following proteomics identification search engines:
608 X!Tandem[78], MS-GF+[79], MyriMatch[80], Comet[81], and OMSSA[82]. SearchGUI parameters
609 were set as follow: maximum precursor charge, 5; maximum number of PTM per peptide,
610 5; X!Tandem minimal fragment m/z, 140; removal of initiator methionine for Comet, 1. A
611 full list of parameters used for SearchGUI and PeptideShaker is available in
612 Supplementary file 2, sheet 1. For PXD000953 dataset[35], precursor and fragment
613 tolerance were set 0.006 Da and 0.1 Da respectively, with carbamidomethylation of C as
614 a fixed modification and Nter-Acetylation and methionine oxidation as variable
615 modifications. For PXD000788[33] and PXD000612[34] datasets, precursor and fragment
616 tolerance were set to 4.5 ppm and 0.1 Da respectively with carbamidomethylation of

617 cysteine as a fixed modification and Nter-Acetylation, methionine oxidation and
618 phosphorylation of serine, threonine and tyrosine as variable modifications. For
619 PXD002815 dataset[32], precursor and fragment tolerance were set to 4.5 ppm and 0.1 Da
620 respectively with carbamidomethylation of cysteine as a fixed modification and Nter-
621 Acetylation and methionine oxidation as variable modifications.Datasets were searched
622 using a target-decoy approach against a composite database composed of a target
623 database [Uniprot canonical and isoform reference proteome (16 January 2015) for a total
624 of 89,861 sequences + custom alternative proteome resulting from the in silico translation
625 of all human altORFs (available to download at
626 https://www.roucoulab.com/p/downloads)], and their reverse protein sequences from the
627 target database used as decoys. In order to separate alternative and reference proteins for
628 FDR analyses, PeptideShaker output files were extracted with target and decoy hits.
629 PSMs matching reference target or decoy proteins were separated from those matching
630 alternative targets or decoys as previously described [83,84]. PSMs that matched both
631 reference and alternative proteins were automatically moved to the reference database
632 group. PSMs were then ranked according to their PeptideShaker score and filtered at 1%
633 FDR separately. Validated PSMs were selected to group proteins using proteoQC R tool
634 [85] , and proteins were separately filtered again using a 1% FDR cut-off.
635 Only alternative proteins identified with at least one unique and specific peptide were
636 considered valid[59]. Any peptide matching both a canonical (annotated in Uniprot) and an
637 alternative protein was attributed to the canonical protein. For non-unique peptides, i.e.
638 peptides matching more than one alternative protein, the different accession IDs are
639 indicated in the MS files. For subsequent analyses (e.g. conservation, protein

signature…), only one protein is numbered in the total count of alternative proteins; we arbitrarily selected the alternative protein with the lowest accession ID.

Peptides matching proteins in a protein sequence database for common contaminants were rejected[86].

For spectral validation (Figure 6-figure supplement1, 2, 3, and 4), synthetic peptides were purchased from the peptide synthesis service at the *Université de Sherbrooke*. Peptides were solubilized in 10% acetonitrile, 1% formic acid and directly injected into a Q-Exactive mass spectrometer (Thermo Scientific) via an electro spray ionization source (Thermo Scientific). Spectra were acquired using Xcalibur 2.2 (RRID:SCR_014593) at 70000 resolution with an AGC target of 3e6 and HCD collision energy of 25. Peaks were assigned manually by comparing monoisotopic m/z theoretical fragments and experimental (PeptideShaker) spectra.

In order to test if the interaction between alternative zinc-finger/reference zinc-finger protein pairs (encoded in the same gene) may have occurred by chance only, all interactions between alternative proteins and reference proteins were randomized with an in-house randomisation script. The number of interactions with reference proteins for each altProt was kept identical as the number of observed interactions. The results indicate that interactions between alternative zinc-finger/reference zinc-finger protein pairs did not occur by chance ($p<10^{-6}$) based on 1 million binomial simulations; highest observed random interactions between alternative zinc-finger proteins and their reference proteins = 3 (39 times out of 1 million simulations), compared to detected interactions=5.

Code availability. Computer codes are available upon request with no restrictions.

662

663 **Data availability.** Alternative protein sequence databases for different species can be

664 accessed at https://www.roucoulab.com/p/downloads with no restrictions.

665

666 **Cloning and antibodies.** Human Flag-tagged altMiD51(WT) and

667 altMiD51(LYR→AAA), and HA-tagged DrP1(K38A) were cloned into pcDNA3.1

668 (Invitrogen) using a Gibson assembly kit (New England Biolabs, E26115). The cDNA

669 corresponding to human MiD51/MIEF1/SMCR7L transcript variant 1 (NM_019008) was

670 also cloned into pcDNA3.1 by Gibson assembly. In this construct, altMiD51 and MiD51

671 were tagged with Flag and HA tags, respectively. $MiD51^{GFP}$ and $altMiD51^{GFP}$ were also

672 cloned into pcDNA3.1 by Gibson assembly. For $MiD51^{GFP}$, a LAP tag[32] was inserted

673 between MiD51 and GFP. gBlocks were purchased from IDT. Human $altDDIT3^{mCherry}$

674 was cloned into pcDNA3.1 by Gibson assembly using coding sequence from transcript

675 variant 1 (NM_004083.5) and mCherry coding sequence from pLenti-myc-GLUT4-

676 mCherry (Addgene plasmid # 64049). Human $DDIT3^{GFP}$ was also cloned into pcDNA3.1

677 by Gibson assembly using CCDS8943 sequence.

678 For immunofluorescence, primary antibodies were diluted as follow: anti-Flag (Sigma,

679 F1804) 1/1000, anti-TOM20 (Abcam, ab186734) 1/500. For western blots, primary

680 antibodies were diluted as follow: anti-Flag (Sigma, F1804) 1/1000, anti-HA (BioLegend,

681 901515) 1/500, anti-actin (Sigma, A5441) 1/10000, anti-Drp1 (BD Transduction

682 Laboratories, 611112) 1/500, anti-GFP (Santa Cruz Biotechnology, sc-9996) 1/10000,

683 anti-mCherry (Abcam, ab125096) 1/2000.

684

685 **Cell culture, immunofluorescence, knockdown and western blots.** HeLa cells (ATCC
686 CRM-CCL-2, authenticated by STR profiling, RRID:CVCL_0030) cultures tested
687 negative for mycoplasma contamination (ATCC 30-1012K), transfections,
688 immunofluorescence, confocal analyses and western blots were carried out as previously
689 described[87]. Mitochondrial morphology was analyzed as previously described[88]. A
690 minimum of 100 cells were counted (n=3 or 300 cells for each experimental condition).
691 Three independent experiments were performed.
692 For Drp1 knockdown, 25,000 HeLa cells in 24-well plates were transfected with 25 nM
693 Drp1 SMARTpool: siGENOME siRNA (Dharmacon, M-012092-01-0005) or ON-
694 TARGET plus Non-targeting pool siRNAs (Dharmacon, D-001810-10-05) with
695 DharmaFECT 1 transfection reagent (Dharmacon, T-2001-02) according to the
696 manufacturer's protocol. After 24h, cells were transfected with pcDNA3.1 or altMiD51,
697 incubated for 24h, and processed for immunofluorescence or western blot. Colocalization
698 analyses were performed using the JACoP plugin (Just Another Co-localization Plugin) [50]
699 implemented in Image J software.
700
701 **Immunoprecipitations.** Immunoprecipitations experiments were conducted using GFP-
702 Trap (ChromoTek) protocol with minor modifications. Briefly, cells were lysed with co-
703 ip lysis buffer (0.5 % NP40, Tris-HCl 50 mM pH 7.5, NaCl 150 mM and two EDTA-free
704 Roche protease inhibitors per 50 mL of buffer). After 5 mins of lysis on ice, lysate was
705 sonicated twice at 11 % amplitude for 5 s with 3 minutes of cooling between sonication
706 cycles. Lysate was centrifuged, supernatant was isolated and protein content was assessed
707 using BCA assay (Pierce). GFP-Trap beads were conditioned with lysis buffer. 40 µL of

708 beads were added to 2 mg of proteins at a final concentration of 1 mg/mL. After
709 overnight immunoprecipitation, beads were centrifuged at 5000 rpm for 5 minutes and
710 supernatant was discarded. Beads were then washed three times with wash buffer (0.5 %
711 NP40, Tris-HCl 50 mM pH 7.5, NaCl 200 mM and two EDTA-free Roche protease
712 inhibitors per 50 mL of buffer) and supernatants were discarded. Immunoprecipitated
713 proteins were eluted from beads by adding 40 µL of Laemmli buffer and boiling at 95 °C
714 for 15 minutes. Eluate was split in halfs which were loaded onto 10 % SDS-PAGE gels to
715 allow western blotting of GFP and mCherry tagged proteins. 40 µg of initial lysates were
716 loaded into gels as inputs.
717
718 **Mitochondrial localization, parameters and ROS production.** Trypan blue quenching
719 experiment was performed as previously described[89].
720 A flux analyzer (XF96 Extracellular Flux Analyzer; Seahorse Bioscience, Agilent
721 technologies) was used to determine the mitochondrial function in HeLa cells
722 overexpressing altMiD51^{Flag}. Cells were plated in a XF96 plate (Seahorse Biosciences) at
723 1×10^4 cells per well in Dulbecco's modified Eagle's medium supplemented with 10%
724 FBS with antibiotics. After 24 hours, cells were transfected for 24 hours with an empty
725 vector (pcDNA3.1) or with the same vector expressing altMiD51^{Flag} with GeneCellin
726 tranfection reagent according to the manufacturer's instructions. Cells were equilibrated
727 in XF assay media supplemented with 25 mM glucose and 1 mM pyruvate and were
728 incubated at 37 °C in a CO_2-free incubator for 1 h. Baseline oxygen consumption rates
729 (OCRs) of the cells were recorded with a mix/wait/measure times of 3/0/3 min
730 respectively. Following these measurements, oligomycin (1 µM), FCCP (0.5 µM), and

731 antimycin A/rotenone (1 μM) were sequentially injected, with oxygen consumption rate
732 measurements recorded after each injection. Data were normalized to total protein in each
733 well. For normalization, cells were lysed in the 96-well XF plates using 15 μl/well of
734 RIPA lysis buffer (1% Triton X-100, 1% NaDeoxycholate, 0.1% SDS, 1 mM EDTA, 50
735 mM Tris-HCl pH 7.5). Protein concentration was measured using the BCA protein assay
736 reagent (Pierce, Waltham, MA, USA).
737 Reactive oxygen species (ROS) levels were measured using Cellular ROS/Superoxide
738 Detection Assay Kit (Abcam #139476). HeLa cells were seeded onto 96-well black/clear
739 bottom plates at a density of 6,000 cells per well with 4 replicates for each condition.
740 After 24 hours, cells were transfected for 24 hours with an empty vector (pcDNA3.1) or
741 with the same vector expressing altMiD51^{Flag} with GeneCellin according to the
742 manufacturer's instruction. Cells were untreated or incubated with the ROS inhibitor (N-
743 acetyl-L-cysteine) at 10 mM for 1 hour. Following this, the cells were washed twice with
744 the wash solution and then labeled for 1 hour with the Oxidative Stress Detection
745 Reagent (green) diluted 1:1000 in the wash solution with or without the positive control
746 ROS Inducer Pyocyanin at 100 μM. Fluorescence was monitored in real time. ROS
747 accumulation rate was measured between 1 to 3 hours following induction. After the
748 assay, total cellular protein content was measured using BCA protein assay reagent
749 (Pierce, Waltham, MA, USA) after lysis with RIPA buffer. Data were normalised for
750 initial fluorescence and protein concentration.
751 ATP synthesis was measured as previously described[90] in cells transfected for 24 hours
752 with an empty vector (pcDNA3.1) or with the same vector expressing altMiD51^{Flag}.
753

Acknowledgements

This research was supported by CIHR grants MOP-137056 and MOP-136962 to X.R; MOP-299432 and MOP-324265 to C.L; a *Université de Sherbrooke* institutional research grant made possible through a generous donation by Merck Sharp & Dohme to X.R; a FRQNT team grant 2015-PR-181807 to C.L. and X.R; Canada Research Chairs in Functional Proteomics and Discovery of New Proteins to X.R, in Evolutionary Cell and Systems Biology to C.L and in Computational and Biological Complexity to A.O; A.A.C is supported by a CIHR New Investigator Salary Award; M.S.S is a recipient of a *Fonds de Recherche du Québec – Santé* Research Scholar Junior 2 Career Award; V.D is supported in part by fellowships from *Région Nord-Pas de Calais* and PROTEO; A.A.C, D.J.H, M.S.S and X.R are members of the *Fonds de Recherche du Québec Santé*-supported *Centre de Recherche du Centre Hospitalier Universitaire de Sherbrooke*. We thank the staff from the Centre for Computational Science at the *Université de Sherbrooke*, Compute Canada and Compute Québec for access to the Mammouth supercomputer.

771 **References**

772 1. Ingolia, N. T., Lareau, L. F. & Weissman, J. S. Ribosome profiling of mouse
773 embryonic stem cells reveals the complexity and dynamics of mammalian
774 proteomes. *Cell* **147,** 789–802 (2011).
775 2. Lee, S. S. *et al.* Global mapping of translation initiation sites in mammalian cells at
776 single-nucleotide resolution. *Proc. Natl. Acad. Sci. U. S. A.* **109,** E2424-2432
777 (2012).
778 3. Mouilleron, H., Delcourt, V. & Roucou, X. Death of a dogma: eukaryotic mRNAs
779 can code for more than one protein. *Nucleic Acids Res.* **44,** 14–23 (2015).
780 4. Pauli, A. *et al.* Toddler: An Embryonic Signal That Promotes Cell Movement via
781 Apelin Receptors. *Science* **343,** 1248636–1248636 (2014).
782 5. Anderson, D. M. *et al.* A Micropeptide Encoded by a Putative Long Noncoding
783 RNA Regulates Muscle Performance. *Cell* **160,** 595–606 (2015).
784 6. Zanet, J. *et al.* Pri sORF peptides induce selective proteasome-mediated protein
785 processing. *Science* **349,** 1356–1358 (2015).
786 7. Nelson, B. R. *et al.* A peptide encoded by a transcript annotated as long noncoding
787 RNA enhances SERCA activity in muscle. *Science (80-.).* **351,** 271–275 (2016).
788 8. Bazzini, A. A. *et al.* Identification of small ORFs in vertebrates using ribosome
789 footprinting and evolutionary conservation. *EMBO J.* **33,** 981–993 (2014).
790 9. Ji, Z., Song, R., Regev, A. & Struhl, K. Many lncRNAs, 5'UTRs, and pseudogenes
791 are translated and some are likely to express functional proteins. *Elife* **4,** e08890
792 (2015).
793 10. Prabakaran, S. *et al.* Quantitative profiling of peptides from RNAs classified as

794 noncoding. *Nat. Commun.* **5,** 5429 (2014).
795 11. Slavoff, S. a *et al.* Peptidomic discovery of short open reading frame-encoded
796 peptides in human cells. *Nat. Chem. Biol.* **9,** 59–64 (2013).
797 12. Andrews, S. J. & Rothnagel, J. A. Emerging evidence for functional peptides
798 encoded by short open reading frames. *Nat. Rev. Genet.* **15,** 193–204 (2014).
799 13. Landry, C. R., Zhong, X., Nielly-Thibault, L. & Roucou, X. Found in translation:
800 Functions and evolution of a recently discovered alternative proteome. *Curr. Opin.*
801 *Struct. Biol.* **32,** 74–80 (2015).
802 14. Fields, A. P. *et al.* A Regression-Based Analysis of Ribosome-Profiling Data
803 Reveals a Conserved Complexity to Mammalian Translation. *Mol. Cell* **60,** 816–
804 827 (2015).
805 15. Saghatelian, A. & Couso, J. P. Discovery and characterization of smORF-encoded
806 bioactive polypeptides. *Nat. Chem. Biol.* **11,** 909–16 (2015).
807 16. Stock, D., Leslie, A. G. & Walker, J. E. Molecular architecture of the rotary motor
808 in ATP synthase. *Science* **286,** 1700–1705 (1999).
809 17. Schmitt, J. P. *et al.* Dilated cardiomyopathy and heart failure caused by a mutation
810 in phospholamban. *Science* **299,** 1410–1413 (2003).
811 18. Nemeth, E. *et al.* Hepcidin regulates cellular iron efflux by binding to ferroportin
812 and inducing its internalization. *Science* **306,** 2090–2093 (2004).
813 19. Carvunis, A.-R. *et al.* Proto-genes and de novo gene birth. *Nature* 3–7 (2012).
814 doi:10.1038/nature11184
815 20. Schlötterer, C. Genes from scratch--the evolutionary fate of de novo genes. *Trends*
816 *Genet.* **31,** 215–9 (2015).

817 21. McLysaght, A. & Hurst, L. D. Open questions in the study of de novo genes: what,
818 how and why. *Nat. Rev. Genet.* **17,** 567–578 (2016).
819 22. Sabath, N., Wagner, A. & Karlin, D. Evolution of viral proteins originated de novo
820 by overprinting. *Mol. Biol. Evol.* **29,** 3767–80 (2012).
821 23. Iacono, M., Mignone, F. & Pesole, G. uAUG and uORFs in human and rodent
822 5'untranslated mRNAs. *Gene* **349,** 97–105 (2005).
823 24. Neafsey, D. E. & Galagan, J. E. Dual modes of natural selection on upstream open
824 reading frames. *Mol. Biol. Evol.* **24,** 1744–51 (2007).
825 25. Smith, E. *et al.* Leaky ribosomal scanning in mammalian genomes: significance of
826 histone H4 alternative translation in vivo. *Nucleic Acids Res.* **33,** 1298–1308
827 (2005).
828 26. Pop, C. *et al.* Causal signals between codon bias, mRNA structure, and the
829 efficiency of translation and elongation. *Mol. Syst. Biol.* **10,** 770 (2014).
830 27. Pollard, K. S., Hubisz, M. J., Rosenbloom, K. R. & Siepel, A. Detection of
831 nonneutral substitution rates on mammalian phylogenies. *Genome Res.* **20,** 110–
832 121 (2010).
833 28. Michel, A. M. *et al.* GWIPS-viz: development of a ribo-seq genome browser.
834 *Nucleic Acids Res.* **42,** D859-864 (2014).
835 29. Raj, A. *et al.* Thousands of novel translated open reading frames in humans
836 inferred by ribosome footprint profiling. *Elife* **5,** 1–24 (2016).
837 30. Miettinen, T. P. & Björklund, M. Modified ribosome profiling reveals high
838 abundance of ribosome protected mRNA fragments derived from 3' untranslated
839 regions. *Nucleic Acids Res.* **43,** 1019–1034 (2015).

840 31. Weingarten-Gabbay, S. *et al.* Systematic discovery of cap-independent translation
841 sequences in human and viral genomes. *Science (80-.).* **351,** 1–24 (2016).
842 32. Hein, M. Y. *et al.* A Human Interactome in Three Quantitative Dimensions
843 Organized by Stoichiometries and Abundances. *Cell* **163,** 712–723 (2015).
844 33. Tong, J., Taylor, P. & Moran, M. F. Proteomic analysis of the epidermal growth
845 factor receptor (EGFR) interactome and post-translational modifications associated
846 with receptor endocytosis in response to EGF and stress. *Mol. Cell. Proteomics* **13,**
847 1644–1658 (2014).
848 34. Sharma, K. *et al.* Ultradeep Human Phosphoproteome Reveals a Distinct
849 Regulatory Nature of Tyr and Ser/Thr-Based Signaling. *Cell Rep.* **8,** 1583–1594
850 (2014).
851 35. Rosenberger, G. *et al.* A repository of assays to quantify 10,000 human proteins by
852 SWATH-MS. *Sci. data* **1,** 140031 (2014).
853 36. Mitchell, A. *et al.* The InterPro protein families database: the classification
854 resource after 15 years. *Nucleic Acids Res.* **43,** D213-221 (2014).
855 37. Vanderperre, B. *et al.* Direct detection of alternative open reading frames
856 translation products in human significantly expands the proteome. *PLoS One* **8,**
857 e70698 (2013).
858 38. Wolfe, S. A., Nekludova, L. & Pabo, C. O. DNA recognition by Cys2His2 zinc
859 finger proteins. *Annu. Rev. Biophys. Biomol. Struct.* **29,** 183–212 (2000).
860 39. Laity, J. H., Lee, B. M. & Wright, P. E. Zinc finger proteins: new insights into
861 structural and functional diversity. *Curr. Opin. Struct. Biol.* **11,** 39–46 (2001).
862 40. Karimpour-Fard, A., Detweiler, C. S., Erickson, K. D., Hunter, L. & Gill, R. T.

863 Cross-species cluster co-conservation: a new method for generating protein
864 interaction networks. *Genome Biol.* **8,** R185 (2007).
865 41. Schmitges, F. W. *et al.* Multiparameter functional diversity of human C2H2 zinc
866 finger proteins. *Genome Res.* **26,** 1742–1752 (2016).
867 42. Andreev, D. E. *et al.* Translation of 5' leaders is pervasive in genes resistant to
868 eIF2 repression. *Elife* **4,** e03971 (2015).
869 43. Kim, M.-S. *et al.* A draft map of the human proteome. *Nature* **509,** 575–581
870 (2014).
871 44. Angerer, H. Eukaryotic LYR Proteins Interact with Mitochondrial Protein
872 Complexes. *Biology (Basel).* **4,** 133–150 (2015).
873 45. Losón, O. C., Song, Z., Chen, H. & Chan, D. C. Fis1, Mff, MiD49, and MiD51
874 mediate Drp1 recruitment in mitochondrial fission. *Mol. Biol. Cell* **24,** 659–667
875 (2013).
876 46. Motori, E. *et al.* Inflammation-Induced Alteration of Astrocyte Mitochondrial
877 Dynamics Requires Autophagy for Mitochondrial Network Maintenance. *Cell*
878 *Metab.* **18,** 844–859 (2013).
879 47. Smirnova, E., Shurland, D. L., Ryazantsev, S. N. & van der Bliek, A. M. A human
880 dynamin-related protein controls the distribution of mitochondria. *J. Cell Biol.*
881 **143,** 351–358 (1998).
882 48. Cui, K., Coutts, M., Stahl, J. & Sytkowski, A. J. Novel interaction between the
883 transcription factor CHOP (GADD153) and the ribosomal protein FTE/S3a
884 modulates erythropoiesis. *J. Biol. Chem.* **275,** 7591–6 (2000).
885 49. Chiribau, C.-B., Gaccioli, F., Huang, C. C., Yuan, C. L. & Hatzoglou, M.

886 Molecular symbiosis of CHOP and C/EBP beta isoform LIP contributes to
887 endoplasmic reticulum stress-induced apoptosis. *Mol. Cell. Biol.* **30,** 3722–31
888 (2010).
889 50. Bolte, S. & Cordelières, F. P. A guided tour into subcellular colocalization analysis
890 in light microscopy. *J. Microsc.* **224,** 213–32 (2006).
891 51. Couso, J.-P. & Patraquim, P. Classification and function of small open reading
892 frames. *Nat. Rev. Mol. Cell Biol.* (2017). doi:10.1038/nrm.2017.58
893 52. Johnstone, T. G., Bazzini, A. A. & Giraldez, A. J. Upstream ORFs are prevalent
894 translational repressors in vertebrates. *EMBO J.* (2016).
895 doi:10.15252/embj.201592759
896 53. Jousse, C. *et al.* Inhibition of CHOP translation by a peptide encoded by an open
897 reading frame localized in the chop 5'UTR. *Nucleic Acids Res.* **29,** 4341–51
898 (2001).
899 54. Young, S. K., Palam, L. R., Wu, C., Sachs, M. S. & Wek, R. C. Ribosome
900 Elongation Stall Directs Gene-specific Translation in the Integrated Stress
901 Response. *J. Biol. Chem.* **291,** 6546–6558 (2016).
902 55. Lee, Y. C. G. & Reinhardt, J. A. Widespread Polymorphism in the Positions of
903 Stop Codons in Drosophila melanogaster. *Genome Biol. Evol.* **4,** 533–549 (2012).
904 56. Andreatta, M. E. *et al.* The Recent De Novo Origin of Protein C-Termini. *Genome*
905 *Biol. Evol.* **7,** 1686–701 (2015).
906 57. Knowles, D. G. & McLysaght, A. Recent de novo origin of human protein-coding
907 genes. *Genome Res.* **19,** 1752–9 (2009).
908 58. Neme, R. & Tautz, D. Phylogenetic patterns of emergence of new genes support a

909 model of frequent de novo evolution. *BMC Genomics* **14,** 117 (2013).
910 59. Vaudel, M. *et al.* PeptideShaker enables reanalysis of MS-derived proteomics data
911 sets. *Nat. Biotechnol.* **33,** 22–24 (2015).
912 60. Shteynberg, D. *et al.* iProphet: multi-level integrative analysis of shotgun
913 proteomic data improves peptide and protein identification rates and error
914 estimates. *Mol. Cell. Proteomics* **10,** M111.007690 (2011).
915 61. Quelle, D. E., Zindy, F., Ashmun, R. A. & Sherr, C. J. Alternative reading frames
916 of the INK4a tumor suppressor gene encode two unrelated proteins capable of
917 inducing cell cycle arrest. *Cell* **83,** 993–1000 (1995).
918 62. Abramowitz, J., Grenet, D., Birnbaumer, M., Torres, H. N. & Birnbaumer, L.
919 XLalphas, the extra-long form of the alpha-subunit of the Gs G protein, is
920 significantly longer than suspected, and so is its companion Alex. *Proc. Natl.*
921 *Acad. Sci. U. S. A.* **101,** 8366–8371 (2004).
922 63. Bergeron, D. *et al.* An out-of-frame overlapping reading frame in the ataxin-1
923 coding sequence encodes a novel ataxin-1 interacting protein. *J. Biol. Chem.* **288,**
924 21824–35 (2013).
925 64. Lee, C. -f. C., Lai, H.-L. H.-L., Lee, Y.-C., Chien, C.-L. C.-L. & Chern, Y. The
926 A2A Adenosine Receptor Is a Dual Coding Gene: A NOVEL MECHANISM OF
927 GENE USAGE AND SIGNAL TRANSDUCTION. *J. Biol. Chem.* **289,** 1257–
928 1270 (2014).
929 65. Yosten, G. L. C. *et al.* A 5′-Upstream short open reading frame encoded peptide
930 regulates angiotensin type 1a receptor production and signaling via the beta-
931 arrestin pathway. *J. Physiol.* **6,** n/a-n/a (2015).

932 66. Rice, P., Longden, I. & Bleasby, A. EMBOSS: the European Molecular Biology
933 Open Software Suite. *Trends Genet.* **16,** 276–277 (2000).
934 67. Kozak, M. Pushing the limits of the scanning mechanism for initiation of
935 translation. *Gene* **299,** 1–34 (2002).
936 68. Fritsch, C. *et al.* Genome-wide search for novel human uORFs and N-terminal
937 protein extensions using ribosomal footprinting. *Genome Res.* **22,** 2208–2218
938 (2012).
939 69. Stern-Ginossar, N. *et al.* Decoding human cytomegalovirus. *Science* **338,** 1088–93
940 (2012).
941 70. Gao, X. *et al.* Quantitative profiling of initiating ribosomes in vivo. *Nat. Methods*
942 **12,** 147–53 (2015).
943 71. Langmead, B. & Salzberg, S. L. Fast gapped-read alignment with Bowtie 2. *Nat.*
944 *Methods* **9,** 357–9 (2012).
945 72. Sonnhammer, E. L. L. & Östlund, G. InParanoid 8: orthology analysis between
946 273 proteomes, mostly eukaryotic. *Nucleic Acids Res.* **43,** D234-239 (2015).
947 73. Remm, M., Storm, C. E. & Sonnhammer, E. L. Automatic clustering of orthologs
948 and in-paralogs from pairwise species comparisons. *J. Mol. Biol.* **314,** 1041–1052
949 (2001).
950 74. Tarailo-Graovac, M. & Chen, N. Using RepeatMasker to identify repetitive
951 elements in genomic sequences. *Curr. Protoc. Bioinformatics* **Chapter 4,** Unit
952 4.10 (2009).
953 75. Jones, P. *et al.* InterProScan 5: genome-scale protein function classification.
954 *Bioinformatics* **30,** 1236–1240 (2014).

955 76. Na, D., Son, H. & Gsponer, J. Categorizer: a tool to categorize genes into user-
956 defined biological groups based on semantic similarity. *BMC Genomics* **15,** 1091
957 (2014).
958 77. Vaudel, M., Barsnes, H., Berven, F. S., Sickmann, A. & Martens, L. SearchGUI:
959 An open-source graphical user interface for simultaneous OMSSA and X!Tandem
960 searches. *Proteomics* **11,** 996–999 (2011).
961 78. Craig, R. & Beavis, R. C. TANDEM: matching proteins with tandem mass spectra.
962 *Bioinformatics* **20,** 1466–1467 (2004).
963 79. Kim, S. & Pevzner, P. A. MS-GF+ makes progress towards a universal database
964 search tool for proteomics. *Nat. Commun.* **5,** 5277 (2014).
965 80. Tabb, D. L., Fernando, C. G. & Chambers, M. C. MyriMatch: highly accurate
966 tandem mass spectral peptide identification by multivariate hypergeometric
967 analysis. *J. Proteome Res.* **6,** 654–661 (2007).
968 81. Eng, J. K., Jahan, T. A. & Hoopmann, M. R. Comet: an open-source MS/MS
969 sequence database search tool. *Proteomics* **13,** 22–24 (2013).
970 82. Geer, L. Y. *et al.* Open mass spectrometry search algorithm. *J. Proteome Res.* **3,**
971 958–64 (2004).
972 83. Menschaert, G. & Fenyö, D. Proteogenomics from a bioinformatics angle: A
973 growing field. *Mass Spectrom. Rev.* **36,** 584–599 (2015).
974 84. Woo, S. *et al.* Proteogenomic strategies for identification of aberrant cancer
975 peptides using large-scale next-generation sequencing data. *Proteomics* **14,** 2719–
976 30 (2014).
977 85. Gatto, L., Breckels, L. M., Naake, T. & Gibb, S. Visualization of proteomics data

978 using R and Bioconductor. *Proteomics* **15,** 1375–1389 (2015).

979 86. Perkins, D. N., Pappin, D. J. C., Creasy, D. M. & Cottrell, J. S. Probability-based
980 protein identification by searching sequence databases using mass spectrometry
981 data. *Electrophoresis* **20,** 3551–3567 (1999).

982 87. Vanderperre, B. *et al.* An overlapping reading frame in the PRNP gene encodes a
983 novel polypeptide distinct from the prion protein. *FASEB J.* **25,** 2373–86 (2011).

984 88. Palmer, C. S. *et al.* MiD49 and MiD51, new components of the mitochondrial
985 fission machinery. *EMBO Rep.* **12,** 565–573 (2011).

986 89. Vanderperre, B. *et al.* MPC1-like: a Placental Mammal-Specific Mitochondrial
987 Pyruvate Carrier Subunit Expressed in Post-Meiotic Male Germ Cells. *J. Biol.*
988 *Chem.* (2016). doi:10.1074/jbc.M116.733840

989 90. Vives-Bauza, C., Yang, L. & Manfredi, G. Assay of Mitochondrial ATP Synthesis
990 in Animal Cells and Tissues. *Methods Cell Biol* **80,** 155–171 (2007).

991

992 **FIGURE LEGENDS**

993

994 **Figure 1. Annotation of human altORFs.**

995 (**a**) AltORF nomenclature. AltORFs partially overlapping the CDS must be in a different
996 reading frame. (**b**) Pipeline for the identification of altORFs. (**c**) Size distribution of
997 alternative (empty bars, vertical and horizontal axes) and reference (grey bars, secondary
998 horizontal and vertical axes) proteins. Arrows indicate the median size. The median
999 alternative protein length is 45 amino acids (AA) compared to 460 for the reference
1000 proteins. (**d**) Distribution of altORFs in the human hg38 transcriptome. (**e, f**) Number of
1001 total altORFs (**e**) or number of altORFs/10kbs (**f**) in hg38 compared to shuffled hg38.
1002 Means and standard deviations for 100 replicates obtained by sequence shuffling are
1003 shown. Statistical significance was determined by using one sample t-test with two-tailed
1004 *p*-values. **** $p<0.0001$. (**g**) Percentage of altORFs with an optimal Kozak motif. The
1005 total number of altORFs with an optimal Kozak motif is also indicated at the top.

1006

1007 **Figure 1-figure supplement 1. 10% of altORFs are present in different classes of**
1008 **repeats.**

1009 While more than half of the human genome is composed of repeated sequences, only
1010 9.83% or 18,003 altORFs are located inside these repeats (**a**), compared to 2,45% or
1011 1,677 CDSs (**b**). AltORFs and CDSs are detected in non-LTR retrotransposons (LINEs,
1012 SINEs, SINE-VNTR-Alus), LTR repeats, DNA repeats, satellites and other repeats.
1013 Proportions were determined using RepeatMasker (version 3.3.0).

1014

1015 **Figure 1-figure supplement 2. The proportion of altORFs with a translation**
1016 **initiation site (TIS) with a Kozak motif in hg38 is significantly different from 100**
1017 **shuffled hg38 transcriptomes.**
1018 Percentage of altORFs with a TIS within an optimal Kozak sequence in hg38 (dark blue)
1019 compared to 100 shuffled hg38 (light blue). Mean and standard deviations for sequence
1020 shuffling are displayed, and significant difference was defined by using one sample t test.
1021 **** $P<0.0001$. Note that shuffling all transcripts in the hg38 transcriptome generates a
1022 total of 489,073 altORFs on average, compared to 539,134 altORFs in hg38. Most
1023 transcripts result from alternative splicing and there are 183,191 unique altORFs in the
1024 hg38 transcriptome, while the 489,073 altORFs in shuffled transcriptomes are all unique.
1025 Figure 1g shows the percentage of unique altORFs with a kozak motif (15%), while the
1026 current Fig. shows the percentage of altORFs with a kozak motif relative to the total
1027 number of altORFs (14%).
1028
1029 **Figure 2. Conservation of alternative and reference proteins across different species.**
1030 (**a**) Number of orthologous and paralogous alternative and reference proteins between *H.*
1031 *sapiens* and other species (pairwise study). (**b**) Phylogenetic tree: conservation of
1032 alternative (blue) and reference (red) proteins across various eukaryotic species. (**c**)
1033 Number and fraction of genes encoding homologous reference proteins or at least 1
1034 homologous alternative protein between *H. sapiens* and other species (pairwise study).
1035
1036 **Figure 3. Number of orthologous and co-conserved alternative and reference**
1037 **proteins between *H. sapiens* and other species (pairwise).** For the co-conservation

1038 analyses, the percentage of observed (Obs.), expected (Exp.) and corresponding *p*-values
1039 relative to the total number of reference-alternative protein pairs are indicated on the right
1040 (see Table 2 for details).
1041
1042 **Figure 4. AltORFs completely nested within CDSs show more extreme PhyloP values**
1043 **(more conserved or faster evolving) than their CDSs.** Differences between altORF and
1044 CDS PhyloP scores (altORF PhyloP – CDS PhyloP, *y*-axis) are plotted against PhyloPs
1045 for their respective CDSs (*x*-axis). We restricted the analysis to altORF-CDS pairs that
1046 were co-conserved from humans to zebrafish. The plot contains 889 CDSs containing at
1047 least one fully nested altORF, paired with one of its altORFs selected at random (to avoid
1048 problems with statistical non-independence). PhyloPs for both altORFs and CDSs are
1049 based on 3rd codons in the CDS reading frame, calculated across 100 vertebrate species.
1050 We compared these differences to those generated based on five random regions in CDSs
1051 with a similar length as altORFs. Expected quantiles of the differences ("DQ" columns)
1052 were identified and compared to the observed differences. We show the absolute numbers
1053 ("n") and observed-to-expected ratios ("O/E") for each quantile. There are clearly
1054 substantial over-representations of extreme values (red signaling conservation DQ 0.95,
1055 and blue signaling accelerated evolution DQ 0.05) with 317 of 889 altORFs (35.7%). A
1056 random distribution would have implied a total of 10% (or 89) of altORFs in the extreme
1057 values. This suggests that 25.7% (35.7%-10%) of these 889 altORFs undergo specific
1058 selection different from random regions in their CDSs with a similar length distribution.
1059 This percentage is very similar to the 26.2% obtained from an analysis of altORFs
1060 without restriction based on co-conservation in vertebrates (see Figure 4-figure

1061 supplement 1), a total which would imply that there are about 4,458 altORFs fully nested
1062 in CDSs undergoing conserved or accelerated evolution relative to their CDSs.
1063
1064 **Figure 4-figure supplement 1. AltORFs completely nested within CDSs show more**
1065 **extreme PhyloP values (more conserved or faster evolving) than their CDSs.**
1066 Differences between altORF and CDS PhyloP scores (altORF PhyloP – CDS PhyloP, *y*-
1067 axis) are plotted against PhyloPs for their respective CDSs (*x*-axis). The plot contains all
1068 20,814 CDSs containing at least one fully nested altORF, paired with one of its altORFs
1069 selected at random (to avoid problems with statistical non-independence). PhyloPs for
1070 both altORFs and CDSs are based on third codon positions in the CDS reading frame,
1071 calculated across 100 vertebrate species. We compared these differences to those
1072 generated based on five random regions in CDSs with a similar length as altORFs.
1073 Expected quantiles of the differences ("DQ" columns) were identified and compared to
1074 the observed differences. We show the absolute numbers ("n") and observed-to-expected
1075 ratios ("O/E") for each quantile. There are clearly substantial over-representations of
1076 extreme values (red signalling conservation DQ≥0.95, and blue signalling accelerated
1077 evolution DQ≤0.05) with 6,428 of 19,705 altORFs (36.2%). A random distribution would
1078 have implied a total of 10% (or 1,970) of altORFs in the extreme values. This suggests
1079 that 26.2% (36.2%-10%) of altORFs (or 4,458) undergo specific selection different from
1080 random regions in their CDSs with a similar length distribution.
1081
1082 **Figure 5. First, second, and third codon nucleotide PhyloP scores for 100 vertebrate**
1083 **species for the CDSs of the *NTNG1*, *RET* and *VTI1A* genes.** Chromosomal coordinates

1084 for the different CDSs and altORFs are indicated on the right. The regions highlighted in
1085 red indicate the presence of an altORF characterized by a region with elevated PhyloP
1086 scores for wobble nucleotides. The region of the altORF is indicated by a black bar above
1087 each graph.
1088
1089 **Figure 6. Expression of human altORFs.**
1090 (**a**) Percentage of CDSs and altORFs with detected TISs by ribosomal profiling and
1091 footprinting of human cells[23]. The total number of CDSs and altORFs with a detected TIS
1092 is indicated at the top. (**b**) Alternative and reference proteins detected in three large
1093 proteomic datasets: human interactome[32], 10,000 human proteins[35], human
1094 phosphoproteome[34], EGFR interactome[33]. Numbers are indicates above each column. (**c**)
1095 Percentage of altORFs encoding alternative proteins detected by MS-based proteomics.
1096 The total number of altORFs is indicated at the top. Localization "Unknown" indicates
1097 that the detected peptides can match more than one alternative protein. Localization ">1"
1098 indicates that the altORF can have more than one localization in different RNA isoforms.
1099
1100 **Figure 6-figure supplement 1. Spectra validation for altSLC35A4$^{5'}$**
1101 Example of validation for altSLC35A4$^{5'}$ specific peptide
1102 RVEDEVNSGVGQDGSLLSSPFLK. (**a**) Experimental MS/MS spectra (PeptideShaker
1103 graphic interface output). (**b**) MS/MS spectra of the synthetic peptide.
1104 Matching peaks are shown with blue masks. A diagram of the transcript with its accession
1105 number and the localization of the altORF and the CDS is shown at the top.
1106

1107 **Figure 6-figure supplement 2. Spectra validation for altRELT$^{5'}$**

1108 Example of validation for altRELT$^{5'}$ specific peptide VALELLK. (**a**) Experimental

1109 MS/MS spectra (PeptideShaker graphic interface output). (**b**) MS/MS spectra of the

1110 synthetic peptide.

1111 Matching peaks are shown with blue masks. A diagram of the transcript with its accession

1112 number and the localization of the altORF and the CDS is shown at the top.

1113

1114 **Figure 6-figure supplement 3. Spectra validation for altLINC01420^{nc}**

1115 Example of validation for altLINC01420^{nc} specific peptide

1116 WDYPEGTPNGGSTTLPSAPPPASAGLK. (**a**) Experimental MS/MS spectra

1117 (PeptideShaker graphic interface output). (**b**) MS/MS spectra of the synthetic peptide.

1118 Matching peaks are shown with blue masks. A diagram of the transcript with its accession

1119 number and the localization of the altORF is shown at the top.

1120

1121 **Figure 6-figure supplement 4. Spectra validation for altSRRM2^{CDS}**

1122 Example of validation for altSRRM2^{CDS} specific peptide EVILDPDLPSGVGPGLHR.

1123 (**a**) Experimental MS/MS spectra (PeptideShaker graphic interface output). (**b**) MS/MS

1124 spectra of the synthetic peptide.

1125 Matching peaks are shown with blue masks. A diagram of the transcript with its accession

1126 number and the localization of the altORF and the CDS is shown at the top.

1127

1128 **Figure 7. The alternative phosphoproteome in mitosis and EGF-treated cells.**

1129 Heatmap showing relative levels of spectral counts for phosphorylated peptides following

1130 the indicated treatment[34]. For each condition, heatmap colors show the percentage of
1131 spectral count on total MS/MS phosphopeptide spectra. Blue bars on the right represent
1132 the number of MS/MS spectra; only proteins with spectral counts above 10 are shown.
1133

1134 **Figure 7-figure supplement 1: Example of a phosphorylated peptide in mitosis -**
1135 **alternative protein AltLINC01420^{nc} (LOC550643, IP_305449.1).**
1136 (**a**) AltLINC01420^{nc} amino acid sequence with detected peptides underlined and
1137 phosphorylated peptide in bold (73,9% sequence coverage). (**b**) MS/MS spectrum for the
1138 phosphorylated peptide (PeptideShaker graphic interface output). The phosphorylation
1139 site is the tyrosine residue, position 2. (**c**) MS/MS spectrum for the non-phosphorylated
1140 peptide. The mass difference between the precursor ions between both spectra
1141 corresponds to that of a phosphorylation, confirming the specific phosphorylation of this
1142 residue in mitosis.
1143

1144 **Figure 8. Number of alternative proteins detected by ribosome profiling and mass**
1145 **spectrometry.**
1146 The expression of 467 alternative proteins was detected by both ribosome profiling
1147 (translation initiation sites, TIS) and mass spectrometry (MS).
1148

1149 **Figure 9. Human alternative proteome sequence analysis and classification using**
1150 **InterProScan.**
1151 (**a**) InterPro annotation pipeline. (**b**) Alternative and reference proteins with InterPro
1152 signatures. (**c**) Number of alternative and reference proteins with transmembrane domains

1153 (TM), signal peptides (S) and both TM and SP. (**d**) Number of all alternative and
1154 reference proteins predicted to be intracellular, membrane, secreted and membrane-
1155 spanning and secreted. [1]Proteins with at least one InterPro signature; [2]Proteins with no
1156 predicted signal peptide or transmembrane features. (**e**) Number of predicted TM regions
1157 for alternative and reference proteins.
1158
1159 **Figure 9-figure supplement 1: Alternative proteome sequence analysis and**
1160 **classification in *P. troglodytes*, *M. musculus*, *B. Taurus*, *D. melanogaster* and *S.***
1161 ***cerevisiae*.**
1162 For each organism, the number of InterPro signatures (top graphs) and proteins with
1163 transmembrane (TM), signal peptide (SP), or TM+SP features (bottom pie charts) is
1164 indicated for alternative and reference proteins.
1165
1166 **Figure 10. Gene ontology (GO) annotations for human alternative proteins.**
1167 GO terms assigned to InterPro entries are grouped into 13 categories for each of the three
1168 ontologies. (**a**) 34 GO terms were categorized into cellular component for 107 alternative
1169 proteins. (**b**) 64 GO terms were categorized into biological process for 128 alternative
1170 proteins. (**c**) 94 GO terms were categorized into molecular function for 302 alternative
1171 proteins. The majority of alternative proteins with GO terms are predicted to be
1172 intracellular, to function in nucleic acid-binding, catalytic activity and protein binding
1173 and to be involved in biosynthesis and nucleic acid metabolism processes.
1174
1175 **Figure 11. Main InterPro entries in human alternative proteins.** (**a**) The top 10

1176 InterPro families in the human alternative proteome. (**b**) A total of 110 alternative
1177 proteins have between 1 and 23 zinc finger domains.
1178
1179 **Figure 12. Reference and alternative proteins share functional domains.**
1180 (**a**) Distribution of the number of shared InterPro entries between alternative and
1181 reference proteins coded by the same transcripts. 138 pairs of alternative and reference
1182 proteins share between 1 and 4 protein domains (InterPro entries). Only
1183 alternative/reference protein pairs that have at least one domain are considered (n = 298).
1184 (**b**) The number of reference/alternative protein pairs that share domains (n = 138) is
1185 higher than expected by chance alone. The distribution of expected pairs sharing domains
1186 and the observed number are shown. (**c**) Matrix of co-occurrence of domains related to
1187 zinc fingers. The entries correspond to the number of times entries co-occur in reference
1188 and alternative proteins. The full matrix is available in figure 12-figure supplement 1.
1189
1190 **Figure 12-figure supplement 1. Matrix of co-occurrence of InterPro entries between**
1191 **alternative/reference protein pairs coded by the same transcript.**
1192 Pixels show the number of times entries co-occur in reference and alternative proteins.
1193 Blue pixels indicate that these domains are not shared, white pixels indicate that they are
1194 shared once, and red that they are shared twice or more.
1195
1196 **Figure 12-figure supplement 2. Reference and alternative proteins share functional**
1197 **domains.**
1198 The number of reference/alternative protein pairs that share domains (n = 49) is higher

1199 than expected by chance alone (p<0.001). The distribution of expected pairs sharing
1200 domains and the observed number are shown. This is the same analysis as the one
1201 presented in figure 12b, with the zinc finger domains taken out.
1202
1203 **Figure 13. AltMiD51$^{5'}$ expression induces mitochondrial fission.**
1204 (**a**) AltMiD51$^{5'}$ coding sequence is located in exon 2 or the *MiD51/MIEF1/SMCR7L* gene
1205 and in the 5'UTR of the canonical mRNA (RefSeq NM_019008). +2 and +1 indicate
1206 reading frames. AltMiD51 amino acid sequence is shown with the LYR tripeptide shown
1207 in bold. Underlined peptides were detected by MS. (**b**) Human HeLa cells transfected
1208 with empty vector (mock), a cDNA corresponding to the canonical MiD51 transcript with
1209 a Flag tag in frame with altMiD51 and an HA tag in frame with MiD51, altMiD51^{Flag}
1210 cDNA or MiD51^{HA} cDNA were lysed and analyzed by western blot with antibodies
1211 against Flag, HA or actin, as indicated. (**c**) Confocal microscopy of mock-transfected
1212 cells, cells transfected with altMiD51^{WT}, altMiD51$^{LYR\rightarrow AAA}$ or Drp1^{K38A} immunostained
1213 with anti-TOM20 (red channel) and anti-Flag (green channel) monoclonal antibodies. In
1214 each image, boxed areas are shown at higher magnification in the bottom right corner. %
1215 of cells with the most frequent morphology is indicated: mock (tubular), altMiD51^{WT}
1216 (fragmented), altMiD51(LYR→AAA) (tubular), Drp1(K38A) (elongated). Scale bar, 10
1217 mm. (**d**) Bar graphs show mitochondrial morphologies in HeLa cells. Means of three
1218 independent experiments per condition are shown (100 cells for each independent
1219 experiment). ***p<0.0005 (Fisher's exact test) for the three morphologies between
1220 altMiD51(WT) and the other experimental conditions.
1221

1222 **Figure 13-figure supplement 1. Spectra validation for altMiD51.**

1223 Example of validation for altMiD51 specific peptides YTDRDFYFASIR and

1224 GLVFLNGK. (**a,c**) Experimental MS/MS spectra (PeptideShaker graphic interface

1225 output). (**b,d**) MS/MS spectra of the synthetic peptides.

1226 Matching peaks are shown with blue masks. A diagram of the transcript with its accession

1227 number and the localization of the altORF and the CDS is shown at the top.

1228

1229 **Figure 13-figure supplement 2. MiD51 expression results in mitochondrial fission.**

1230 (**a**) Confocal microscopy of HeLa cells transfected with $MiD51^{GFP}$ immunostained with

1231 anti-TOM20 (red channel) monoclonal antibodies. In each image, boxed areas are shown

1232 at higher magnification in the bottom right corner. The localization of MiD51 in fission

1233 sites is shown in merged higher magnification inset. Scale bar, 10 mm. (**b**) Human HeLa

1234 cells transfected with empty vector (mock) or $MiD51^{GFP}$ were lysed and analyzed by

1235 western blot to confirm $MiD51^{GFP}$ expression.

1236

1237 **Figure 13-figure supplement 3: AltMiD51 is localized in the mitochondrial matrix.**

1238 Trypan blue quenching experiment performed on HeLa cells stably expressing the

1239 indicated constructs. The fluorescence remaining after quenching by trypan blue is shown

1240 relative to Matrix-Venus (Mx-Venus) indicated by the dashed line. (**** p <0,0001, one-

1241 way ANOVA). The absence of quenching of the fluorescence compared to IMS-Venus

1242 indicates the matricial localization of altMiD51. n≥3 cells were quantified per

1243 experiment, and results are from 6 independent experiments. Data are mean ±SEM.

1244

1245 **Figure 13-figure supplement 4. Mitochondrial function parameters.**

1246 (**a**) Oxygen consumption rates (OCR) in HeLa cells transfected with empty vector (mock)
1247 or altMiD51^{Flag}. Mitochondrial function parameters were assessed in basal conditions
1248 (basal), in the presence of oligomycin to inhibit the ATP synthase (oxygen consumption
1249 that is ATP-linked), FCCP to uncouple the mitochondrial inner membrane and allow for
1250 maximum electron flux through the respiratory chain (maximal OCR), and antimycin
1251 A/rotenone to inhibit complex III (non-mitochondrial). The balance of the basal OCR
1252 comprises oxygen consumption due to proton leak and nonmitochondrial sources. The
1253 mitochondrial reserve capacity (maximal OCR- basal OCR) is an indicator of rapid
1254 adaptation to stress and metabolic changes. Mean values of replicates are plotted with
1255 error bars corresponding to the 95% confidence intervals. Statistical significance was
1256 estimated using a two-way ANOVA with Tukey's post-hoc test (**p = 0,004). (**b**) ROS
1257 production in mock and altMiD51-expressing cells. Cells were untreated, treated with a
1258 ROS inducer or a ROS inhibitor. Results represent the mean value out of three
1259 independent experiments, with error bars corresponding to the standard error of the mean
1260 (s.e.m.). Statistical significance was estimated using unpaired T-test. (**c**) ATP synthesis
1261 rate in mock and altMiD51-expressing cells. No significant differences in ATP production
1262 were observed between mock and altMiD51 transfected cells.
1263 Results represent the mean of three independent experiments (8 technical replicates
1264 each). Error bars represent the standard error of the mean. At the end of the experiments,
1265 cells were collected and proteins analyzed by western blot with antibodies against the
1266 Flag tag (altMiD51) or actin, as indicated, to verify the expression of altMiD51. A
1267 representative western blot is shown on the right. Molecular weight markers are shown

1268 on the left (kDa).

1269

1270 **Figure 13-figure supplement 5. Representative confocal images of cells co-expressing**

1271 **altMiD51^{GFP} and Drp1(K38A)^{HA}.**

1272 (**a**) Confocal microscopy of HeLa cells co-transfected with altMiD51^{GFP} and

1273 Drp1(K38A)^{HA} immunostained with anti-TOM20 (blue channel) and anti-HA (red

1274 channel) monoclonal antibodies. In each image, boxed areas are shown at higher

1275 magnification in the bottom right corner. % of cells with the indicated morphology is

1276 indicated on the TOM20 panels. (**b**) Confocal microscopy of HeLa cells co-transfected

1277 with altMiD51^{GFP} and Drp1(wt)^{HA} immunostained with anti-TOM20 (blue channel) and

1278 anti-HA (red channel) monoclonal antibodies. In each image, boxed areas are shown at

1279 higher magnification in the bottom right corner. Scale bar, 10 mm.

1280

1281 **Figure 13-figure supplement 6. Protein immunoblot showing the expression of**

1282 **different constructs in HeLa cells.**

1283 HeLa cells were transfected with empty vector (pcDNA3.1), altMiD51(WT)^{Flag},

1284 altMID51(LYR→AAA)^{Flag}, Drp1(K38A)^{HA}, or Drp1(K38A)^{HA} and altMiD51(WT)^{Flag}, as

1285 indicated. Proteins were extracted and analyzed by western blot with antibodies against

1286 the Flag tag (altMiD51), the HA tag (Drp1K38A) or actin, as indicated. Molecular weight

1287 markers are shown on the left (kDa). Representative experiment of three independent

1288 biological replicates.

1289

1290 **Figure 14. AltMiD51-induced mitochondrial fragmentation is dependent on Drp1.**

1291 (**a**) Bar graphs show mitochondrial morphologies in HeLa cells treated with non-target or
1292 Drp1 siRNAs. Cells were mock-transfected (pcDNA3.1) or transfected with
1293 altMiD51^{Flag}. Means of three independent experiments per condition are shown (100 cells
1294 for each independent experiment). ***p<0.0005 (Fisher's exact test) for the three
1295 morphologies between altMiD51 and the other experimental conditions. (**b**) HeLa cells
1296 treated with non-target or Drp1 siRNA were transfected with empty vector (pcDNA3.1)
1297 or altMiD51^{Flag}, as indicated. Proteins were extracted and analyzed by western blot with
1298 antibodies against the Flag tag (altMiD51), Drp1 or actin, as indicated. (**c**) Confocal
1299 microscopy of Drp1 knockdown cells transfected with altMiD51^{GFP} immunostained with
1300 anti-TOM20 (blue channel) and anti-Drp1 (red channel) monoclonal antibodies. In each
1301 image, boxed areas are shown at higher magnification in the bottom right corner. % of
1302 cells with the indicated morphology is indicated on the TOM20 panels. Scale bar, 10 mm.
1303 (**d**) Control Drp1 immunostaining in HeLa cells treated with a non-target siRNA. For (**c**)
1304 and (**d**), laser parameters for Drp1 and TOM20 immunostaining were identical.
1305

1306 **Figure 15. AltDDIT3$^{5'}$ co-localizes and interacts with DDIT3.**

1307 (**a**) AltDDIT3$^{5'}$ coding sequence is located in exons 1 and 2 or the
1308 *DDIT3/CHOP/GADD153* gene and in the 5'UTR of the canonical mRNA (RefSeq
1309 NM_004083.5). +2 and +1 indicate reading frames. AltDDIT3 amino acid sequence is
1310 also shown. (**b**) Confocal microscopy analyses of HeLa cells co-transfected with
1311 altDDIT3^{GFP} (green channel) and DDIT3^{mCherry} (red channel). Scale bar, 10 µm. (**c, d**)
1312 Colocalization analysis of the images shown in (**b**) performed using the JACoP plugin
1313 (Just Another Co-localization Plugin) implemented in Image J software (two independent

1314 biological replicates). (**c**) Scatterplot representing 50 % of green and red pixel intensities
1315 showing that altDDIT3^{GFP} and DDIT3^{mCherry} signal highly correlate (with Pearson
1316 correlation coefficient of 0.92 (p-value < 0.0001)). (**d**) Binary version of the image shown
1317 in (**b**) after Costes' automatic threshold. White pixels represent colocalization events (p-
1318 value < 0.001, based on 1000 rounds of Costes' randomization colocalization analysis).
1319 The associated Manders Correlation Coefficient, M_1 and M_2, are shown in the right upper
1320 corner. M_1 is the proportion of altDDIT3^{GFP} signal overlapping DDIT3^{mCherry} signal and
1321 M_2 is the proportion of DDIT3^{mCherry} signal overlapping altDDIT3^{GFP}. (**e**) Representative
1322 immunoblot of co-immunoprecipitation with GFP-Trap agarose beads performed on
1323 HeLa lysates co-expressing DDIT3^{mcherry} and altDDIT3^{GFP} or DDIT3^{mcherry} with
1324 pcDNA3.1^{GFP} empty vector (two independent experiments).
1325
1326 **Figure 15-figure supplement 1. Protein immunoblot showing the expression of**
1327 **different constructs in HeLa cells.**
1328 HeLa cells were co-transfected with GFP and mCherry, or altDDIT3^{GFP} and
1329 DDIT3^{mCherry}, as indicated. Proteins were extracted and analyzed by western blot with
1330 antibodies, as indicated. Molecular weight markers are shown on the left (kDa).
1331 AltDDIT3 has a predicted molecular weight of 4.28 kDa and thus migrates at its expected
1332 molecular weight when tagged with GFP (~32 kDa). Representative experiment of two
1333 independent biological replicates.
1334
1335 **Figure 15–figure supplement 2. Colocalization of altDDIT3 with DDIT3.**
1336 Scatter plots of Pearson's Correlation Coefficient and Manders' Correlation Coefficient

1337 after Costes' automatic threshold (p-value < 0.001, based on 1000 rounds of Costes'
1338 randomization colocalization analysis). M1 is the proportion of altDDIT3^{GFP} signal
1339 overlapping DDIT3^{mCherry} signal and M2 is the proportion of DDIT3^{mCherry} signal
1340 overlapping altDDIT3^{GFP}. Error bars represent the mean +/- SD of three independent
1341 experiments (28 cells).

1342 **SUPPLEMENTARY FILES**

1343

1344 **Supplementary file 1: 12,616 alternative proteins and 26,531 reference proteins with**
1345 **translation initiation sites detected by ribosome profiling after re-analysis of large**
1346 **scale studies. Sheet 1: general information.** Sheet 2: list of alternative proteins; sheet 3:
1347 pie chart of corresponding altORFs localization. Sheet 4: Sheet 2: list of reference
1348 proteins

1349

1350 **Supplementary file 2: 4,872 alternative proteins detected by mass spectrometry**
1351 **(MS) after re-analysis of large proteomic studies.** Sheet 1: MS identification
1352 parameters; sheet 2: raw MS output; sheet 3: list of detected alternative proteins; sheet 4:
1353 pie chart of corresponding altORFs localization.

1354

1355 **Supplementary file 3: list of phosphopeptides.**

1356

1357 **Supplementary file 4: linker sequences separating adjacent zinc finger motifs.**

1358

1359 **Supplementary file 5: 383 alternative proteins detected by mass spectrometry in the**
1360 **interactome of 118 zinc finger proteins.** Sheet 1: MS identification parameters; sheet 2:
1361 raw MS output; sheet 3: list of detected alternative proteins.

1362

1363 **Supplementary file 6: high-confidence list of predicted functional and co-operating**
1364 **alternative proteins based on co-conservation and expression analyses.** Sheet 1: high

1365 confidence list in mammals; sheet 2: high confidence list in in vertebrates.

Table 1: AltORFs and alternative protein annotations in different organisms

Genomes	Features					
	Transcripts		Current annotations		Annotations of alternative protein coding sequences	
	mRNAs	Others[1]	CDSs	Proteins	altORFs	Alternative proteins
H. sapiens GRCh38 RefSeq GCF_000001405.26	67,765	11,755	68,264	54,498	539,134	183,191
P. troglodytes 2.1.4 RefSeq GCF_000001515.6	55,034	7,527	55,243	41,774	416,515	161,663
M. musculus GRCm38p2, RefSeq GCF_000001635.22	73,450	18,886	73,551	53,573	642,203	215,472
B. Taurus UMD3.1.86	22,089	838	22,089	21,915	79,906	73,603
X. tropicalis Ensembl JGI_4.2	28,462	4,644	28,462	22,614	141,894	69,917
D rerio Ensembl ZV10.84	44,198	8,196	44,198	41,460	214,628	150,510
D. melanogaster RefSeq GCA_000705575.1	30,255	3,474	30,715	20,995	174,771	71,705
C. elegans WBcel235, RefSeq GCF_000002985.6	28,653	25,256	26,458	25,750	131,830	45,603
S. cerevisiae YJM993_v1, RefSeq GCA_000662435.1	5,471	1,463	5,463	5,423	12,401	9,492

[1]Other transcripts include miRNAs, rRNAs, ncRNAs, snRNAs, snoRNAs, tRNAs. [2]Annotated retained-intron and processed transcripts were classified as mRNAs.

Table 2: orthology and co-conservation assessment of alternative-reference protein pairs between H. sapiens and other species

	A	B	C	D	E	F	G	H	I	J
						Observed	Mean expected		Max expected	
	Orthologous altProts (of 183,191 total)	Orthologous refProts	Co-conserved altProt-refProt pairs	Non-orthologous altProts	Non-orthologous altProts paired with orthologous refProts	Co-conservation (C/A)	% orthologous refProts (B/54,498)	% non-orthologous altProts paired with an orthologous refProt (E/D)	Max % of 1 million binomial simulations, p=max(G, H), n=A	Inferred *p*-value
P. troglodytes	113,687	25,755	100,839	69,504	30,772	88.69	47.20	44.27	50.39	<1e-06
M. musculus	25,930	22,304	24,862	157,261	106,987	95.88	40.09	68.031	69.39	<1e-06
B. taurus	25,868	16,887	24,426	157,323	99,369	94.42	30.98	63.16	64.67	<1e-06
X. tropicalis	2,470	12,458	1,974	180,721	95,499	79.91	22.85	52.84	57.81	<1e-06
D. rerio	2,023	12,791	1,203	181,168	94,426	59.46	23.47	52.12	57.29	<1e-06
D. melanogaster	115	4,881	51	183,076	34,352	44.34	8.95	18.76	38.26	<1e-06
C. elegans	34	3,954	8	183,157	26,839	23.52	7.25	14.65	50.00	0.02
S. cerevisiae	6	1,854	2	183,185	10,935	33.33	3.40	5.96	83.33	0.04

In order to compare the observed co-conservation to expected co-conservation, we used the more conservative of two expected values: either the percentage of all refProts (called here reference proteins) that were defined as orthologous (column G), or the percentage of non-orthologous altProts (called here alternative proteins) that were paired with an orthologous refProt. Both of these methods are themselves conservative, as they do not account for the conservation of the pairing. The larger of these values for each species was then used to generate 1 million random binomial distributions with n=# of orthologous altProts; the maximum of these percentages is reported in column I.

Table 3: alternative zinc finger proteins detected by mass spectrometry (MS) and ribosome profiling (RP)

Formatted: Numbering: Continuous

Alternative protein accession	Detection method[1]	Gene	Amino acid sequence	AltORF localization
IP_238718.1	MS	RP11	MLVEVACSSCRSLLHKGAGASEDGAALEPAHTGGKENGATT	nc
IP_278905.1	RP	ZNF761	MSVARPLVGSHILYAIIDFILERNLISVMSVARTLVRSHPLYAT IDFILERNLTSVMSVARPLVRSQTLHAIVDFILEKNKCNECGE VFNQQAHLAGHHRIHTGEKP	CDS
IP_278745.1	MS and RP	ZNF816	MSVARPSVRNHPFNAIIYFTLERNLTNVKNVTMFTFADHTLK DIGRFILERDHTNVRFVTRFSGVIHTLQNIREFILERNHTSVINV AGVSVGSHPFNTIIHFTLERNLTHVMNVARFLVEEKTLHVIID FMLERNLTNVKNVTKFSVADHTLKDIGEFILGKNHTNVRFVT RLSGVIHALQTIREFILERNLTSVINVRRFLIKKESLHNIREFILE RNLTSVMNVARFLIKKQALQNIREFILQRNLTSVMSVAKPLL DSQHLFTIKQSMGVGKLYKCNDCHKVFSNATTIANHYRIHIE ERSTSVINVANFSDVIHNL	CDS
IP_138289.1	MS	ZSCAN31	MNIGGATLERNPINVRSVGKPSVPAMASLDTEESTQGKNHM NAKCVGRLSSSAHALFSIRGYTLERSAISVVSVAKPSFRMQGF SSISESTLVRNPISAVSAVNSLVSGHFLRNIRKSTLERDHKGDE FGKAFSHHCNLIRHFRIHTVPAELD	CDS
IP_278564.1	MS	ZNF808	MIVTKSSVTLQQLQIIGESMMKRNLLSVINVACFSDIVHTLQFI GNLILERNLTNVMIEARSSVKLHPMQNRRIHTGEKPHKCDDC GKAFTSHSHLVGHQRIHTGQKSCKCHQCGKVFSPRSLLAEHE KIHF	3'UTR
IP_275012.1	MS	ZNF780A	MKPCECTECGKTFSCSSNIVQHVKIHTGEKRYNVRNMGKHLL WMISCLNIRKFRIVRNFVTIRSVDKPSLCTKNLLNTRELILMRN LVNIKECVKNFHHGLGFAQLLSIHTSEKSLSVRNVGRFIATLN TLEFGEDNSCEKVFE	3'UTR
IP_270595.1[2]	MS	ZNF440	MHSVERPYKCKICGRGFYSAKSFQIHEKSYTGEKPYECKQCG KAFVSFTSFRYHERTHTGENPYECKQFGKAFRSVKNLRFHKR THTGEKPCECKKCRKAFHNFSSLQIHERMHRGEKLCECKHCG KAFISAKIL	CDS
IP_270643.1[2]	MS	ZNF763	MKKLTLERNPINACHVVKPSIFPVPFSIMKGLTLERNPMSVSV GKPSDVPHTFEGMVGLTGEKPYECKECGKAFRSASHLQIHER TQTHIRIHSGERPYKCKTCGKGFYSPTSFQRHEKTHTAEKPYE CKQCGKAFSSSSSFWYHERTHTGEKPYECKQCGKAFRSASIQ MHAGTHPEEKPYECKQCGKAFRSAPHLRIHGRTHTGEKPYEC KECGKAFRSAKNLRIHERTQTHVRMHSVERPYKCKICGKGFY SAKSFQIPEKSYTGEKPYECKQCGKAFISFTSFR	3'UTR
IP_270597.1[3]	MS	ZNF440	MKNLTLERNPMSVSNVGKPLFPSLPFDIMKGLTLERTPMSVS NLGKPSDLSKIFDFIKGHTLERNPVNVRNVEKHSIISLLCKYM KGCTEERSSVNVSIVGKHSYLPRSFEYMQEHTMERNPMNVK NAEKHSACLLPFIDMKRLTLEGNTMNASNVAKLSLLPVLFNI MKEHTREKPYQCKQCAKAFISSTSFQYHERTHMGEKPYECM PSGKAFISSSSLQYHERTHTGEKPYEYKQCGKAFRSASHLQM HGRTHTGEKPYECKQYGKAFRPDKIL	3'UTR
IP_270609.1[3]	MS	ZNF439	MNVSNVAKAFTSSSSFQYHERTHTGEKPYQCKQCGKAVRSA SRLQMHGSTHTWQKLYECKQYGKAFRSARIL	3'UTR
IP_270663.1[3]	MS	ZNF844	MHGRTHTQEKPYECKQCGKAFIFSTSFRYHERTHTGEKPYEC KQCGKAFRSATQLQMHRKIHTGEKPYECKQCGKAYRSVSQL LVHERTHTVEQPYEYKQYGKAFRFAKNLQIQTMNVNN	CDS
IP_270665.1[3]	MS	ZNF844	MHRKIHTGEKPYECKQCGKAYRSVSQLLVHERTHTVEQPYE YKQYGKAFRFAKNLQIQTMNVNN	CDS
IP_270668.1[3]	MS	ZNF844	MSSTAFQYHEKTHTREKHYECKQCGKAFISSGSLRYHERTHT GEKPYECKQCGKAFRSATQLQMHRKIHTGEKPYECKQCGKA YRSVSQLLVHERTHTVEQPYEYKQYGKAFRFAKNLQIQTMN	3'UTR

			VNN	
IP_138139.1	MS	ZNF322	MLSPSRCKRIHTGEQLFKCLQCQLCCRQYEHLIGPQKTHPGE KPQQV	3'UTR
IP_204754.1	RP	ZFP91-CNTF	MPGETEEPRPPEQQDQEGGEAAKAAPEEPQQRPPEAVAAAPA GTTSSRVLRGGRDRGRAAAAAAAAAVSRRRKAEYPRRRRSS PSARPPDVPGQQPQAAKSPSPVQGKKSPRLLCIEKVTTDKDPK EEKEEEDDSALPQEVSIAASRPSRGWRSSRTSVSRHRDTENTR SSRSKTGSLQLICKSEPNTDQLDYDVGEEHQSPGGISSEEEEEE EEEMLISEEEIPFKDDPRDETYKPHLERETPKPRRKSGKVKEE KEKKEIKVEVEVEVKEEENEIREDEEPPRKRGRRRKDDKSPRL PKRRKKPPIQYVRCEMEGCGTVLAHPRYLQHHIKYQHLLKK KYVCPHPSCGRLFRLQKQLLRHAKHHTDQRDYICEYCARAF KSSHNLAVHRMIHTGEKPLQCEICGFTCRQKASLNWHMKKH DADSFYQFSCNICGKKFEKKDSVVAHKAKSHPEVLIAEALAA NAGALITSTDILGTNPESLTQPSDGQGLPLLPEPLGNSTSGECL LLEAEGMSKSYCSGTERSIHR	nc
IP_098649.1	RP	INO80B-WBP1	MSKLWRRGSTSGAMEAPEPGEALELSLAGAHGHGVHKKKH KKHKKKHKKKHHQEEDAGPTQPSPAKPQLKLKIKLGGQVLG TKSVPTFTVIPEGPRSPSPLMVVDNEEEPMEGVPLEQYRAWL DEDSNLSPSPLRDLSGGLGGQEEEEEQRWLDALEKGELDDNG DLKKEINERLLTARQRALLQKARSQPSPMLPLPVAEGCPPPAL TEEMLLKREERARKRRLQAARRAEEHKNQTIERLTKTAATSG RGGRGGARGERRGGRAAAPAPMVRYCSGAQGSTLSFPPGVP APTAVSQRPSPSGPPPRCSVPGCPHPRRYACSRTGQALCSLQC YRINLQMRLGGPEGPGSPLLATFESCAQE	nc
IP_115174.1	RP	ZNF721	MYIGEFILERNPTHVENVAKPLDSLQIFMRIRKFILERNPTRVE TVAKPLDSLQIFMHIRKFILEIKPYKCKECGKAFKSYYSILKHK RTHTRGMSYEGDECRGL	CDS
IP_275016.1	RP	ZNF780A	MNVRSVGKALIVVHTLFSIRKFIPMRNLLYVGNVRWPLDIIAN LLNILEFILVTSHLNVKTVGRPSIVAQALFNIRVFTLVRSPMNV RSVGRLLDFTYNFPNIRKLTQVKNHLNVRNVGNSFVVVQILI NIEVFILERNPLNVRNVGKPFDFICTLFDIRNCILVRNPLNVRS VGKPFDFICNLFDIRNCILVRNPLNVRNVERFLVFPPSLIAIRTF TQVRRHLECKECGKSFNRVSNHVQHQSIRAGVKPCECKGCG KGFICGSNVIQHQKIHSSEKLFVCKEWRTTFRYHYHLFNITKF TLVKNPLNVKNVERPSVF	CDS or 3'UTR
IP_278870.1	RP	ZNF845	MNVARFLIEKQNLHVIIEFILERNIRNMKNVTKFTVVNQVLKD RRIHTGEKAYKCKSL	CDS
IP_278888.1	RP	ZNF765	MSVARPSAGRHPLHTIIDFILDRNLTNVKIVMKLSVSNQTLKD IGEFILERNYTCNECGKTFNQELTLTCHRRLHSGEKPYKYEEL DKAYNFKSNLEIHQKIRTEENLTSVMSVARP	CDS
IP_278918.1	RP	ZNF813	MNVARVLIGKHTLHVIIDFILERNLTSVMNVARFLIEKHTLHIII DFILEINLTSVMNVARFLIKKHTLHVTIDFILERNLTSVMNVAR FLIKKQTLHVIIDFILERNLTSLMSVAKLLIEKQSLHIIIQFILER NKCNECGKTFCHNSVLVIHKNSYWRETSVMNVAKFLINKHT FHVIIDFIVERNLRNVKHVTKFTVANRASKDRRIHTGEKAYK GEEYHRVFSHKSNLERHKINHTAEKP	CDS
IP_280349.1	RP	ZNF587	MNAVNVGNHFFPALRFMFIKEFILDKSLISAVNVENPFLNVPV SLNTGEFTLEKGLMNAPNVEKHFSEALPSFIIRVHTGERPYEC SEYGKSFAEASRLVKHRRVHTGERPYECCQCGKHQNVCCPR S	CDS
IP_280385.1	RP	ZNF417	MNAMNVGNHFFPALRFMFIKEFILDKSLISAVNVENPLLNVP VSLNTGEFTLEKGLMNVPNVEKHFSEALPSFIIRVHTGERPYE CSEYGKSFAETSRLIKHRRVHTGERPYECCQSGKHQNVCSPW S	CDS

[1]MS, mass spectrometry; RP, ribosome profiling.

[2] These two proteins were not detected with unique peptides but with shared peptides. One protein only was counted in subsequent analyses.

[3] These five proteins were not detected with unique peptides but with shared peptides. One protein only was counted in subsequent analyses.

1 **Table 4: Examples of proteins encoded in the same gene and functionally interacting**

Gene	Polypeptides[1]	Reference	altORF localization	altORF size aa	Conservation	Summary of functional relationship with the annotated protein
CDKN2A, INK4	Cyclin-dependent kinase inhibitor 2A or p16-INK4 (P42771), and p19ARF (Q8N726)	(61)	5'UTR	169	Unknown	the unitary inheritance of p16INK4a and p19ARF may underlie their dual requirement in cell cycle control.
GNAS, XLalphas	Guanine nucleotide-binding protein G(s) subunit alpha isoforms XL□s (Q5JWF2) and Alex (P84996)	(62)	5'UTR	+700	Human, mouse, rat	Both subunits transduce receptor signals into stimulation of adenylyl cyclase.
ATXN1	Ataxin-1 (P54253) and altAtaxin-1	(63)	CDS	185	Unknown	Direct interaction
Adora2A	A2A adenosine receptor (P30543) and uORF5	(64)	5'UTR	134	Human, chimpanzee, rat, mouse	A2AR stimulation increases the level of the uORF5 protein via post-transcriptional regulation.

AGTR1	Angiotensin type 1a receptor (P25095) and PEP7	(65)	5'UTR	7	Highly conserved across mammalian species	Inhibits non-G protein-coupled signalling of angiotensin II, without altering the classical G protein-coupled pathway activated by the ligand.

[1]The UniProtKB accession is indicated when available.

Figure 1

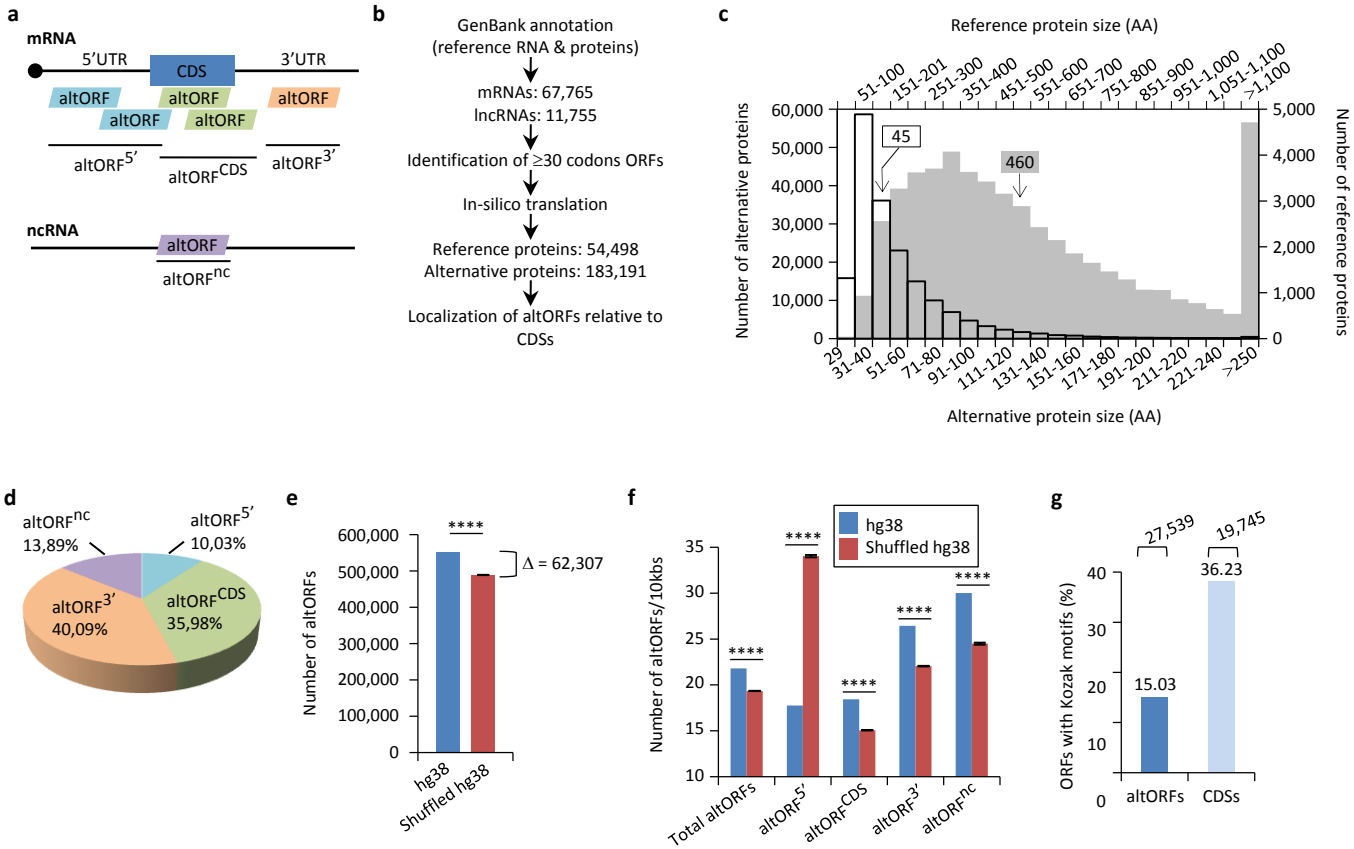

Figure 1. Annotation of human altORFs.
(**a**) AltORF nomenclature. AltORFs partially overlapping the CDS must be in a different reading frame. (**b**) Pipeline for the identification of altORFs. (**c**) Size distribution of alternative (empty bars, vertical and horizontal axes) and reference (grey bars, secondary horizontal and vertical axes) proteins. Arrows indicate the median size. The median alternative protein length is 45 amino acids (AA) compared to 460 for the reference proteins. (**d**) Distribution of altORFs in the human hg38 transcriptome. (**e, f**) Number of total altORFs (**e**) or number of altORFs/10kbs (**f**) in hg38 compared to shuffled hg38. Means and standard deviations for 100 replicates obtained by sequence shuffling are shown. Statistical significance was determined by using one sample t-test with two-tailed *p*-values. **** $p<0.0001$. (**g**) Percentage of altORFs with an optimal Kozak motif. The total number of altORFs with an optimal Kozak motif is also indicated at the top.

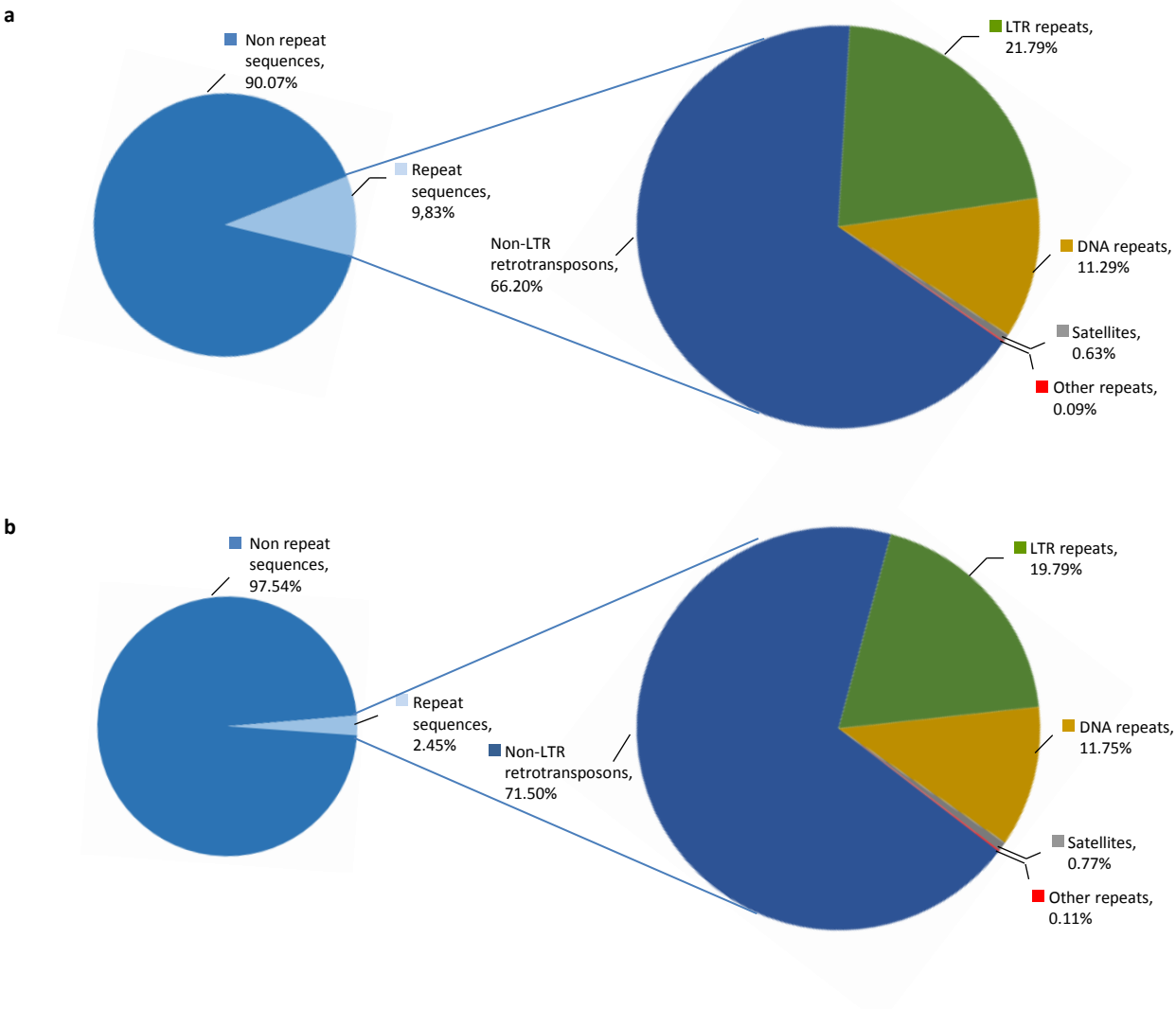

Figure 1-figure supplement 1: 10% of altORFs are present in different classes of repeats.

While more than half of the human genome is composed of repeated sequences, only 9.83% or 18,003 altORFs are located inside these repeats (**a**), compared to 2,45% or 1,677 CDSs (**b**). AltORFs and CDSs are detected in non-LTR retrotransposons (LINEs, SINEs, SINE-VNTR-Alus), LTR repeats, DNA repeats, satellites and other repeats. Proportions were determined using RepeatMasker (version 3.3.0).

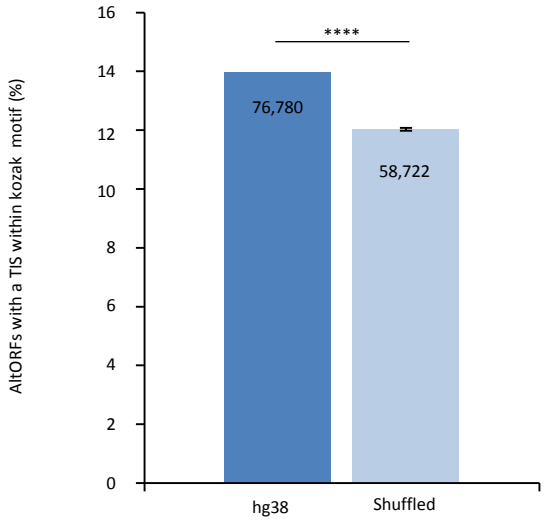

Figure 1-figure supplement 2: The proportion of altORFs with a translation initiation site (TIS) with a Kozak motif in hg38 is significantly different from 100 shuffled hg38 transcriptomes.

Percentage of altORFs with a TIS within an optimal Kozak sequence in hg38 (dark blue) compared to 100 shuffled hg38 (light blue). Mean and standard deviations for sequence shuffling are displayed, and significant difference was defined by using one sample t test. **** $P<0.0001$. Note that shuffling all transcripts in the hg38 transcriptome generates a total of 489,073 altORFs on average, compared to 539,134 altORFs in hg38. Most transcripts result from alternative splicing and there are 183,191 unique altORFs in the hg38 transcriptome, while the 489,073 altORFs in shuffled transcriptomes are all unique. Figure 1g shows the percentage of unique altORFs with a kozak motif (15%), while the current Fig. shows the percentage of altORFs with a kozak motif relative to the total number of altORFs (14%).

Figure 2

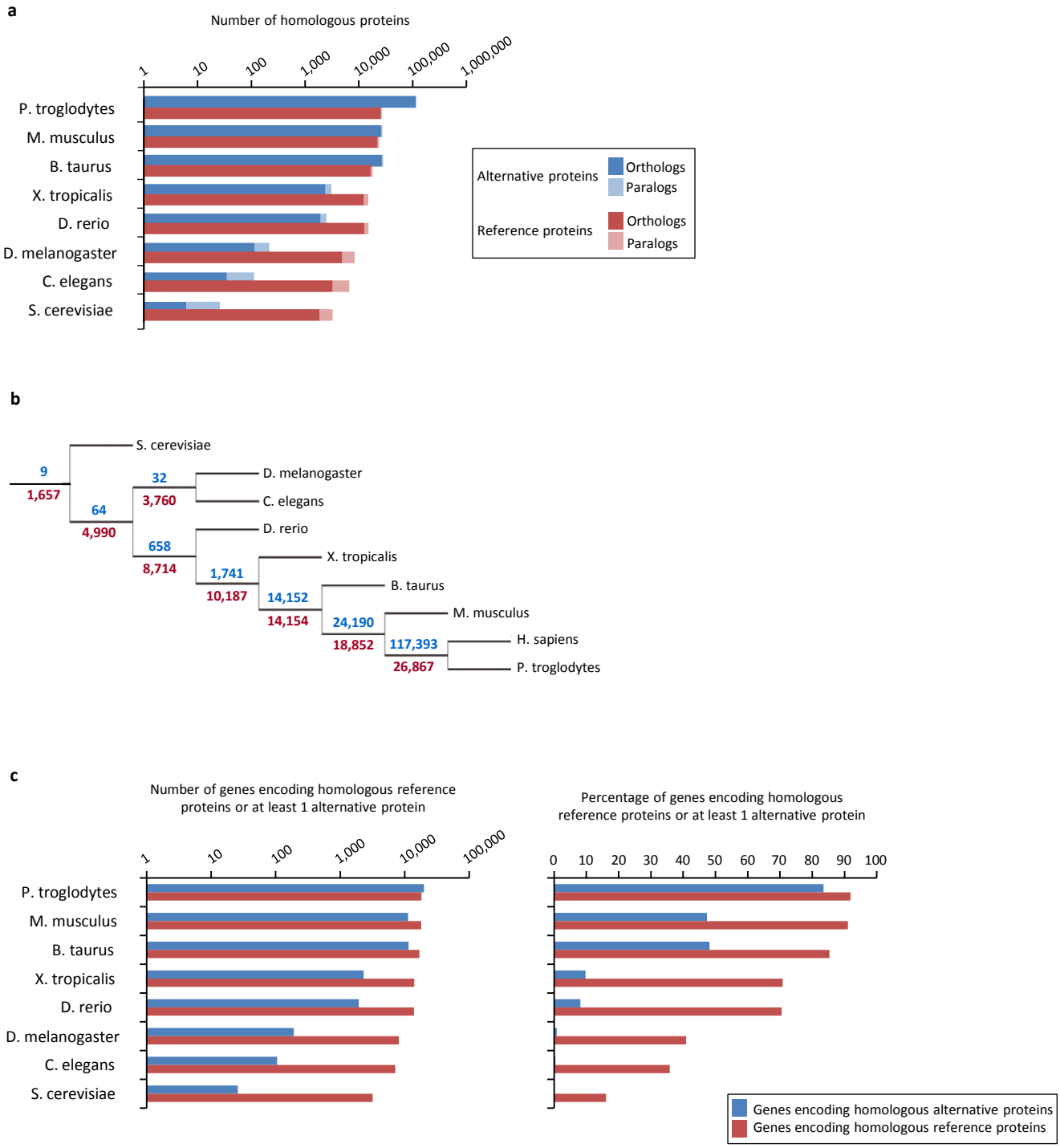

Figure 2. Conservation of alternative and reference proteins across different species. (**a**) Number of orthologous and paralogous alternative and reference proteins between *H. sapiens* and other species (pairwise study). (**b**) Phylogenetic tree: conservation of alternative (blue) and reference (red) proteins across various eukaryotic species. (**c**) Number and fraction of genes encoding homologous reference proteins or at least 1 homologous alternative protein between *H. sapiens* and other species (pairwise study).

Figure 3

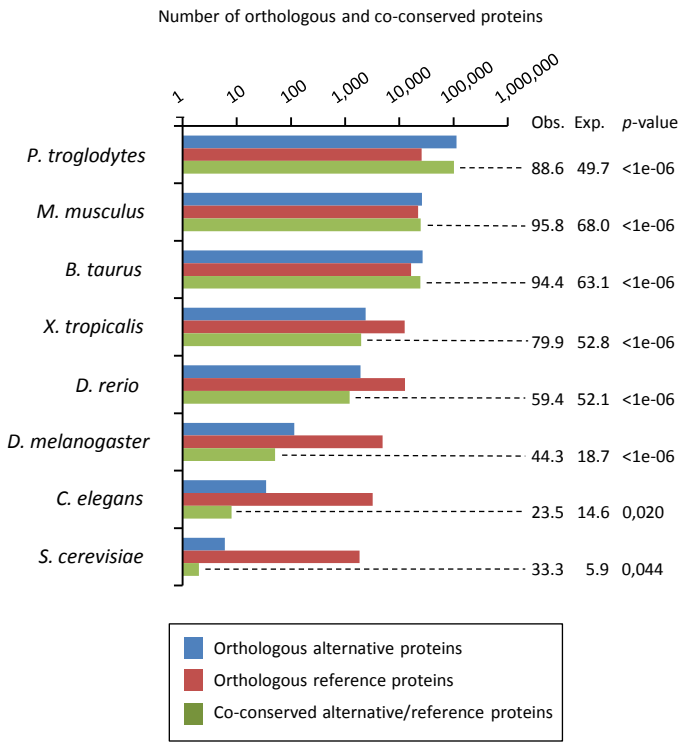

Figure 3. Number of orthologous and co-conserved alternative and reference proteins between *H. sapiens* and other species (pairwise). For the co-conservation analyses, the percentage of observed (Obs.), expected (Exp.) and corresponding *p*-values relative to the total number of reference-alternative protein pairs are indicated on the right (see Table 2 for details).

Figure 4

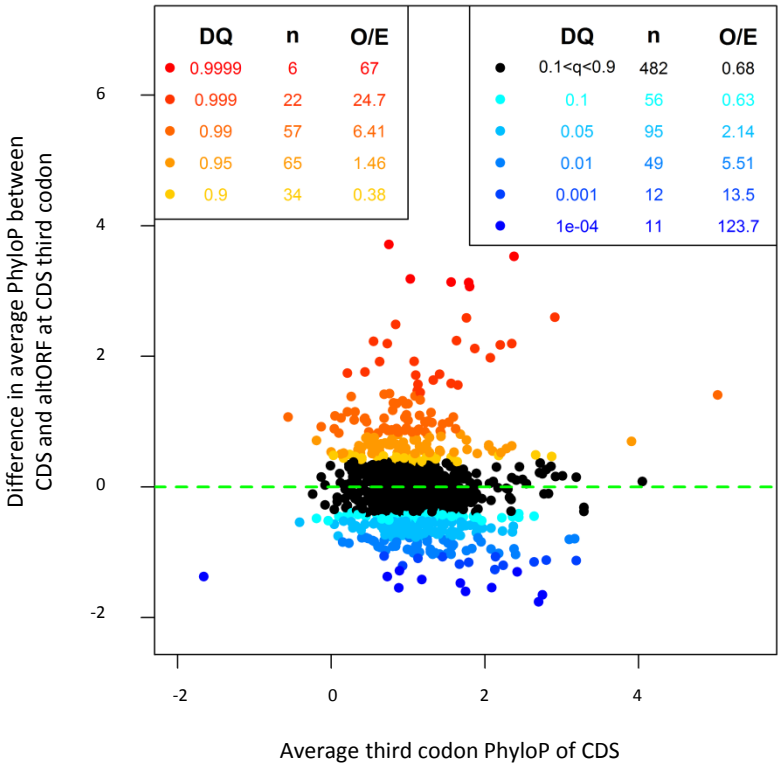

Figure 4. AltORFs completely nested within CDSs show more extreme PhyloP values (more conserved or faster evolving) than their CDSs. Differences between altORF and CDS PhyloP scores (altORF PhyloP – CDS PhyloP, *y*-axis) are plotted against PhyloPs for their respective CDSs (*x*-axis). We restricted the analysis to altORF-CDS pairs that were co-conserved from humans to zebrafish. The plot contains 889 CDSs containing at least one fully nested altORF, paired with one of its altORFs selected at random (to avoid problems with statistical non-independence). PhyloPs for both altORFs and CDSs are based on 3rd codons in the CDS reading frame, calculated across 100 vertebrate species. We compared these differences to those generated based on five random regions in CDSs with a similar length as altORFs. Expected quantiles of the differences ("DQ" columns) were identified and compared to the observed differences. We show the absolute numbers ("n") and observed-to-expected ratios ("O/E") for each quantile. There are clearly substantial over-representations of extreme values (red signaling conservation DQ 0.95, and blue signaling accelerated evolution DQ 0.05) with 317 of 889 altORFs (35.7%). A random distribution would have implied a total of 10% (or 89) of altORFs in the extreme values. This suggests that 25.7% (35.7%-10%) of these 889 altORFs undergo specific selection different from random regions in their CDSs with a similar length distribution. This percentage is very similar to the 26.2% obtained from an analysis of altORFs without restriction based on co-conservation in vertebrates (see Figure 4-figure supplement 1), a total which would imply that there are about 4,458 altORFs fully nested in CDSs undergoing conserved or accelerated evolution relative to their CDSs.

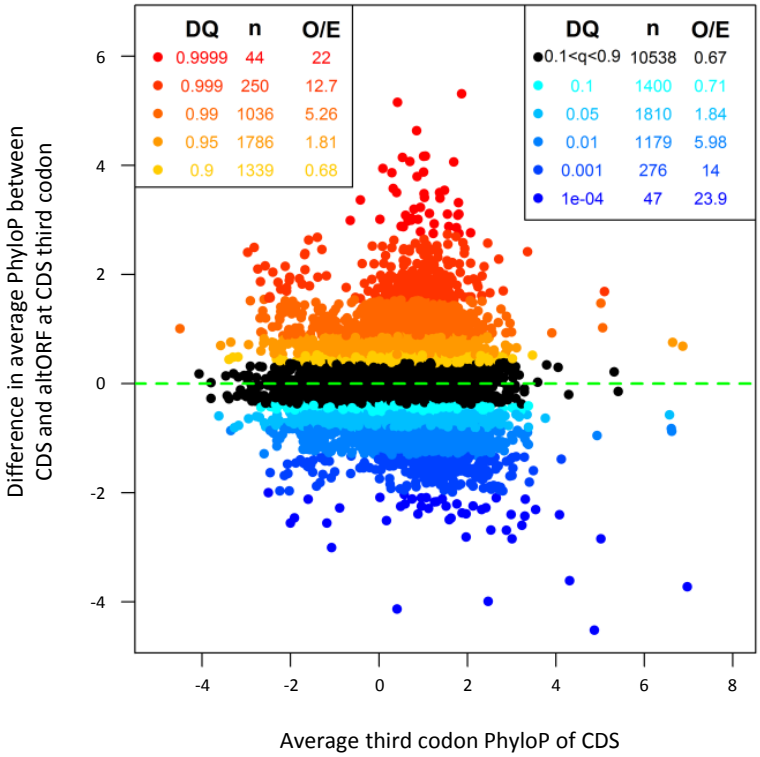

Figure 4-figure supplement 1. AltORFs completely nested within CDSs show more extreme PhyloP values (more conserved or faster evolving) than their CDSs. Differences between altORF and CDS PhyloP scores (altORF PhyloP – CDS PhyloP, *y*-axis) are plotted against PhyloPs for their respective CDSs (*x*-axis). The plot contains all 20,814 CDSs containing at least one fully nested altORF, paired with one of its altORFs selected at random (to avoid problems with statistical non-independence). PhyloPs for both altORFs and CDSs are based on third codon positions in the CDS reading frame, calculated across 100 vertebrate species. We compared these differences to those generated based on five random regions in CDSs with a similar length as altORFs. Expected quantiles of the differences ("DQ" columns) were identified and compared to the observed differences. We show the absolute numbers ("n") and observed-to-expected ratios ("O/E") for each quantile. There are clearly substantial over-representations of extreme values (red signalling conservation DQ≥0.95, and blue signalling accelerated evolution DQ≤0.05) with 6,428 of 19,705 altORFs (36.2%). A random distribution would have implied a total of 10% (or 1,970) of altORFs in the extreme values. This suggests that 26.2% (36.2%-10%) of altORFs (or 4,458) undergo specific selection different from random regions in their CDSs with a similar length distribution.

Figure 5

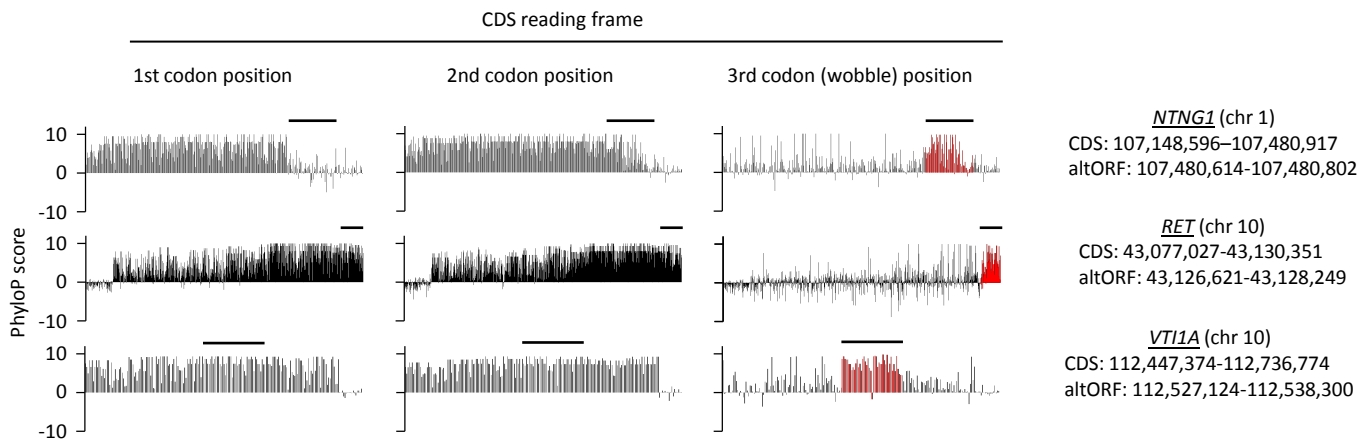

Figure 5. First, second, and third codon nucleotide PhyloP scores for 100 vertebrate species for the CDSs of the *NTNG1*, *RET* and *VTI1A* genes. Chromosomal coordinates for the different CDSs and altORFs are indicated on the right. The regions highlighted in red indicate the presence of an altORF characterized by a region with elevated PhyloP scores for wobble nucleotides. The region of the altORF is indicated by a black bar above each graph.

Figure 6

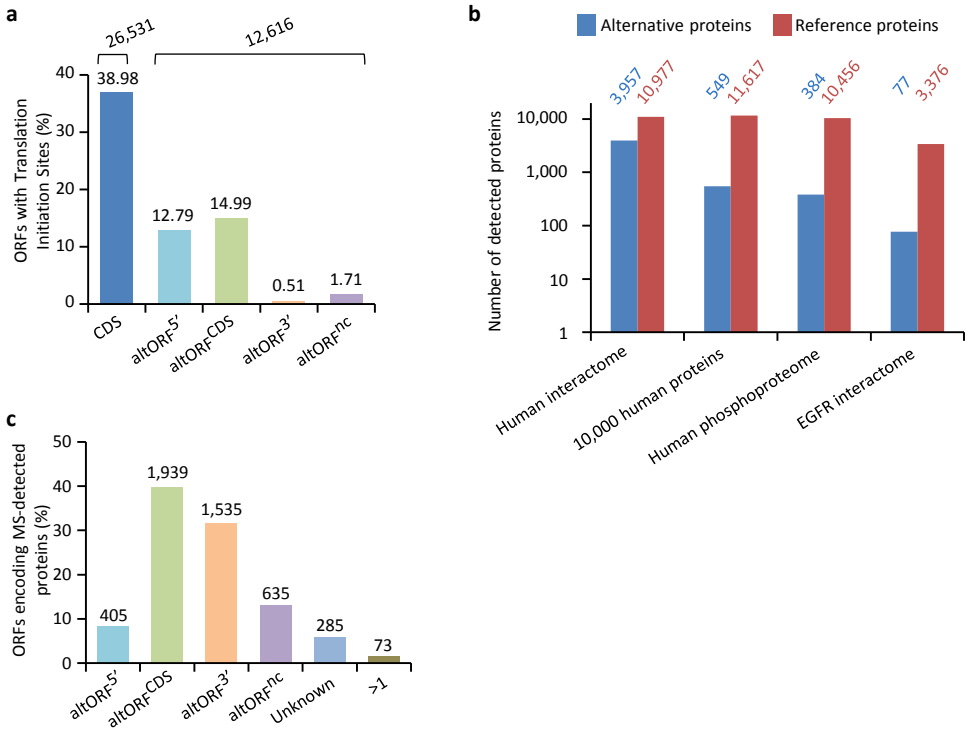

Figure 6. Expression of human altORFs.
(**a**) Percentage of CDSs and altORFs with detected TISs by ribosomal profiling and footprinting of human cells[23]. The total number of CDSs and altORFs with a detected TIS is indicated at the top. (**b**) Alternative and reference proteins detected in three large proteomic datasets: human interactome[32], 10,000 human proteins[35], human phosphoproteome[34], EGFR interactome[33]. Numbers are indicates above each column. (**c**) Percentage of altORFs encoding alternative proteins detected by MS-based proteomics. The total number of altORFs is indicated at the top. Localization “Unknown” indicates that the detected peptides can match more than one alternative protein. Localization ">1" indicates that the altORF can have more than one localization in different RNA isoforms.

Figure 7

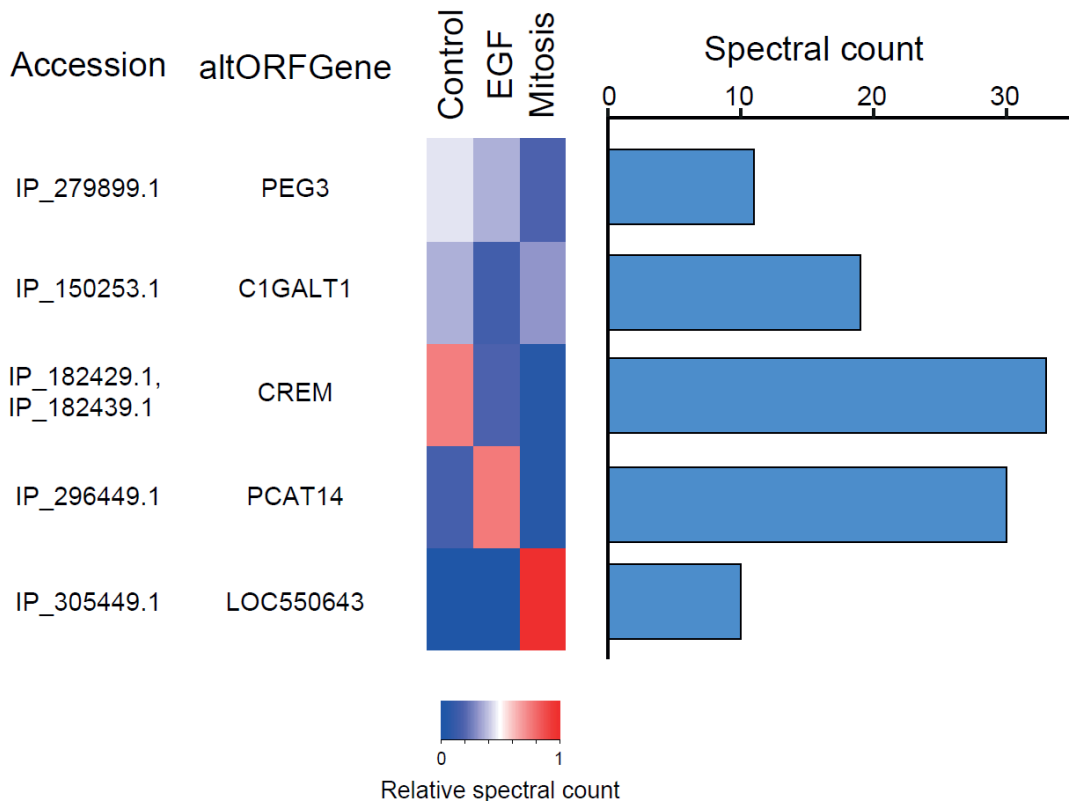

Figure 7. The alternative phosphoproteome in mitosis and EGF-treated cells. Heatmap showing relative levels of spectral counts for phosphorylated peptides following the indicated treatment[34]. For each condition, heatmap colors show the percentage of spectral count on total MS/MS phosphopeptide spectra. Blue bars on the right represent the number of MS/MS spectra; only proteins with spectral counts above 10 are shown.

a

AltLINC01420^{nc}

MGDQPCASGRSTLPPGNAREAKPPKKRCLLAPR**WDYPEGTPNGGSTTLPSAPPPASAGLK**SHPPPPEK

b

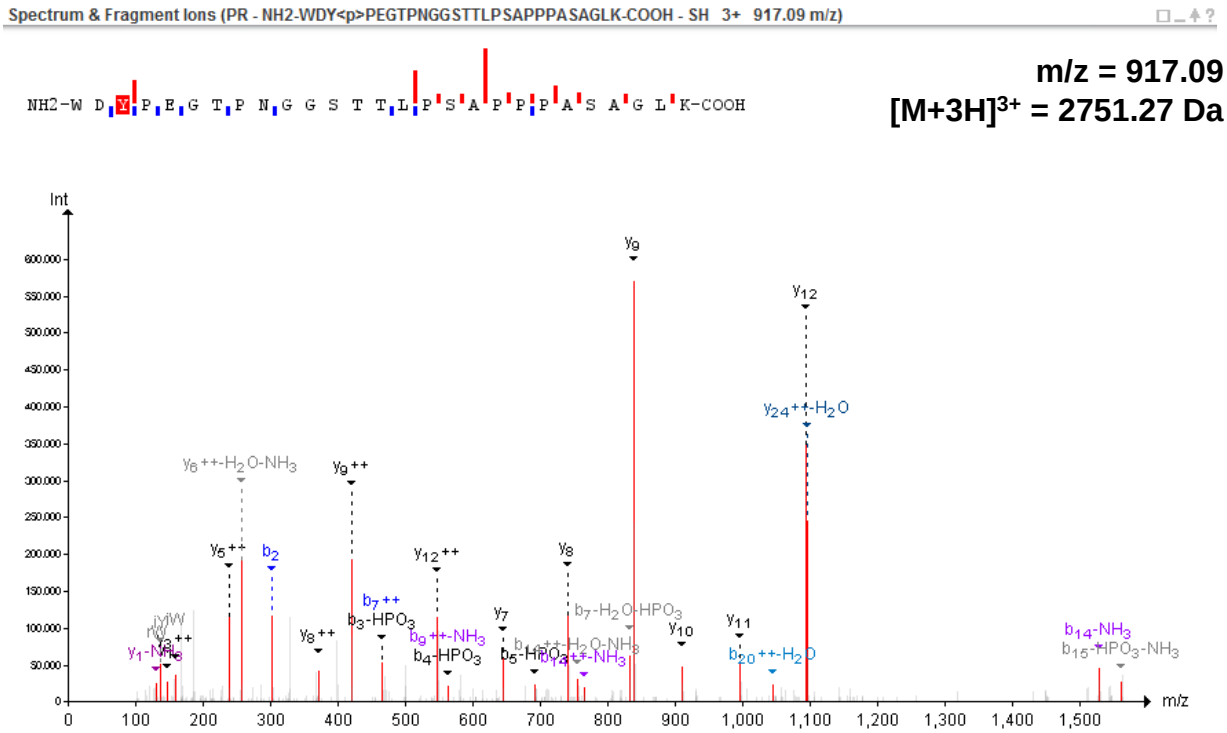

c

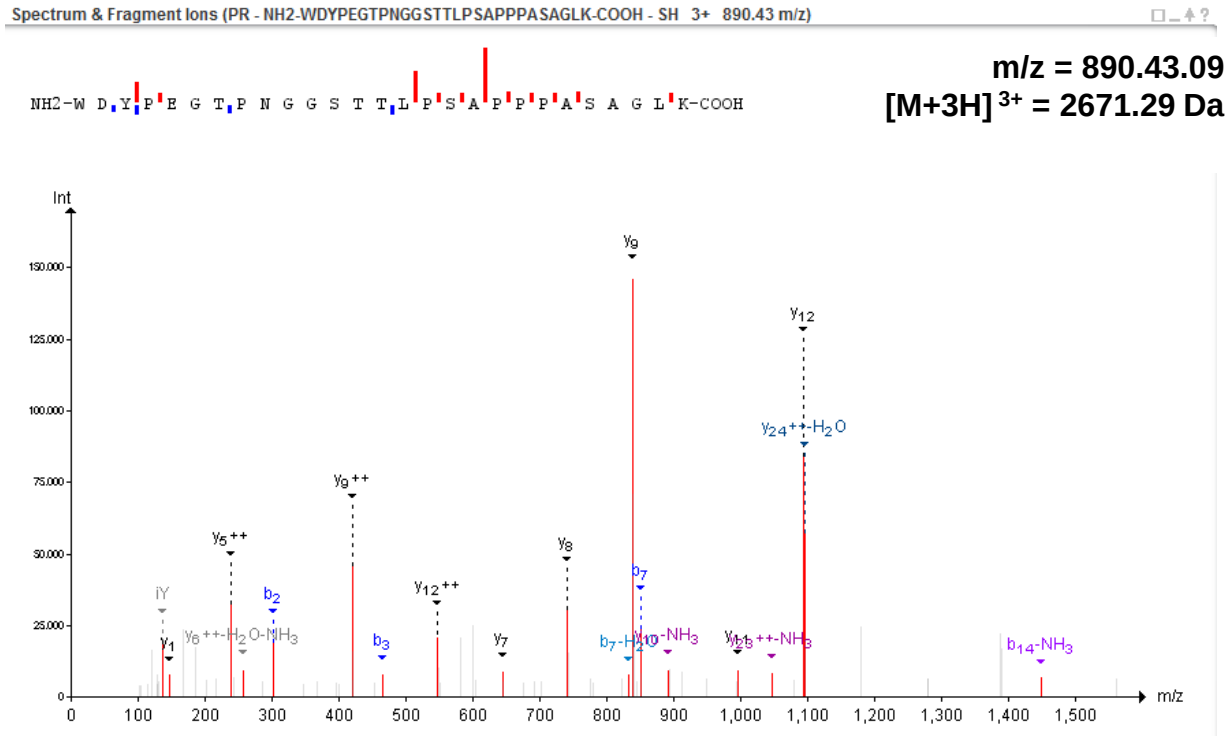

Figure 7-figure supplement 1: Example of a phosphorylated peptide in mitosis - alternative protein AltLINC01420^{nc} (LOC550643, IP_305449.1).

(**a**) AltLINC01420^{nc} amino acid sequence with detected peptides underlined and phosphorylated peptide in bold (73,9% sequence coverage). (**b**) MS/MS spectrum for the phosphorylated peptide (PeptideShaker graphic interface output). The phosphorylation site is the tyrosine residue, position 2. (**c**) MS/MS spectrum for the non-phosphorylated peptide. The mass difference between the precursor ions between both spectra corresponds to that of a phosphorylation, confirming the specific phosphorylation of this residue in mitosis.

Figure 8

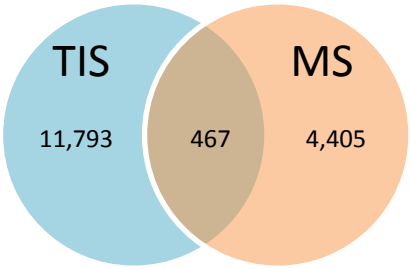

Figure 8. Number of alternative proteins detected by ribosome profiling and mass spectrometry.
The expression of 467 alternative proteins was detected by both ribosome profiling (translation initiation sites, TIS) and mass spectrometry (MS).

Figure 9

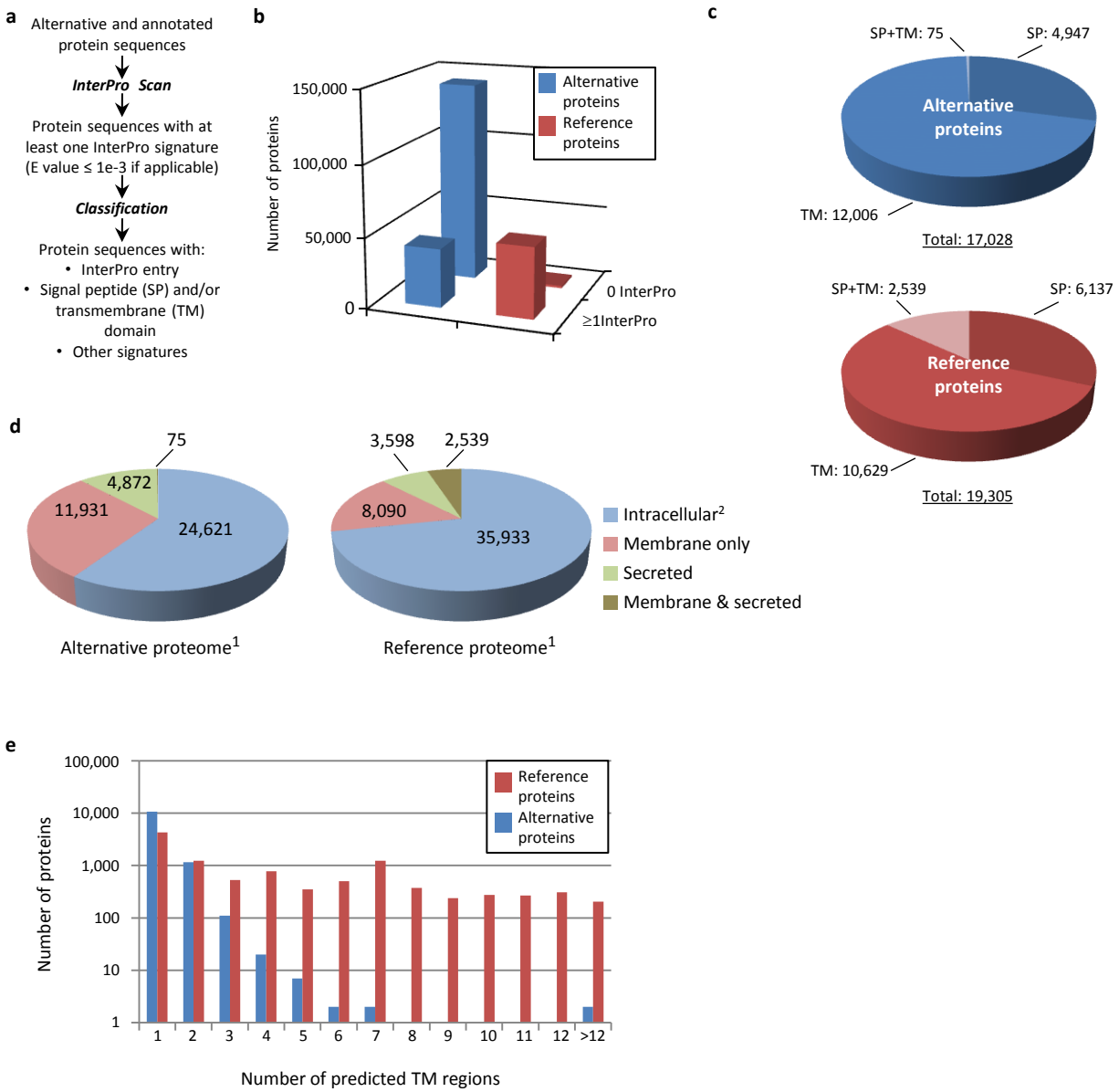

Figure 9. Human alternative proteome sequence analysis and classification using InterProScan.

(**a**) InterPro annotation pipeline. (**b**) Alternative and reference proteins with InterPro signatures. (**c**) Number of alternative and reference proteins with transmembrane domains (TM), signal peptides (S) and both TM and SP. (**d**) Number of all alternative and reference proteins predicted to be intracellular, membrane, secreted and membrane-spanning and secreted. [1]Proteins with at least one InterPro signature; [2]Proteins with no predicted signal peptide or transmembrane features. (**e**) Number of predicted TM regions for alternative and reference proteins.

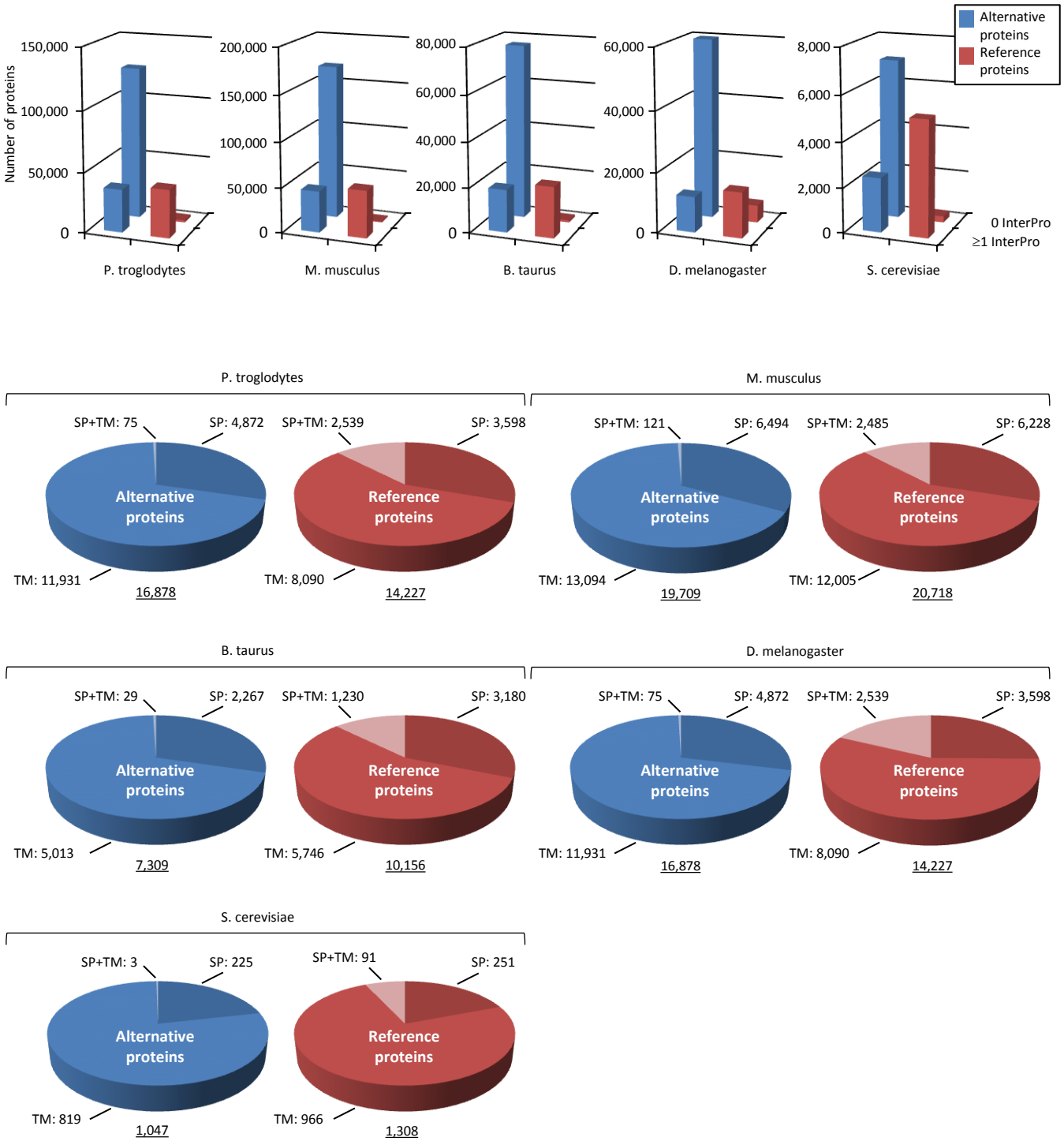

Figure 9-figure supplement 1: Alternative proteome sequence analysis and classification in *P. troglodytes*, *M. musculus*, *B. Taurus*, *D. melanogaster* and *S. cerevisiae*.
For each organism, the number of InterPro signatures (top graphs) and proteins with transmembrane (TM), signal peptide (SP), or TM+SP features (bottom pie charts) is indicated for alternative and reference proteins.

Figure 10

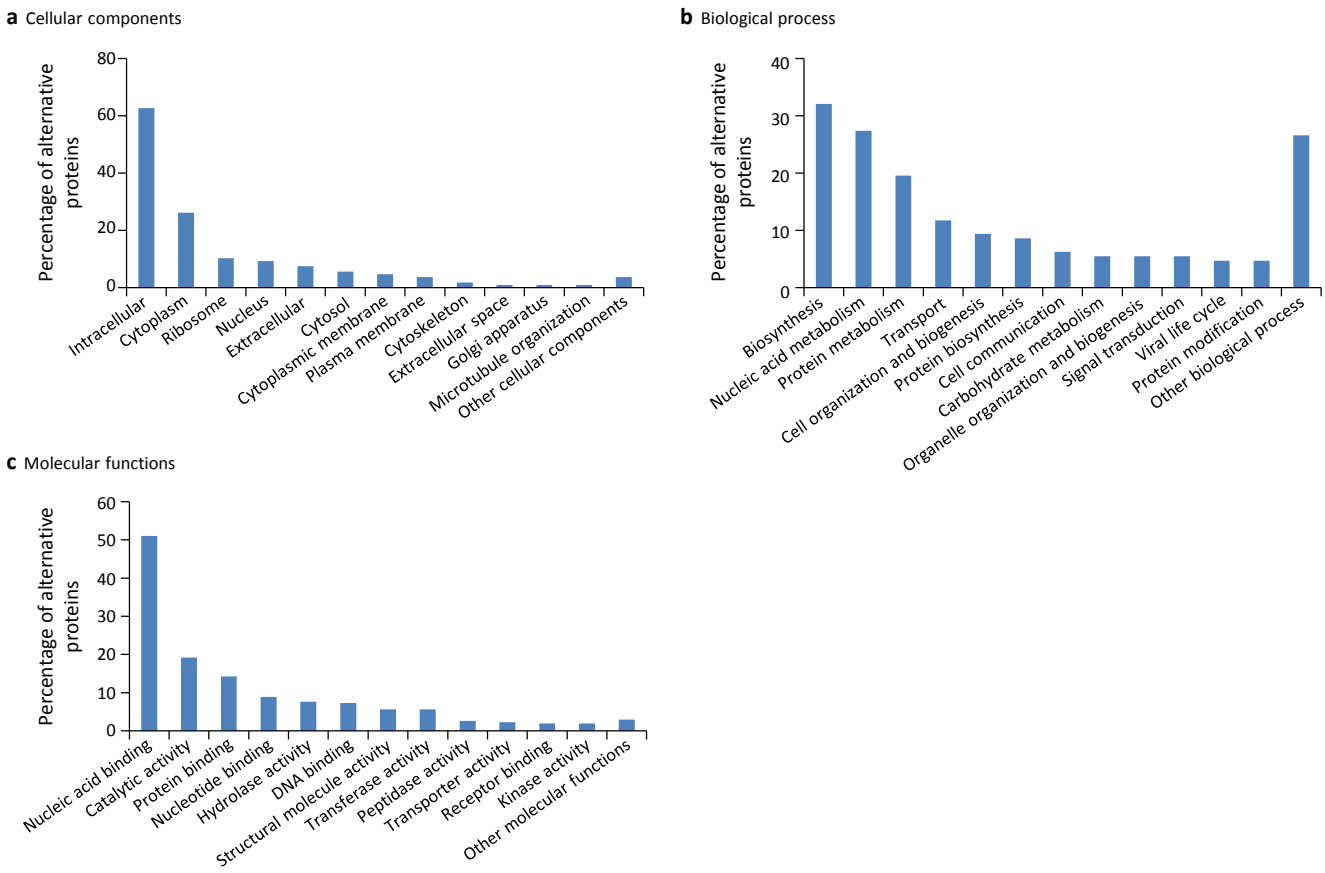

Figure 10. Gene ontology (GO) annotations for human alternative proteins.
GO terms assigned to InterPro entries are grouped into 13 categories for each of the three ontologies. (**a**) 34 GO terms were categorized into cellular component for 107 alternative proteins. (**b**) 64 GO terms were categorized into biological process for 128 alternative proteins. (**c**) 94 GO terms were categorized into molecular function for 302 alternative proteins. The majority of alternative proteins with GO terms are predicted to be intracellular, to function in nucleic acid-binding, catalytic activity and protein binding and to be involved in biosynthesis and nucleic acid metabolism processes.

Figure 11

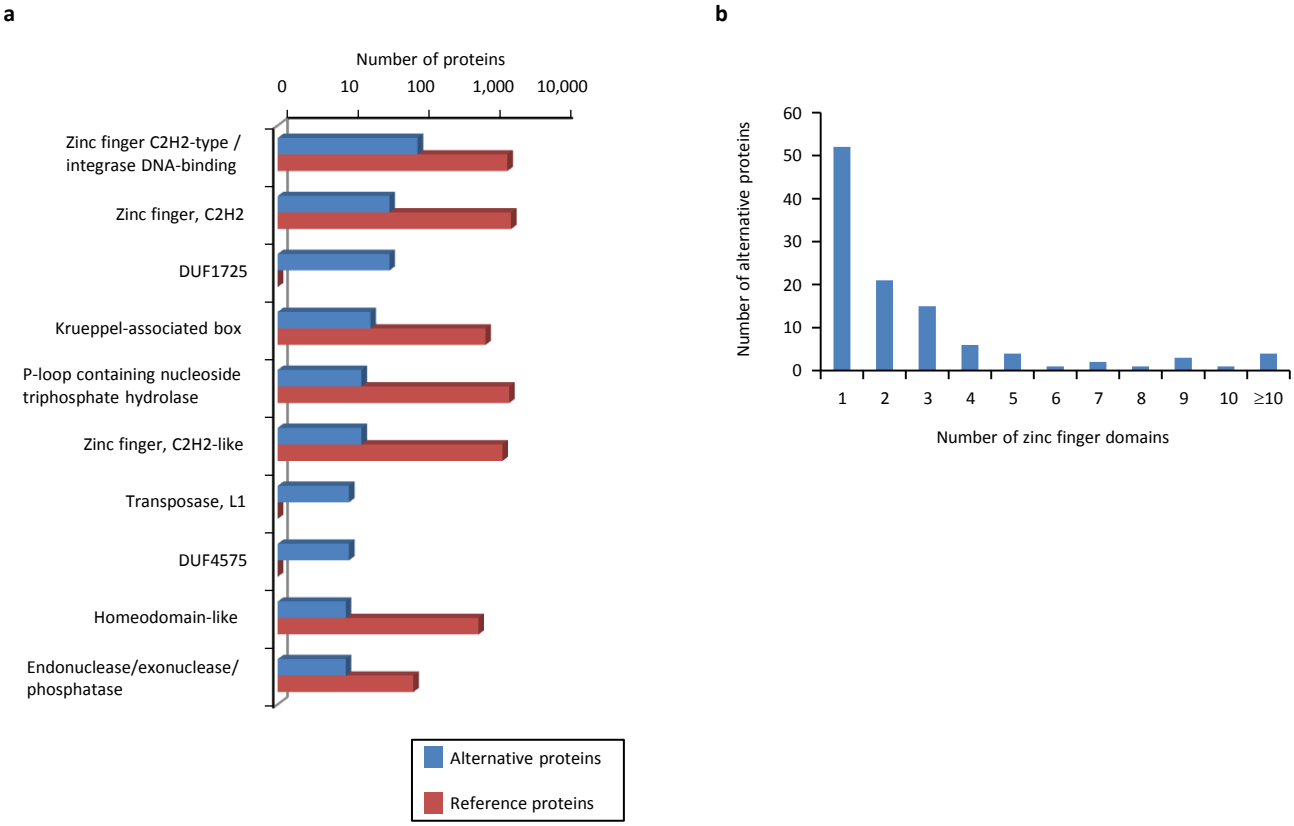

Figure 11. Main InterPro entries in human alternative proteins. (**a**) The top 10 InterPro families in the human alternative proteome. (**b**) A total of 110 alternative proteins have between 1 and 23 zinc finger domains.

Figure 12

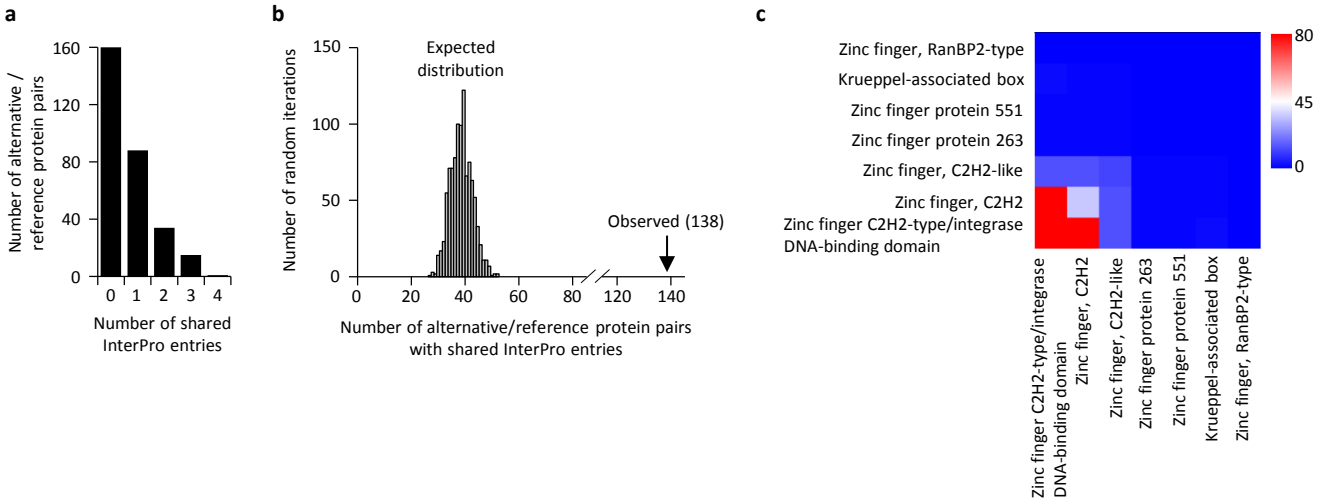

Figure 12. Reference and alternative proteins share functional domains.
(**a**) Distribution of the number of shared InterPro entries between alternative and reference proteins coded by the same transcripts. 138 pairs of alternative and reference proteins share between 1 and 4 protein domains (InterPro entries). Only alternative/reference protein pairs that have at least one domain are considered (n = 298). (**b**) The number of reference/alternative protein pairs that share domains (n = 138) is higher than expected by chance alone. The distribution of expected pairs sharing domains and the observed number are shown. (**c**) Matrix of co-occurrence of domains related to zinc fingers. The entries correspond to the number of times entries co-occur in reference and alternative proteins. The full matrix is available in figure 12-figure supplement 1.

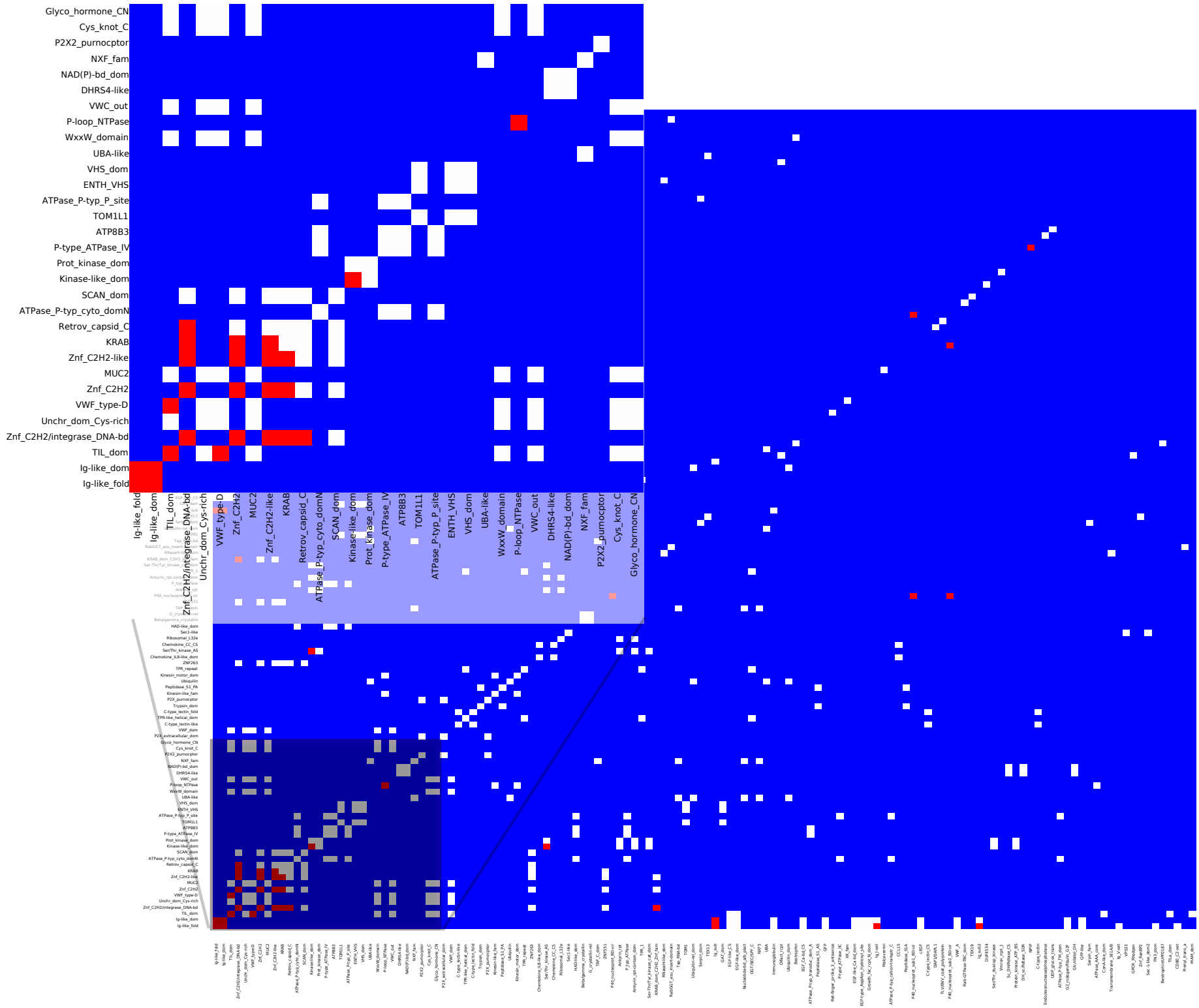
Glyco_hormone_CN
Cys_knot_C
P2X2_purnocptor
NXF_fam
NAD(P)-bd_dom
DHRS4-like
VWC_out
P-loop_NTPase
WxxW_domain
UBA-like
VHS_dom
ENTH_VHS
ATPase_P-typ_P_site
TOM1L1
ATP8B3
P-type_ATPase_IV
Prot_kinase_dom
Kinase-like_dom
SCAN_dom
ATPase_P-typ_cyto_domN
Retrov_capsid_C
KRAB
Znf_C2H2-like
MUC2
Znf_C2H2
VWF_type-D
Unchr_dom_Cys-rich
Znf_C2H2/integrase_DNA-bd
TIL_dom
Ig-like_dom
Ig-like_fold

Figure 12-figure supplement 1: Matrix of co-occurrence of InterPro entries between alternative/reference protein pairs coded by the same transcript.
Pixels show the number of times entries co-occur in reference and alternative proteins. Blue pixels indicate that these domains are not shared, white pixels indicate that they are shared once, and red that they are shared twice or more.

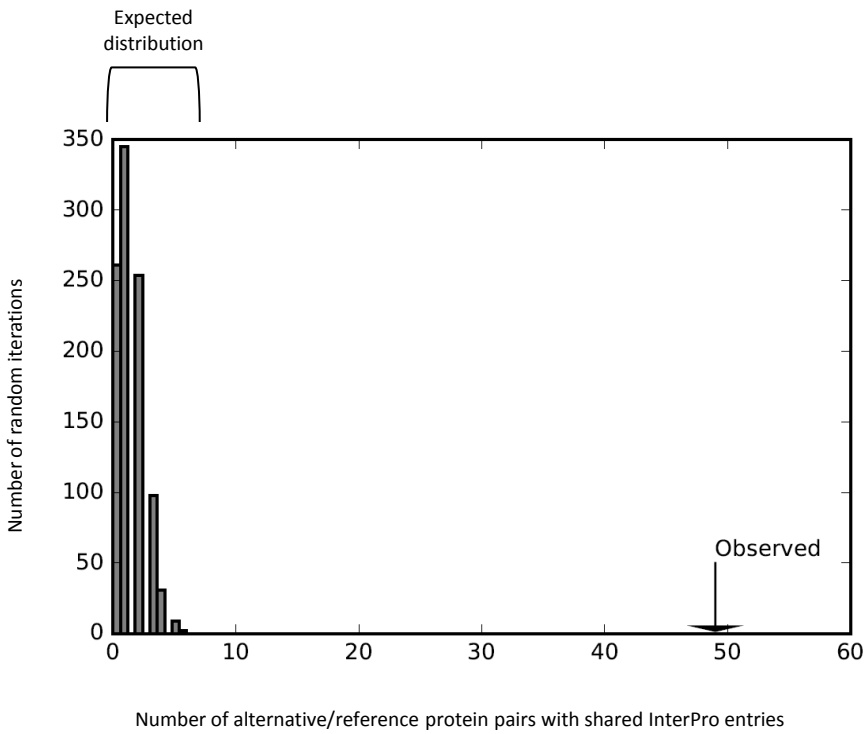

Figure 12-figure supplement 2: Reference and alternative proteins share functional domains.

The number of reference/alternative protein pairs that share domains (n = 49) is higher than expected by chance alone (p<0.001). The distribution of expected pairs sharing domains and the observed number are shown. This is the same analysis as the one presented in figure 12b, with the zinc finger domains taken out.

Figure 13

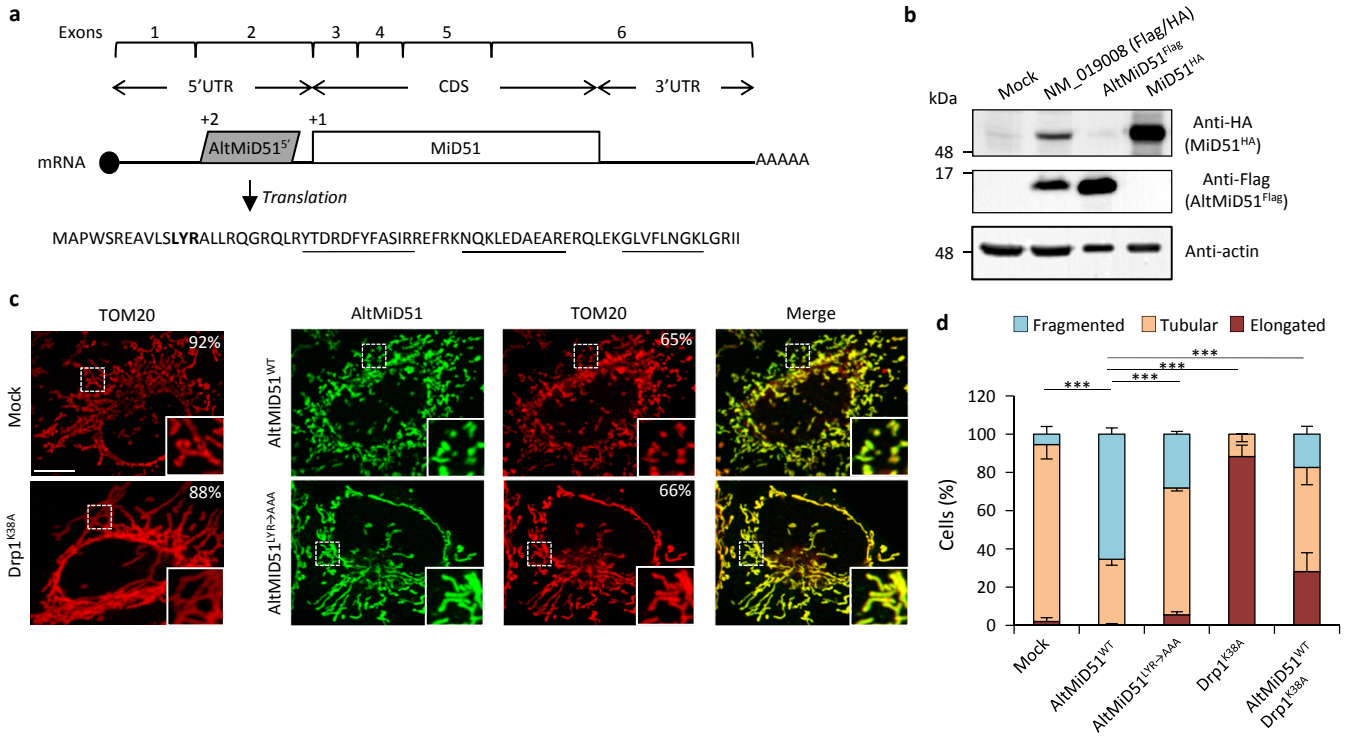

Figure 13. AltMiD51$^{5'}$ expression induces mitochondrial fission.
(**a**) AltMiD51$^{5'}$ coding sequence is located in exon 2 or the *MiD51/MIEF1/SMCR7L* gene and in the 5'UTR of the canonical mRNA (RefSeq NM_019008). +2 and +1 indicate reading frames. AltMiD51 amino acid sequence is shown with the LYR tripeptide shown in bold. Underlined peptides were detected by MS. (**b**) Human HeLa cells transfected with empty vector (mock), a cDNA corresponding to the canonical MiD51 transcript with a Flag tag in frame with altMiD51 and an HA tag in frame with MiD51, altMiD51^{Flag} cDNA or MiD51^{HA} cDNA were lysed and analyzed by western blot with antibodies against Flag, HA or actin, as indicated. (**c**) Confocal microscopy of mock-transfected cells, cells transfected with altMiD51^{WT}, altMiD51$^{LYR\rightarrow AAA}$ or Drp1^{K38A} immunostained with anti-TOM20 (red channel) and anti-Flag (green channel) monoclonal antibodies. In each image, boxed areas are shown at higher magnification in the bottom right corner. % of cells with the most frequent morphology is indicated: mock (tubular), altMiD51^{WT} (fragmented), altMiD51(LYR→AAA) (tubular), Drp1(K38A) (elongated). Scale bar, 10 µm. (**d**) Bar graphs show mitochondrial morphologies in HeLa cells. Means of three independent experiments per condition are shown (100 cells for each independent experiment). ***$p<0.0005$ (Fisher's exact test) for the three morphologies between altMiD51(WT) and the other experimental conditions.

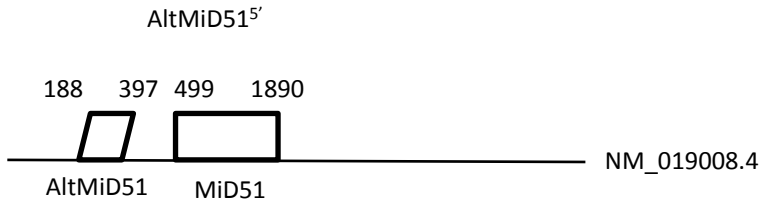

a. Experimental peptide

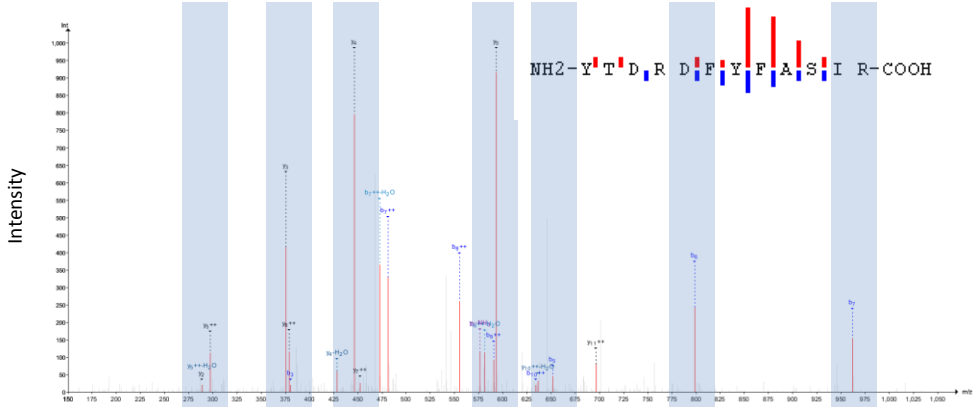

b. Synthetic peptide

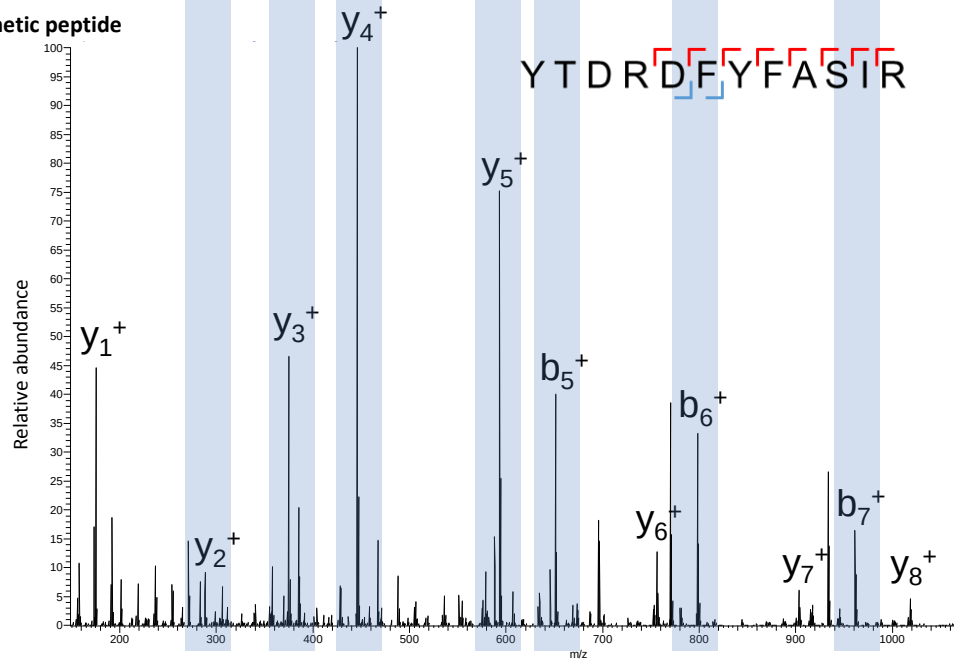

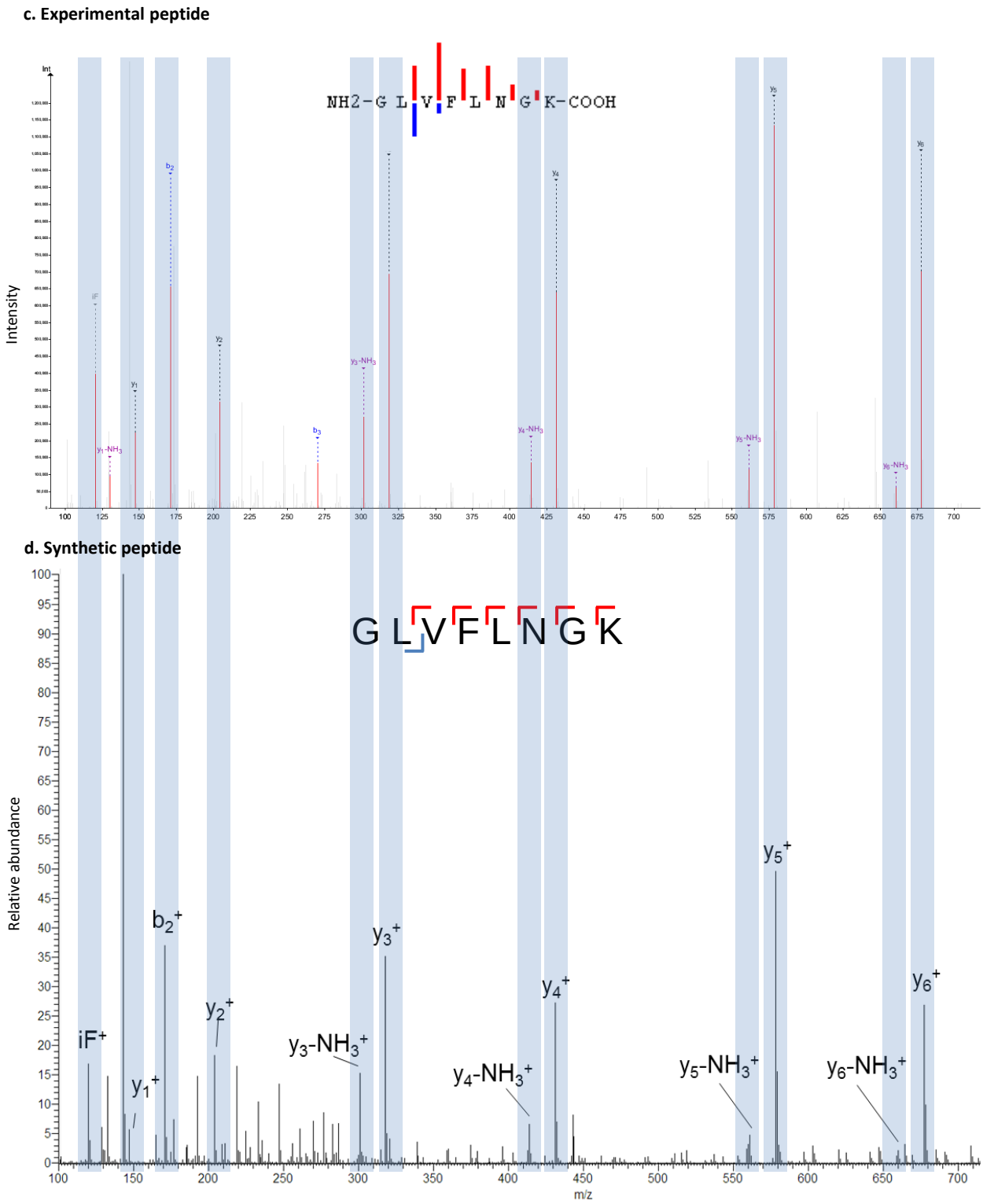

Figure 13-figure supplement 1: Spectra validation for altMiD51.
Example of validation for altMiD51 specific peptides YTDRDFYFASIR and GLVFLNGK. (**a,c**) Experimental MS/MS spectra (PeptideShaker graphic interface output). (**b,d**) MS/MS spectra of the synthetic peptides.
Matching peaks are shown with blue masks. A diagram of the transcript with its accession number and the localization of the altORF and the CDS is shown at the top.

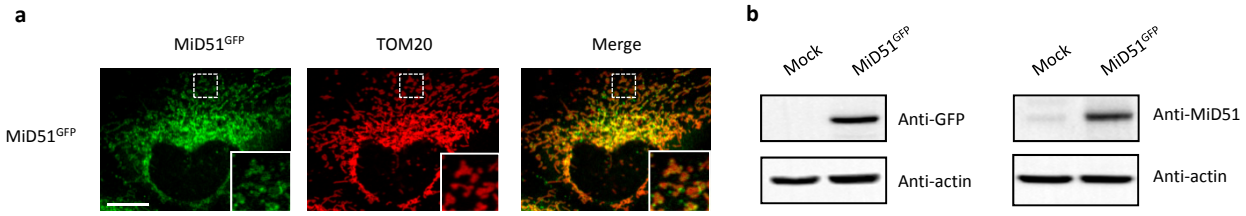

Figure 13-figure supplement 2: MiD51 expression results in mitochondrial fission. (**a**) Confocal microscopy of HeLa cells transfected with MiD51^{GFP} immunostained with anti-TOM20 (red channel) monoclonal antibodies. In each image, boxed areas are shown at higher magnification in the bottom right corner. The localization of MiD51 in fission sites is shown in merged higher magnification inset. Scale bar, 10 µm. (**b**) Human HeLa cells transfected with empty vector (mock) or MiD51^{GFP} were lysed and analyzed by western blot to confirm MiD51^{GFP} expression.

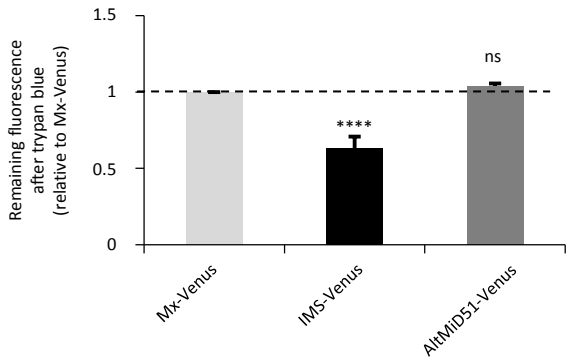

Figure 13-figure supplement 3: AltMiD51 is localized in the mitochondrial matrix. Trypan blue quenching experiment performed on HeLa cells stably expressing the indicated constructs. The fluorescence remaining after quenching by trypan blue is shown relative to Matrix-Venus (Mx-Venus) indicated by the dashed line. (**** p <0,0001, one-way ANOVA). The absence of quenching of the fluorescence compared to IMS-Venus indicates the matricial localization of altMiD51. n≥3 cells were quantified per experiment, and results are from 6 independent experiments. Data are mean ±SEM.

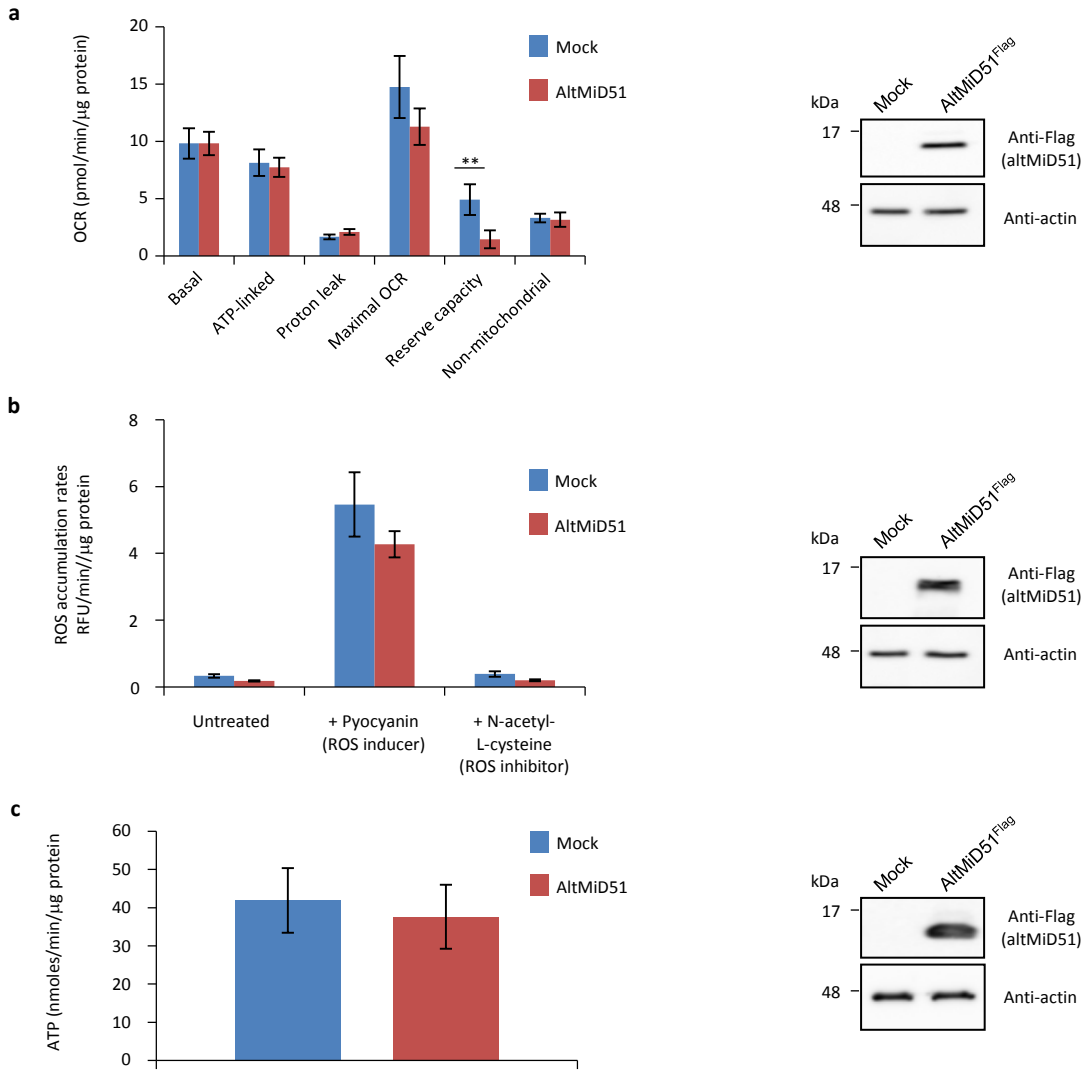

Figure 13-figure supplement 4: Mitochondrial function parameters.
(**a**) Oxygen consumption rates (OCR) in HeLa cells transfected with empty vector (mock) or altMiD51^{Flag}. Mitochondrial function parameters were assessed in basal conditions (basal), in the presence of oligomycin to inhibit the ATP synthase (oxygen consumption that is ATP-linked), FCCP to uncouple the mitochondrial inner membrane and allow for maximum electron flux through the respiratory chain (maximal OCR), and antimycin A/rotenone to inhibit complex III (non-mitochondrial). The balance of the basal OCR comprises oxygen consumption due to proton leak and nonmitochondrial sources. The mitochondrial reserve capacity (maximal OCR- basal OCR) is an indicator of rapid adaptation to stress and metabolic changes. Mean values of replicates are plotted with error bars corresponding to the 95% confidence intervals. Statistical significance was estimated using a two-way ANOVA with Tukey's post-hoc test (**p = 0,004). (**b**) ROS production in mock and altMiD51-expressing cells. Cells were untreated, treated with a ROS inducer or a ROS inhibitor. Results represent the mean value out of three independent experiments, with error bars corresponding to the standard error of the mean (s.e.m.). Statistical significance was estimated using unpaired T-test. (**c**) ATP synthesis rate in mock and altMiD51-expressing cells. No significant differences in ATP production were observed between mock and altMiD51 transfected cells.
Results represent the mean of three independent experiments (8 technical replicates each). Error bars represent the standard error of the mean. At the end of the experiments, cells were collected and proteins analyzed by western blot with antibodies against the Flag tag (altMiD51) or actin, as indicated, to verify the expression of altMiD51. A representative western blot is shown on the right. Molecular weight markers are shown on the left (kDa).

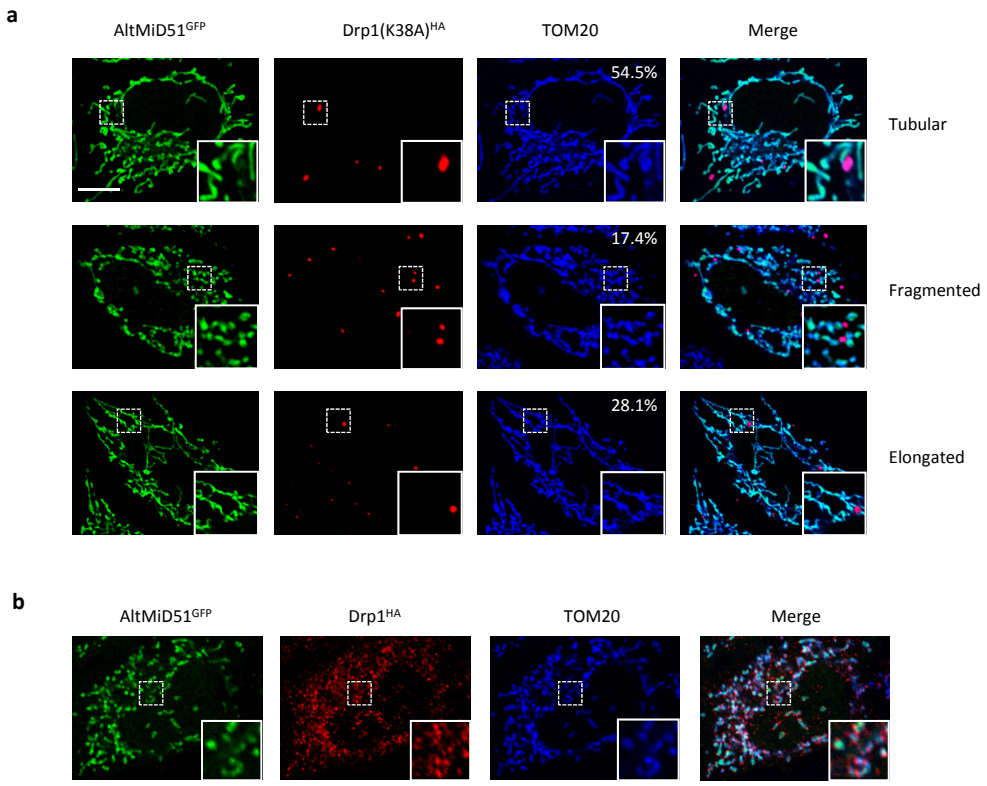

Figure 13-figure supplement 5: Representative confocal images of cells co-expressing altMiD51^{GFP} and Drp1(K38A)^{HA}.

(**a**) Confocal microscopy of HeLa cells co-transfected with altMiD51^{GFP} and Drp1(K38A)^{HA} immunostained with anti-TOM20 (blue channel) and anti-HA (red channel) monoclonal antibodies. In each image, boxed areas are shown at higher magnification in the bottom right corner. % of cells with the indicated morphology is indicated on the TOM20 panels. (**b**) Confocal microscopy of HeLa cells co-transfected with altMiD51^{GFP} and Drp1(wt)^{HA} immunostained with anti-TOM20 (blue channel) and anti-HA (red channel) monoclonal antibodies. In each image, boxed areas are shown at higher magnification in the bottom right corner. Scale bar, 10 μm.

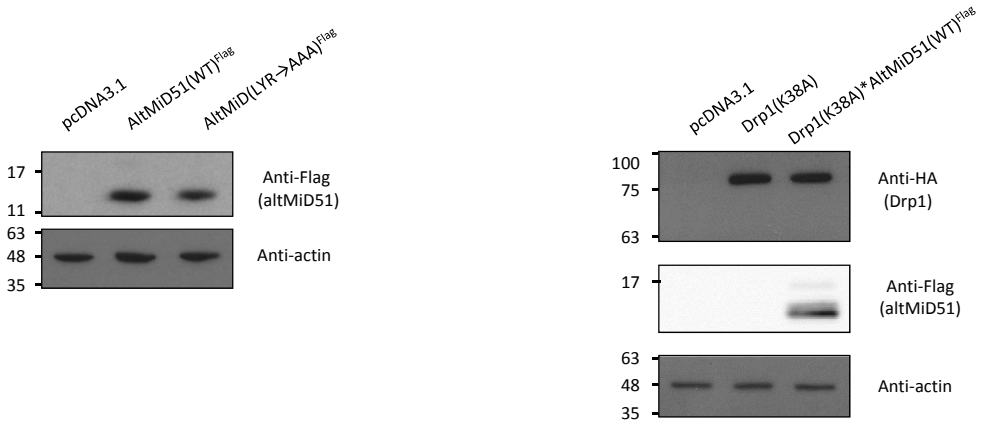

Figure 13-figure supplement 6: Protein immunoblot showing the expression of different constructs in HeLa cells.

HeLa cells were transfected with empty vector (pcDNA3.1), altMiD51(WT)^{Flag}, altMID51(LYR→AAA)^{Flag}, Drp1(K38A)^{HA}, or Drp1(K38A)^{HA} and altMiD51(WT)^{Flag}, as indicated. Proteins were extracted and analyzed by western blot with antibodies against the Flag tag (altMiD51), the HA tag (Drp1K38A) or actin, as indicated. Molecular weight markers are shown on the left (kDa). Representative experiment of three independent biological replicates.

Figure 14

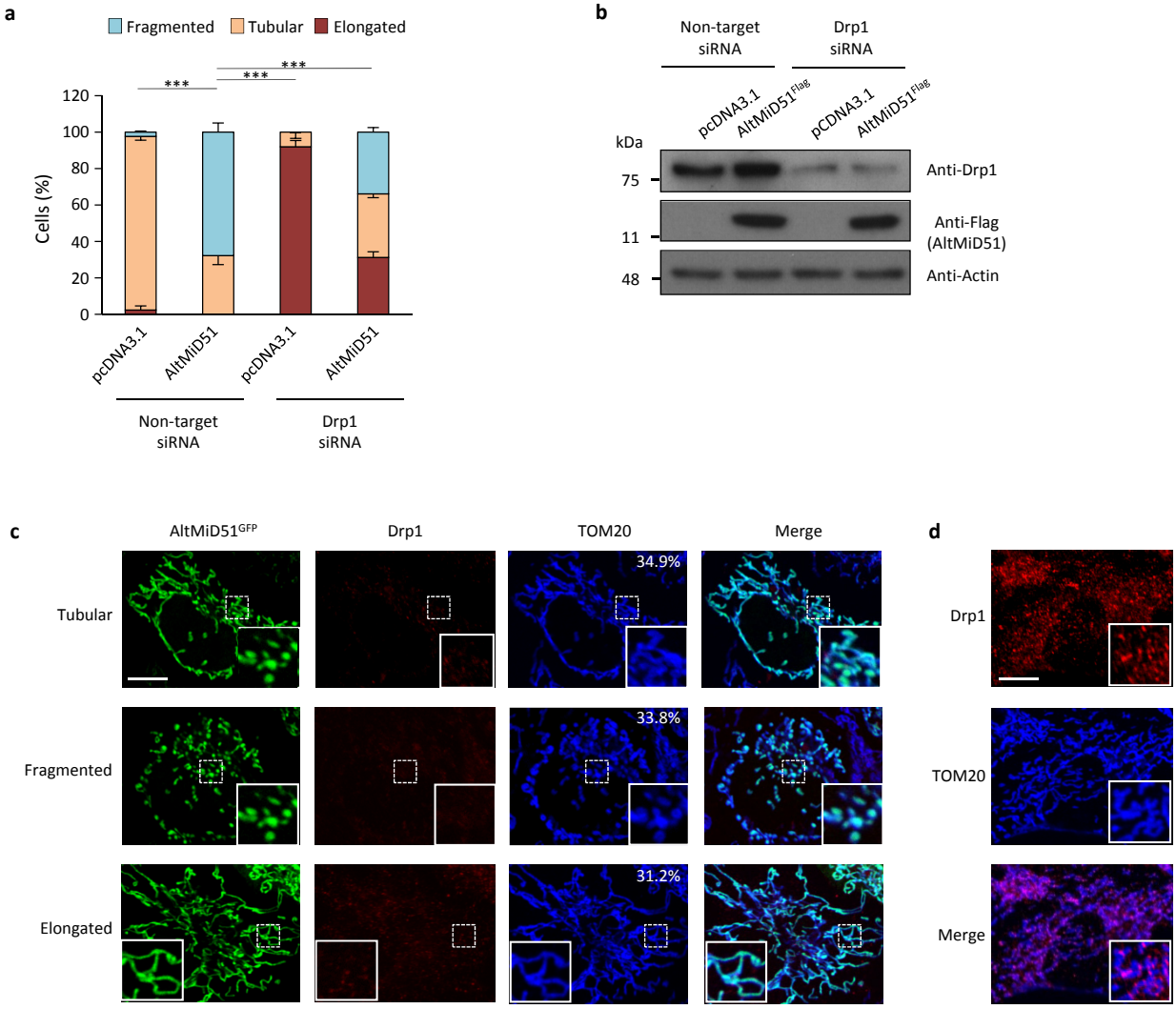

Figure 14. AltMiD51-induced mitochondrial fragmentation is dependent on Drp1. (**a**) Bar graphs show mitochondrial morphologies in HeLa cells treated with non-target or Drp1 siRNAs. Cells were mock-transfected (pcDNA3.1) or transfected with altMiD51^{Flag}. Means of three independent experiments per condition are shown (100 cells for each independent experiment). ***p<0.0005 (Fisher's exact test) for the three morphologies between altMiD51 and the other experimental conditions. (**b**) HeLa cells treated with non-target or Drp1 siRNA were transfected with empty vector (pcDNA3.1) or altMiD51^{Flag}, as indicated. Proteins were extracted and analyzed by western blot with antibodies against the Flag tag (altMiD51), Drp1 or actin, as indicated. (**c**) Confocal microscopy of Drp1 knockdown cells transfected with altMiD51^{GFP} immunostained with anti-TOM20 (blue channel) and anti-Drp1 (red channel) monoclonal antibodies. In each image, boxed areas are shown at higher magnification in the bottom right corner. % of cells with the indicated morphology is indicated on the TOM20 panels. Scale bar, 10 µm. (**d**) Control Drp1 immunostaining in HeLa cells treated with a non-target siRNA. For (**c**) and (**d**), laser parameters for Drp1 and TOM20 immunostaining were identical.

Figure 15

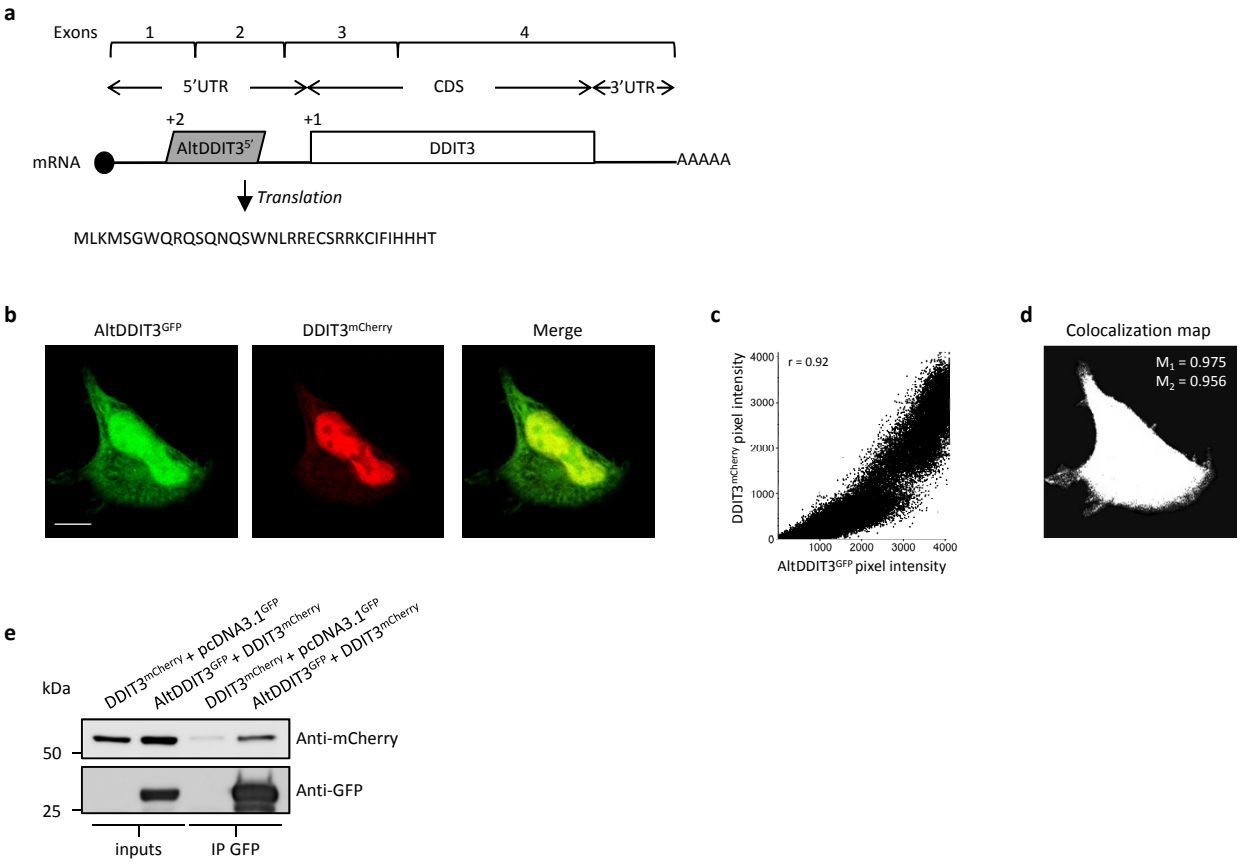

Figure 15. AltDDIT3$^{5'}$ co-localizes and interacts with DDIT3.
(**a**) AltDDIT3$^{5'}$ coding sequence is located in exons 1 and 2 or the *DDIT3/CHOP/GADD153* gene and in the 5'UTR of the canonical mRNA (RefSeq NM_004083.5). +2 and +1 indicate reading frames. AltDDIT3 amino acid sequence is also shown. (**b**) Confocal microscopy analyses of HeLa cells co-transfected with altDDIT3^{GFP} (green channel) and DDIT3^{mCherry} (red channel). Scale bar, 10 µm. (**c, d**) Colocalization analysis of the images shown in (**b**) performed using the JACoP plugin (Just Another Co-localization Plugin) implemented in Image J software (two independent biological replicates). (**c**) Scatterplot representing 50 % of green and red pixel intensities showing that altDDIT3^{GFP} and DDIT3^{mCherry} signal highly correlate (with Pearson correlation coefficient of 0.92 (p-value < 0.0001)). (**d**) Binary version of the image shown in (**b**) after Costes' automatic threshold. White pixels represent colocalization events (p-value < 0.001, based on 1000 rounds of Costes' randomization colocalization analysis). The associated Manders Correlation Coefficient, M_1 and M_2, are shown in the right upper corner. M_1 is the proportion of altDDIT3^{GFP} signal overlapping DDIT3^{mCherry} signal and M_2 is the proportion of DDIT3^{mCherry} signal overlapping altDDIT3^{GFP}. (**e**) Representative immunoblot of co-immunoprecipitation with GFP-Trap agarose beads performed on HeLa lysates co-expressing DDIT3^{mcherry} and altDDIT3^{GFP} or DDIT3^{mcherry} with pcDNA3.1^{GFP} empty vector (two independent experiments).

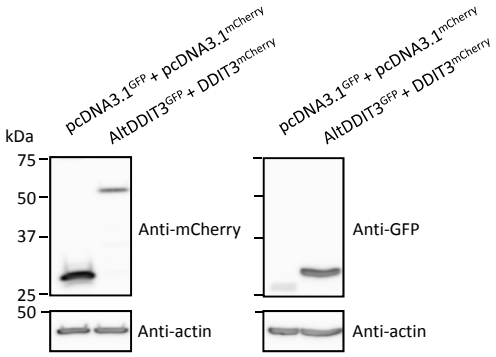

Figure 15-figure supplement 1: Protein immunoblot showing the expression of different constructs in HeLa cells.

HeLa cells were co-transfected with GFP and mCherry, or altDDIT3^{GFP} and DDIT3^{mCherry}, as indicated. Proteins were extracted and analyzed by western blot with antibodies, as indicated. Molecular weight markers are shown on the left (kDa). AltDDIT3 has a predicted molecular weight of 4.28 kDa and thus migrates at its expected molecular weight when tagged with GFP (~32 kDa). Representative experiment of two independent biological replicates.

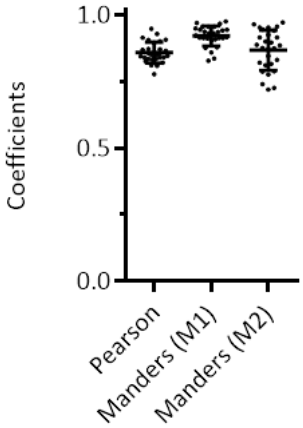

Figure 15–figure supplement 2 : Colocalization of altDDIT3 with DDIT3.
Scatter plots of Pearson's Correlation Coefficient and Manders' Correlation Coefficient after Costes' automatic threshold (*p*-value < 0.001, based on 1000 rounds of Costes' randomization colocalization analysis). M1 is the proportion of altDDIT3^{GFP} signal overlapping DDIT3^{mCherry} signal and M2 is the proportion of DDIT3^{mCherry} signal overlapping altDDIT3^{GFP}. Error bars represent the mean +/- SD of three independent experiments (28 cells).